ABSTRACT

WANG, JUN. Effect of Electric Field on the Processing and Propeties of Yttria-stabilized Zirocnia (YSZ). (Under the supervision of Prof. Hans Conrad).

It is well-known that the processing and properties of polycrystalline ceramics are grain size dependent; the grain size is usually controlled by thermo-mechanical treatments and the addition of solutes. More recently, application of an electric field has been found to retard grain growth and in turn influence the annealing, sintering and plastic deformation rate of ceramic materials. Moreover, it is well-established that the bulk conductivity of polycrystalline ceramics decreases with decrease in grain size.

This research deals with the effect of an applied electric field on the processing and properties of 3 mole percent yttria-stabilized tetragonal zirconia polycrystals (3Y-TZP), whereby DC and AC fields were applied during sintering and isothermal annealing of 3Y-TZP. Regarding sintering, it was found that grain growth during sintering was retarded with the application of electric field compared to without. The ratio of the grain size with field to that without $\bar{d}_E/\bar{d}$ decreased with increase in field strength up to ~ 26 V/cm and then remained constant with further increase in field strength to ~ 60 V/cm, the transition occurred at the ratio of $\bar{d}_E/\bar{d}$ = 0.4. It was further found that an AC field had a greater effect on grain growth retardation compared to DC. In the isothermal annealing study a modest DC field with an initial strength of 14 V/cm was applied during the isothermal annealing at 1300 ^{o}C and 1400 ^{o}C. It was again found that the grain growth rate was retarded by the field.

SEM micrographs showed that the grains were tetrakaidecahedral in shape and essentially isotropic both with electric field and without. The grain size distribution was consistent with the Bitti-Di Nunzio model for both fully sintered and isothermally annealed

conditions, which gives that the entire size distribution shifted to a smaller grain size. The retardation of grain growth rate was attributed to a reduction in grain boundary energy by the interaction of the applied electric field with the space charge at the grain boundary.

Physical models are proposed for the magnitudes of the GB energy components, namely electrostatic (space charge) γ_b^e, crystallographic mismatch (γ_b^Σ) and the ionic size misfit (γ_b^s) components. It was determined that the former two components combined comprised 40% of the total grain boundary energy in 3YSZ and the electrostatic component 60%. The reduction in γ_b^e by electric field is considered to result from the bias exerted by the applied field on the space charge potential that occurs with the segregation of the yttrium ions at the grain boundaries, and is proposed to be the major factor responsible for the retardation of grain growth in 3YSZ by an electric field.

The electrical conductivity of 3 Y-TZP was investigated during the sintering and annealing processes. It was found that the bulk resistivity ρ_Ω increased with applied field E to ~ 20-25 V/cm and then becomes relatively independent of E with further increase to ~ 65-70 V/cm. The bulk resistivity with ac field ρ_Ω(AC) was greater than that with dc ρ_Ω(DC) at all but the highest sintering temperatures. Employing with brick layer model, the grain boundary resistivity ρ_b was 131 Ω-cm and 114 Ω-cm at 1300 ^{o}C and 1400 ^{o}C, respectively, and in turn gave the ratio of ρ_b/ρ_g(resistivity of the grain interior) =257 and 124, which are in good accord with the results obtained by impedance spectroscopy (IS) and 4-probe method. The value of ρ_b obtained was 173Ω-cm and 128 Ω-cm at 1300 ^{o}C and 1400 ^{o}C respectively, taking that the observed increase in bulk resistivty ρ_Ω with applied field strength E results from the corresponding decrease in grain size.

Effect of Electric Field on the Processing and Properties of Yttria-stabilized Zirconia (YSZ)

by
Jun Wang

A dissertation submitted to the Graduate Faculty of
North Carolina State University
in partial fulfillment of the
requirements for the degree of
Doctor of Philosophy

Materials Science and Engineering

Raleigh, North Carolina

2014

APPROVED BY:

_____	_____
Prof. Hans Conrad Committee Chair	Prof. Jay Narayan
_____	_____
Prof. Yuntian Zhu	Prof. Carl C. Koch

_____
Prof. Fuh-Gwo Yuan

DEDICATION

This work is dedicated to my loving family.

My forever love, Aihua Du, and my cute girl, Carrisa, who means the world to me.

My parents, Quanwen and Hongmei, who have been always supporting to me.

My elder sisters, Ling, Xiuhua and Xinhua, whom I am proud of.

BIOGRAPHY

Jun Wang was born in Henan, China on February 10, 1981 to Mr. Quanwen Wang and Ms. Hongmei Zhang. After finishing high school in Xinxian senior high school, he got admission to Henan University of Science and Technology (Luoyang) majoring in Materials Science and Engineering. Jun Wang attended graduate studies and got admitted to the South China University of Technology in 2005. He came to US and joined in Prof. Zhu's group at North Carolina State University as a visiting scholar in 2009. In 2011, Jun Wang joined Prof. Conrad's group to continue his graduate studies at NCSU, he got the Master of Materials Science and Engineering in 2012 and took his PhD in Materials Science and Engineering in March 2014.

ACKNOWLEDGMENTS

I would like to sincerely thank all the members of my research group for their helpful discussion all over my PhD. Special appreciation is dedicated to Dr. Conrad for his great supervision, guidance, and support throughout this work. I also would like to thank Dr. Narayan, Dr. Zhu, Dr. Koch and Dr. Yuan for being members of my PhD committee and for thoughtful comments on editing this dissertation.

Many thanks to Dr. Di Yang and Dr. Chunmin Jin for helping me in experimental work, sharing their experience and useful discussion related to this work. I am also grateful to other group members (Mr. Song Pang, Mr. Daniel Minsk, Mr. John Obare, Mr. William D. Griffin, Mr. Kenneth Plunkett)for their help and contribution to this work.

I would also like to thank Edna Deas and Mary Ann Lofgren who gave me so much help during the course of my Ph.D. program.

Financial support from Nation Science Foundation under contract DMR-1002751, Forging Industry Educational and Research Foundation (FIERF) are gratefully acknowledged. Especially, Teaching Assistantships from the Materials Science and Engineering Department at NCSU are also sincerely appreciated.

Finally, I would like to thank my wife, Aihua, for her great encouragement, patience and understanding all along the way. I would also like to thank my cute girl, Carrisa, whose recent birth gives me strong incentive.

TABLE OF CONTENTS

LIST OF TABLES

CHAPTER THREE

CHAPTER FOUR

CHAPTER FIVE

LIST OF FIGURES

CHAPTER TWO

CHAPTER THREE

CHAPTER FOUR

CHAPTER FIVE

APPENDIX

CHAPTER ONE

1.0 INTRODUCTION

Ceramic materials, especially advanced ceramics, have attracted extensive attention in the recent decades, due to their broad range of applications. As a result, the developmentof bulk ceramics with excellent properties, i.e. mechanical properties and electrical properties, is desired. Since the properties of ceramics are mainly processing and structure dependent, numerous researches have been devoted to understanding the processing-structure-property relationships of these materials.

Grain size dependence of the mechanical properties have been investigated in ceramic materials processed by different experimental techniues, i. e. conventional (e.g. [1.1,1.2]) and field assisted methods (e. g. [1.3-5]). The application of electric field (DC and AC) has been reported to retard grain growth and in turn influence the processing and properties of these materials, namely enhancement of sintering rate (densification rate) and reduction of the plastic deformation flow stress. The mechanism(s) in terms of the grain growth retardation by the applied electric field however still remain questionable. Although there has been some progress in exploring and explaining the mechanism at relatively high electric fieldsin terms of grain growth retardation by DC field(e.g."Joule heating"[1.6] and selected "melting" of grain boundary [1.7]), work still needs to be done with respected to the mechansims pertaining on the grain growth retardation by an application of a small or modest electric field.

The bulk electrical properties of ceramics consists of two components: the grain boundary (GB) conductivity and conductivity of the grain interior, the GB conductivity being

orders of magnitude smaller than that of the grain interior. The birck layer model gives for the bulk resistivity

$$\rho_{bulk} = \rho_g + \rho_b = \rho_g + \rho_b^* \delta_b / d \qquad (1.1)$$

where ρ_g is the resistivity of the grain interior and ρ_b the contribution of the grain boundaries to the bulk resistivity. ρ_b^* is the so-called "specific grain boundary resistivity", $\delta_b$the width of the GB including the space charge zone and the core and d the grain size. Experimental results using impedance spectroscopy (IS) and 4-probe methods and employing the brick layer model give that the GB conductivity in 3 Y-TZP is one-to-three magnitude lower than that of grain interior. However, these two methods are limited in measuring the GB resistivity of oxide ceramics to relatively low temperatures ($<$ 1000 ^{o}C). Measurements of the conductivity at higher temperatures still remains unexplored.

3 mol.% yttria-stabilized zirconia polycrystals (3 Y-TZP) was selected as the starting materials since it had been discovered that an electric field retarded grain growth in this materials [1.8] and moreover enhanced plastic deformation rate [1.5]. In this study, our research focused on two phenonema: the effect of electric field (DC and AC) on: (a) grain growth and (b) electric conductivity.

The sintering rate (densification rate) and corresponding grain growth of 3Y-TZP were determined in the temperature range from 800 ^{o}C to 1500 ^{o}C employing without field and initial field strengths in the range of 1-50 V/cm. Isothermal annealing was performed at the selected temperatures of 1300 ^{o}C and 1400 ^{o}C with an initial applied field strength of 14 V/cm. The effect of electric field on grain growth during these two processes was

determined. Also investigated was the related stereologicalparameters of grain shape and grain size distribution.The governing mechanism(s) are discussed.

In this study, the electric conductivity of 3 Y-TZP was determined employing brick layer model. The bulk conductivity, the conductivity of grain boundary and that of the grain interior were determined.

1.1 References

[1.1] R. M. Cannon, W. H. Rhodes, A. H. Heuer,: J. Am. Ceram. Soc. 63(1980)46-53.

[1.2] F. Wakai, S. J. Sakaguchi, Y. Matsuno,: Adv. Ceram. Mater., 1(1986)259-263.

[1.3] K. S. Tun, M. Gupta,: Comp. Sci. and Tech., 67(2007)2657-2664.

[1.4] Z. Shen, H. Peng, M. Nygren, : Adv. Mater., 15(2003)1006-1009.

[1.5] H. Conrad, D. Yang,: Phil. Mag., 90(2010) 1141-1157.

[1.6] R. Raj,: J. Euro. Ceram. Soc., 32(2012)2293-2301.

[1.7] J. Narayan,: Scripta Mater. , 68(2013)785-788.

[1.8] Di Yang, H. Conrad, Scripta Mater., 36(1997)1431-1435.

CHAPTER TWO

2.0 LITERATURE REVIEW

2.1 Synthesis, properties and application of yttria-stabilized zirconia(YSZ)

2.1.1 Structural property of YSZ ceramics

Zirconium dioxide is one of the most studied ceramics due to its broad application. The crystal structure of ZrO_2 is polymorphous with temperature as monoclinic (1173 ^oC)↔ tetragonal (2370 ^oC)↔ cubic(2690 ^oC)↔melt. It is difficult to get pure zirconia stabilized since there exists a large volume difference between these polymorphs, for instance, there is an approximately 9% volume difference between the monoclinic and tetragonal phases.

Stabilization of zirconia is usually obtained through the addition of a stabilizer such as yttria, calcia, magnesia, ceria and alumina. Among these stabilizers, yttria is one of the most generally employed and the combined compound is named yttira-stabilized zirconia (YSZ). In YSZ, the doped Y^{3+} ions (ionic radius of 1.04 Å) goes into the crystal lattice and replaces some of the Zr^{4+} ions (0.86 Å), see Fig.2.1[2.1]. A fully and/or partial YSZ is obtained by controlling the dopant concentration.

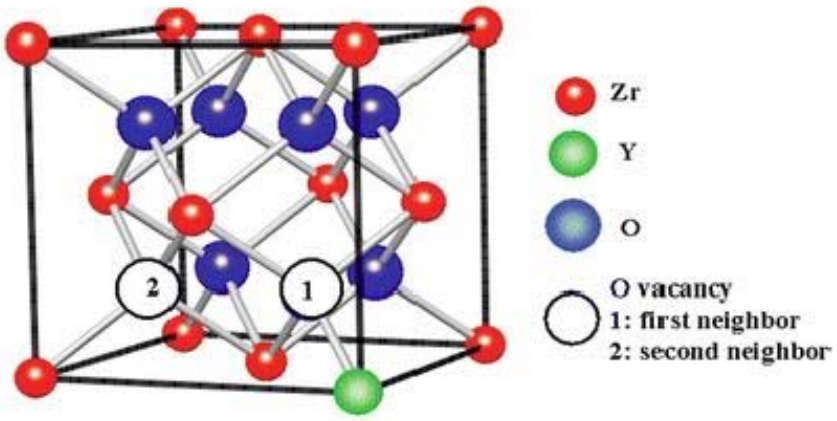

Fig.2.1Structure of YSZ. From Ref. [2.1].

The phase diagram of Y_2O_3-ZrO_2 system, Fig. 2.2[2.2], shows that YSZ is highly stoichiometric with respect to yttria and zirconia. The polymorphous phases of YSZ are dependent on the temperature and the compositions of its compounds. According to the phase diagram, from room temperature to near 3000 ^oC, 3 mole percent YSZ undertakes the following phase evolutions :

M (monoclinic) → M + T (tetragonal) → T → T + F (cubic) → F → L(liquid)

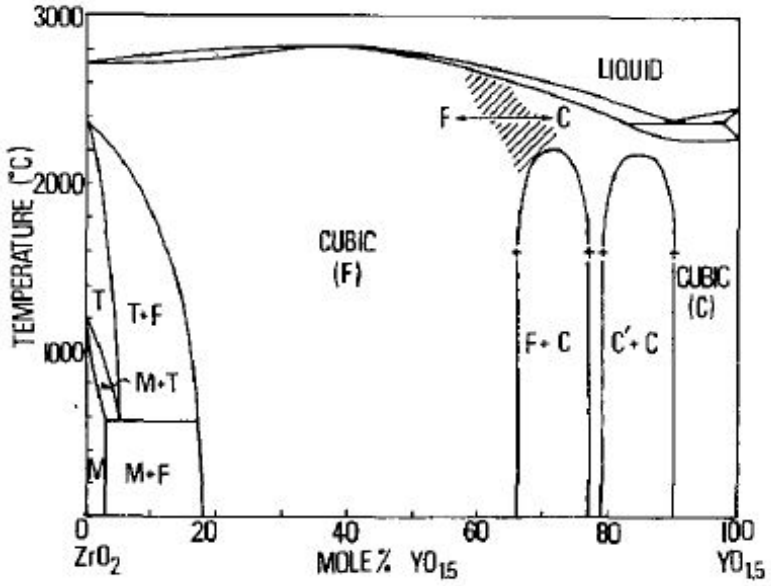

Fig.2.2 Phase diagram of Y_2O_3-ZrO_2. From Ref. [2.2].

With the addition of 3 mol. % yttria and appropriate cooling rate, zirconia can remain tetragonal even at room temperature. The lattice parameters of tetragonal YSZ are a function of the dopants, the a and c values change with the variable concentration of doped Y^{3+}, see Fig. 2.3 [2.3].

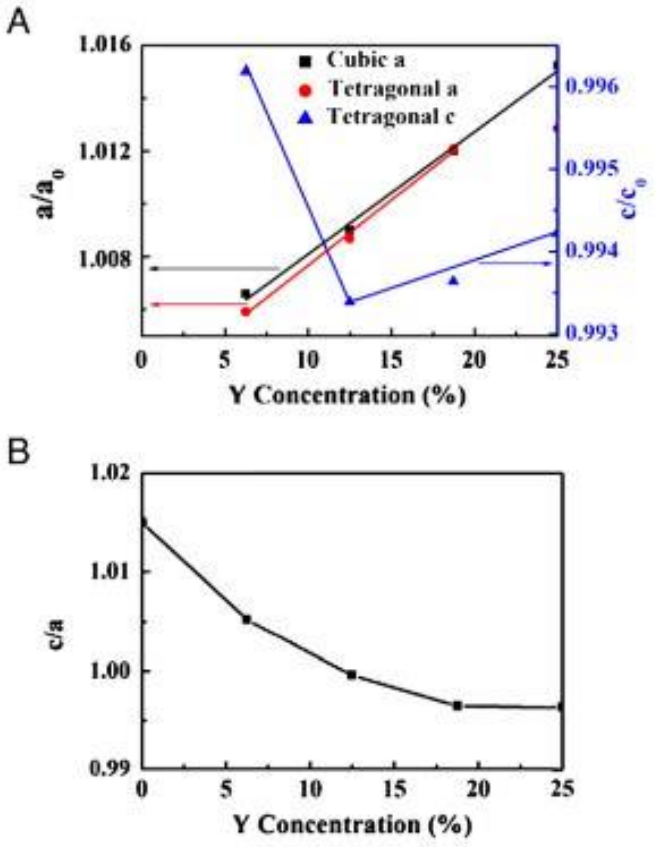

Fig.2.3 The lattice constants of cubic and tetragonal YSZ vs Y concentration: (A) pure lattice constant, a_0 and c_0 and (B) the c/a vs Y concentration in tetragonal YSZ. From Ref.[2.3].

Prevailing defects in YSZ are oxygen vacancies, which are introduced to maintain the charge neutrality following the reaction: $Y_2O_3 + 2\,Zr_{Zr}^{\times} + O_O^{\times} \xrightarrow{ZrO_2} 2Y'_{Zr} + V_O^{\cdot\cdot} + 2ZrO_2$ [2.4]. The vacancies have preferred aligned directions with respect to the dopant concentration. For example, as reported by H. P. Ding et al. [2.3] by using first principles, the vacancy pair in tetragonal YSZ has an alignment in the directions of $<1, \frac{1}{2}, 0>$ at low Y concentration and $<1, \frac{1}{2}, \frac{1}{2}>$ at high Y concentration, see Fig.2.4.

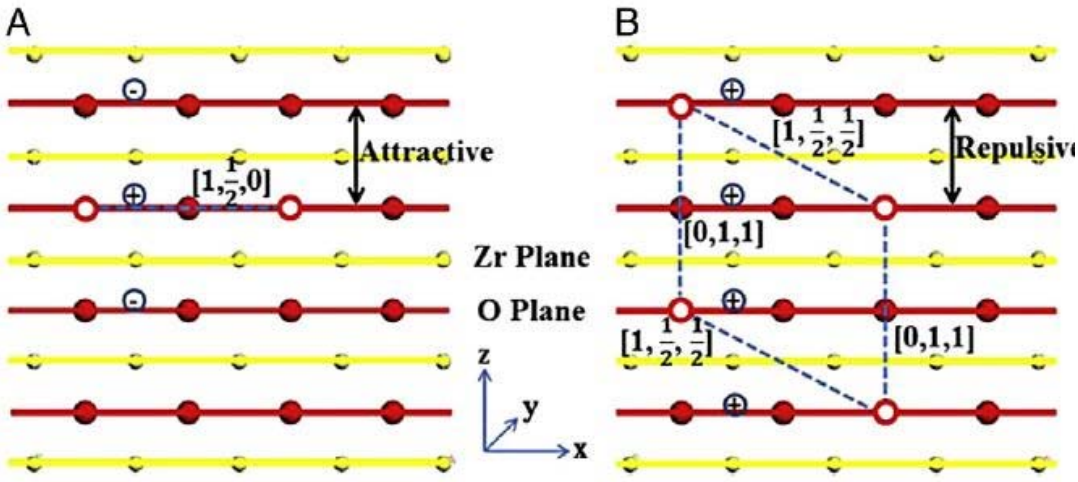

Fig.2.4 Vacancy alignment in tetragonal YSZ: (A) low Y concentration and (B) high Y concentration, Zr/Y atoms are small balls, oxygen atoms are large balls and oxygen vacancies are open circles. From Ref.[2.3].

2.1.2 Synthesis and processing of YSZ ceramics

2.1.2.1 Synthesis of YSZ powders

Numerous routes are used to synthesis YSZ powders and these routes are classified as conventional methods and wet chemical methods [2.5]. Compared to conventional methods, the powders are better and cheaper when synthesized using chemical counterparts (such as hydrothermal, solvothermal, aqueous, hydrolysis, co-precipitation and sol-gel [2.6]). The principle of the wet chemical methods is that the YSZ powders are produced via the chemical reaction between the zirconium solution and the yttrium solution, and followed by the transparent solutions heating process. Compositions of the YSZ powders are controlled by the mole fraction of the added solutions.

Commercial 3 mol.% Y-TZP powders used in the present study was purchased from Tosoh Inc., Japan. This highly pure, nano-particles were made by the chemical coprecipita-

ting process with the reaction of aqueous $ZrOCl_2$ solution and YCl_3 solution.

2.1.2.2 Specimen fabrication routes from ceramic powders

Various methods have been developed to process powders (ceramic particles or metallic particles) to fabricate products with complex structures and desirable properties. The methods generally include pressing (cold pressing, hot pressing, warm compaction and warm flow compaction), centrifugal casting, slip casting, iso-static moulding, and high-velocity compaction. Of these, cold pressing, used in the present research, is simplest and most convenient. The principle of cold pressing is that a "green" specimen is produced by applying optimized compressive force to the punch at the room temperature to fill the powders in the die. The green products with high density and strength can be achieved via appropriate powder mixing and compressive parameters optimization. A schematic of cold pressing is shown in Fig.2.5.

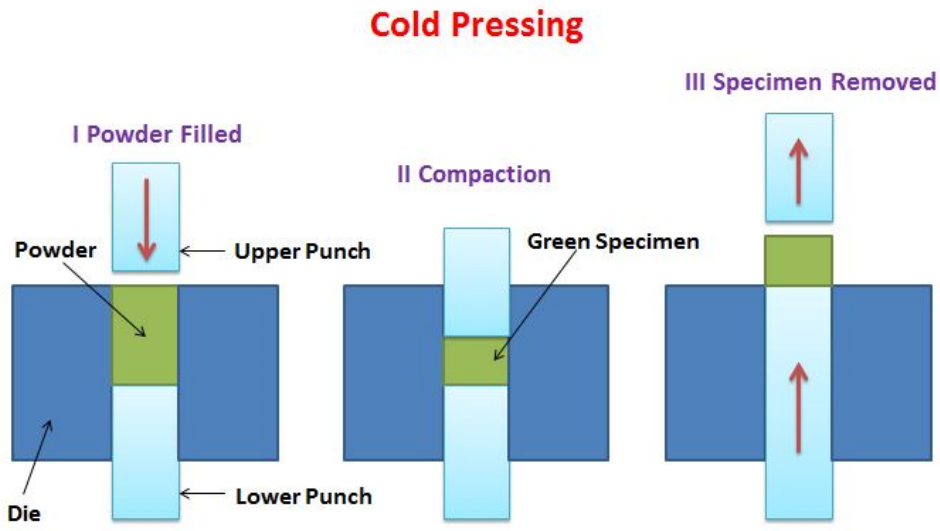

Fig.2.5 Schematic of cold pressing used in the present study.

2.1.2.3 Sintering of ceramic powders

Sintering at elevated temperatures is used to consolidate the green specimen into a solid body with desired structure and properties at an elevated temperature through mass (atom or vacancy) transport. Generally, sintering of the powders occurs in three stages [2.7]: (i) initial stage: rapid interparticles neck growth by diffusion, (ii) intermediate stage: the resulting pores reach equilibrium shape and are connected, and (iii) final stage: pores reach an equilibrium shape and become isolated. Sintering usually occurs by mass transport from the regions with high chemical potential to the regions with lower chemical potential, accompanied by bonding and neck growths between particles.

The driving force of sintering is the surface curvature (surface tension) reduced by the roughness and shrinkage of the pores or voids, which gives a reduction in the associated surface energy due to the surface curvature flatting promoted by the mass transport and the densification of the compacts. This driving force is controlled by geometry and size of the pores or voids.

Kinetics of sintering involves both the direction and velocity of the mass transport. Due to the bulk pressure, vacancy concentration and vapor pressure difference, the mass is diffused via different paths, such as surface diffusion, lattice diffusion, GB diffusion and bulk diffusion [2.7]. The sources of mass transportation are the grain boundary and the surface of grain or bulk; the sink is the pores/voids. In the initial sintering stage, the atoms from the surface, the grain boundary, and the bulk move toward the pores/voids via different paths. Employing a model of three particles with spherical geometry, the mass transport

mechanisms are illustrated in Fig.2.6 [2.8]. The shrinkage during sintering is due to the atom movements by these mechanisms.

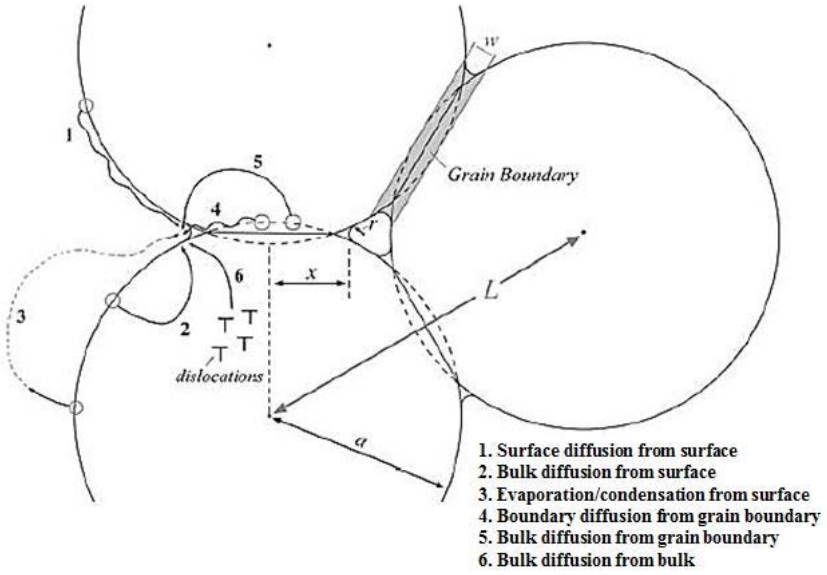

Fig.2.6 Illustation of the sintering mechanisms in a three particles array. From Ref.[2.8].

2.1.2.4 Field assisted sintering

Sintering of powders is influenced by many factors. Besides temperature, time, heating rate, initial particle size and impurities, the sintering behavior of the ceramics is also influenced by the application of the external fields. Field assisted sintering such as microwaves [2.9, 2.10], spark plasma sintering (SPS) [2.11, 2.12] and simple two-electrodes [2.13-15, 2.16-22] have been reported to be efficient ways to produce bulk oxide ceramics with excellent properties. The principle is that the application of the fields had a strong influence on mass transport and related grain boundary mobility [2.8].

2.2 Role of grain boundaries during the processing and properties of ceramics

2.2.1 Role of grain boundary on sintering and grain growth

The grain boundary is an important parameter in the sintering of polycrystalline powders. The tension of the pore and the GB interface provide the driving force, they act either as sinks or as diffusion paths for diffusion [2.23]. GB diffusion and lattice diffusion are governing mechanisms which promote the shrinkage and densification which occur during sintering.

Regarding shrinkage and densification, corresponding to GB diffusion [2.24], Chen and Wang proposed two-stage sintering dense nanocyrtalline ceramics without final-stage grain growth, the densification of matter was derived as following equation,

$$\frac{1}{\rho}\frac{d\rho}{dt} = F(\rho)\left(\frac{\gamma_{sv}\Omega}{dkT}\right)\left(\frac{\delta_{gb}D_{gb}}{d^3}\right) \qquad (2.1)$$

where ρ is relative density, γ_{sv} is surface energy, Ω is the volume of an atom or vacancy, d is grain size, δ_{gb} is GB thickness, and D_{gb} is GB diffusion coefficient. F(ρ) is density dependent and is $\frac{4}{3}\frac{1}{\rho(1-\rho)^{1/2}}$ given by M. N. Rahaman [2.25]. In the above equation, the term of $\gamma_{sv}\Omega/dkT$ is viewed as the normalized driving force, $\delta_{gb}D_{gb}/d^3$ is the standard kinetic factor involving GB process during sintering [2.24].

Grain growth is the process by which the mean grain size of an aggregated of crystals increases [2.26], the driving force is the decrease of the surface energy accompanied by the reduction in the GB area [2.27-29]. Grain growth of ceramics is usually discussed from thermodynamic and kinetic standpoints. Thermodynamically, decrease in the GB energy

control the grain growth; kinetically, the associated GB migration toward it's center of curvature is controlled by the chemical or concentration gradient between the GB and the grain interior [2.30].

Assuming the probability of the associated atom/vacancy jumping across the boundary (an atom moves from the GB to grain interior or exterior surface, or an atom moves from the grain exterior to the GB) is equal, Burke and Turnbull [2.31], Conrad [2.32]and Narayan [2.33] subsequently derived the grain growth rate formula in terms of the diffusion energy barrier and gain of free energy, see schematic of Fig. 2.7 [2.33],

$$\dot{d} = \upsilon\lambda exp(-\Delta G^*/kT)[1 - exp\,(-\Delta G/kT)] \qquad (2.2)$$

where υ is atom/vacancy jump frequency, λ is jump distance, k is Boltzmann constant, T is temperature, ΔG^* is activation energy barrier for atom/vacancy diffusion and ΔG is the resulting gain in free energy. The gain in free energy ΔG was affected by the solute, space charge and the elastic energy at the GB [2.33].

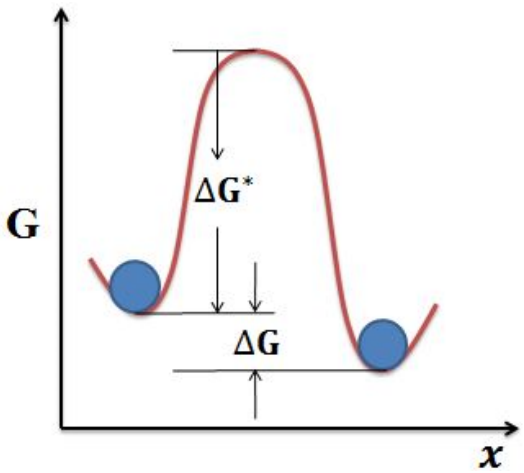

Fig.2.7 Schematic of energy change for atom jump. From Ref.[2.33].

A parabolic grain growth model established by Burke and Turnbull [2.31] presented that the grain growth was driven by the atom transport across the GB due to surface curvature and chemical potential gradient. The grain growth model was derived into power law type as,

$$d^n - {d_0}^n = K(t - t_0) \qquad (2.3)$$

where d_0 is the grain size at time t_0, d is the grain size at t, n is the grain growth exponent and equal 2 or 3 depend on GB diffusion or lattice diffusion mechanisms, K is a temperature dependent growth factor written as,

$$K=2\alpha\gamma_{gb}M_b \qquad (2.4)$$

where α is geometrical constant depending on GB shape, γ_{gb} is the specific GB energy, M_b is the GB mobility. Taking the grain growth velocity as instantaneous grain growth rate, the mobility M_b is defined by [2.30],

$$M_b = \frac{D}{kT}\frac{\Omega}{\delta_{gb}} \qquad (2.5)$$

where D is the governing atom/vacancy diffusion coefficient, k is Boltzmann constant , T is temperature, Ω is atomic volume and δ_{gb} is GB thickness. Substitute Eqs. 2.4 and 2.5 into Eq. (2.3), one obtains,

$$d^n - {d_0}^n = 2(\frac{\alpha D\Omega}{kT})(\frac{\gamma_{gb}}{\delta_{gb}})(t - t_0) \qquad (2.6)$$

Writing Eq.2.5 into an Arrhenius equation, gives

$$d^n - {d_0}^n = K_0 \exp(-Q/RT)\,(t - t_0) \qquad (2.7)$$

where K_0 is a constant, t_0 is the initial time, t is time, R is gas constant, Q is activation energy for grain growth.

The concept that solute segregation at the GB decreases the GB energy is well-established [2.8]. Since the mobility of the solute is frequently slower than that of the solute-free GB, the solute segregation at the grain boundary provides a drag force on GB motion. By considering solute drag, the derived grain growth exponent has values greater than 1in a so-called transition regime [2.34, 2.35]. The grain growth velocity changes due to the interaction between the GB and the segregated solutes, with respect to their diffusivities and concentration [2.36, 2.37].

Considering the intrinsic GB migration (no solute drag effect) and solute drag migration (see Fig.2.8), the driving force for grain growth of polycrystalline ceramics presented by Powers and Glaeser [2.38] gave,

$$F = \frac{V_b}{M_0} + \frac{\alpha C_\infty V_b}{(1+\beta^2 V_b^2)} \qquad (2.8)$$

where V_b is the GB migration velocity, α is the solute drag force per unit velocity and per unit solute concentration depending on temperature, C_∞ the bulk solute concentration, β^{-1} the approximately drift velocity near the GB area. $M_0 = \frac{fD_b\Omega}{\delta_{gb}kT}$ is the boundary mobility without considering solute addition, D_b the corresponding self-diffusion coefficient, Ω atomic volume, δ_{gb} the boundary width, kT the usual meaning.

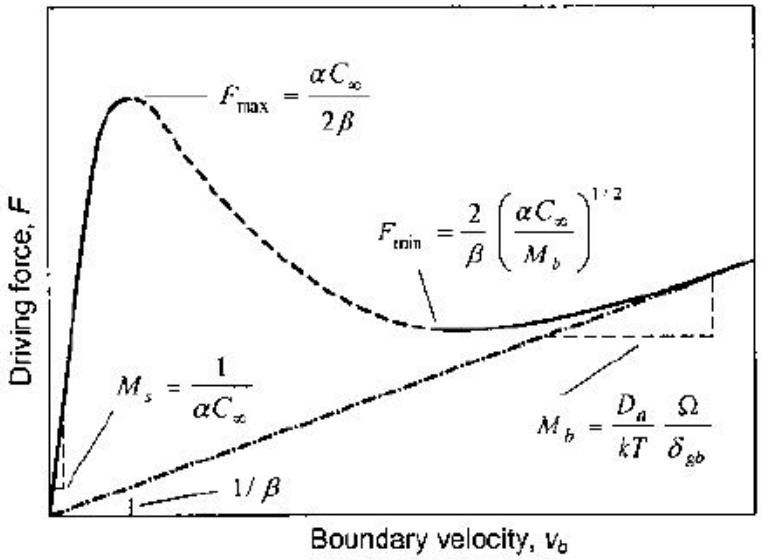

Fig.2.8 Driving force vs velocity of the grain boundary migration controlled by solute drag and in the intrinsic regime. From Ref. [2.38].

Since the GB energy is reduced by the drag effect due to the solute segregation at the GB, grain growth can be retarded or inhibited [2.39-42]. For example in a Lead-Tin alloy [2.43], the average grain diameter during annealing was reduced at 210 ^{o}C with the presence of tin, the magnitude increasing with tin concentration increased; also, grain growth in Al_2O_3 was inhibited by doping with MgO[2.44].

2.2.2 Role of grain boundary on superplastic deformation

Creep or superplastic, grain size dependent, plastic deformation takes place when the nanocrystalline metals or ceramics are subjected to a tensile stress at elevated temperature [2.45]. For the steady-state condition, the strain rate-controlling creep and super-plasticity is usually given as

$$\dot{\epsilon} = \frac{ADGb}{kT}\left(\frac{b}{d}\right)^{p}\left(\frac{\sigma}{G}\right)^{n} \qquad (2.9)$$

where A is a dimensional constant, G is the shear modulus, b is the Burgers vector, k is Boltzmann constant, T is the absolute temperature, d is the grain size, σ is the applied stress, D is the appropriate diffusion coefficient ($D= D_0 \exp(-Q/RT)$, where D_0 is the pre-exponent factor, Q the activation energy and R is the gas constant), n is the stress exponent, and p is the grain size exponent.The magnitudes of the exponents n and p depend on the governing mechanisms [2.45, 2.46]. As reported by London [2.45] and Rachinger [2.46], at high enough temperature, the values of p and n for the creep of Al were 1.0 and 3.0 respectively due to lattice self-diffusion. The values were both 2 when the superplastic deformation occurred and GB sliding prevailed. However, both governing mechanisms were associated with the same activation energy (Q). The superplasticity behavior of YSZ at a ultra-fine grain size resembled that of metals and metal alloys [2.46, 2.47]. Investigations by Manuel et al. [2.48] showed that the mechanical behavior of fine-grained YSZ with solute content less than 10% exhibited transient characteristics at elevated temperatures in the range of 1250 ^{o}C to 1450 ^{o}C, the parameters of n, p and Q being 2, 2 and 460 kJ/mol, respectively.

GB sliding mechanism plays an important role in the plastic deformation behavior of ceramics [2.47]. In YSZ, the GB started to slide at an applied stress higher than the threshold stress due to yttrium segregating at the GBs, or at the dislocations. The GB sliding was usually accompanied by mass and dislocation diffusion [2.48, 2.49]. Investigations by Chokshi et al. [2.49] gave for the GB and lattice diffusion in YSZ: $D_l^{zr} = 5 \times 10^{-4} \exp((-515\,\text{kJ/mol})/\text{RT}\ \text{m}^2\ \text{s}^{-1}$, $D_{gb}^{zr} = 10^{-3} \exp((-370\,\text{kJ/mol})/\text{RT}\ \text{m}^2\ \text{s}^{-1}$,

$D_I^Y = 4 \times 10^{-3} \exp((-500\,\mathrm{kJ/mol})/\mathrm{RT}\ \mathrm{m}^2\ \mathrm{s}^{-1}$, $D_{gb}^Y = 1 \times 10^{-2} \exp(-390\,\mathrm{kJ/mol}/\mathrm{RT}\ \mathrm{m}^2\ \mathrm{s}^{-1}$. The activation energy for the oxygen ion (O^{2-}) diffusion was 127 kJ/mol.

2.3 Grain boundaryconductivity of polycrystalline ceramics

The bulk electrical conductivity of polycrystalline ceramics is attributed to both GB conductivity and the conductivity of grain interior. GB conductivity has been reported to be several orders of magnitude lower than that of grain interior [2.50-53]. The GB conductivity is influenced by GB structure [2.54], impurity phase [2.54], grain size [2.50, 2.55], dopant concentration [2.50, 2.56] and temperature [2.54, 2.57].

2.3.1 Grain boundary structure

Grain boundaries, a planar defect [2.58-60], have a significant influence on the properties of the polycrystalline ceramics. From a structural viewpoint, the GB of ceramics is crystallographic mismatch zone (namely, grain boundary core). From an electronic viewpoint, the GB core is compensated by two adjacent symmetrical space charge layers (see Fig.2.9), which carry an opposite charge sign compared to that of the core.

Dopants segregation at the GB not only introduces an elastic strain (size misfit between the solute and host ions), but also an electrostatic reaction, which occurs due to the Coulomb interaction between the doped ions and the charge potential at the GB core. Regarding the space charge, the charge sign of the GB core is compensated by the charge valence of the doped ions. For example, in YSZ, the concentration oxygen vacancies at the grain boundary established a positive potential in the GB core of ZrO_2 [2.61]. Oxygen vacancy depletion zone with Y^{3+} ions segregation, then presented a negative charge potential

in the space charge layers.

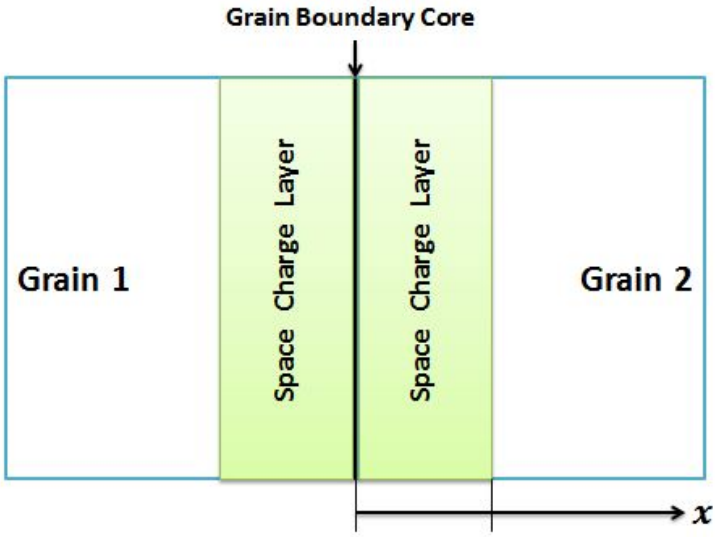

Fig.2.9 Schematic representation of a “electrical grain boundary”.

2.3.2 Effect of impurity phase on grain boundary conductivity

It is well-reported that an impurity phase at the GBs significantly affects the GB electrical property in ceramics [2.62-64], since blocking effect exhibits [2.54]. Based on its nature and location, the GB impurity phase has been classified into three categories: (a) continuous impurity phase surrounding the entire GBs [2.65], (b) partially wetting with direct grain-to-grain contact and (c) clean GBs [2.66].

In zirconia, SiO_2 is one of major impurities. The siliceous phase significantly affects the GB electrical property [2.54]; and the magnitude of the effect is related to the impurity concentration. Observations by TEM on 8 mol. % Y_2O_3 doped ZrO_2 showed that the siliceous phase was situated at the GBs triple junction [2.62, 2.67], see Fig.2.10. Hence, the ions transport across the GBs occurs through two paths, one is through the grain-to-grain

direct contact region, the other is the siliceous glass phase region.

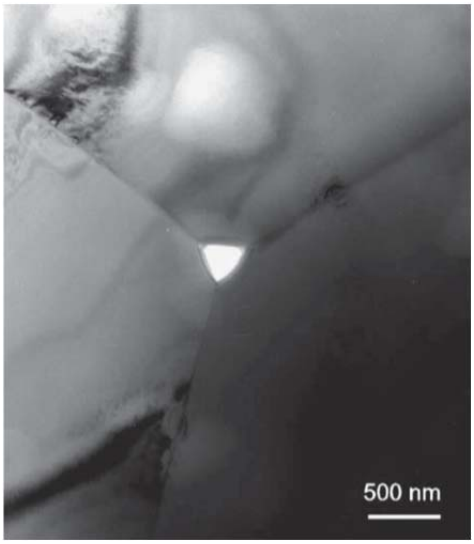

Fig. 2.10 Transmission Electron Microscopy (TEM) micrograph of impurity phase situated at a triple grain junction in 8 mol% Y_2O_3-ZrO_2. From Ref. [2.54].

2.3.3 Effect of grain size on the grain boundary conductivity

The grain size is important parameter in the mechanical [2.68, 2.69], electrical [2.70, 2.71] and magnetic [2.72] properties of ceramics. Regarding the electrical behavior, Martirena and Burffoot [2.73] reported that, due to the "suppression" in the spontaneous polarization, the maximum dielectric constant of ferroelectric ceramics such as barium titanate decreased with decrease in grain size. This phenomenon also occurred in the Ba-Sr titanate system [2.74].

YSZ is an important electrical conductor at the elevated temperature due to the high ionic conductivity [2.75]. The ionic conductivity of YSZ is grain size dependent or independent, depending on the grain size. With grain size in the range of 90-200 nm, ionic

conductivity of polycrystalline YSZ was independent of the average grain size [2.76]. However, with the grain size in the range of 1-8 μm, X. J .Chen reported [2.77] that the intergranular ionic conductivity of 8 mol% YSZ was sensitive to the grain size, but the intragranular term was not.

2.3.4 Effect of space charge and solute segregation on grain boundary conductivity

In pure ionic crystals, Frenkel [2.78], Eshelby et al. [2.79] and Kliewer and Koehler [2.80] proposed that the surface, GBs and dislocation cores had a compensating charge (namely space charge)with an opposite sign adjacent to the lattice discontinuity region, and further that the net charge was given by the effective charge of the aliovalent impurities. Suppose that dopants with a positive effective charge are presented in the bulk, then in equilibrium condition, the surface possess a negative countercharge to maintain the bulk essentially neutral. The establishment of a space charge at the GBs depended on the formation energy of cation and anion vacancies in ionic ceramics [2.80-84]; see Fig.2.11. The accumulation or depletion of the charge carriers in the space charge zone significantly influences the electric property of ionic ceramics [2.85, 2.86].

Segregation of solutes at the GBs will affect the magnitude (and can even reverse the polarity) of the space charge electrostatic potential, depending on the effective valence of the solute compared to the host [2.87-89].

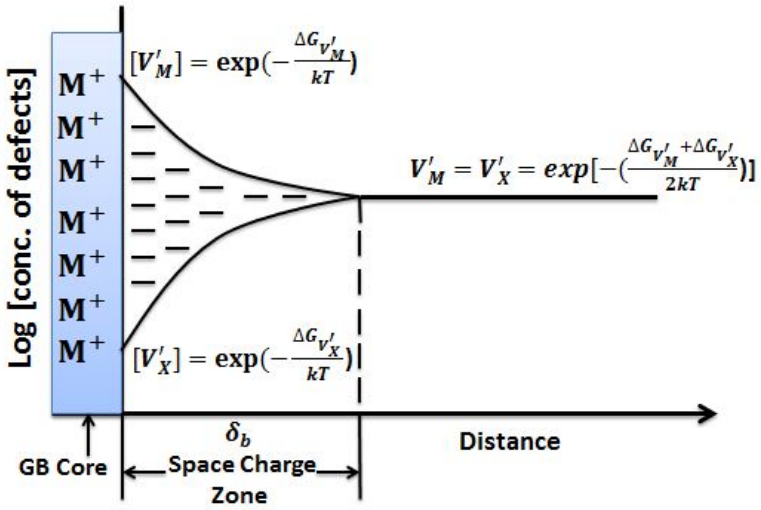

Fig. 2.11 Space charge at the grain boundary in an MX compound and the corresponding charge distribution when the Gibbs free energy for formation of anion vacancies $\Delta G_{V'_X}$ is greater than that ($\Delta G_{V'_M}$) for cation vacancies.

The degree of solute segregation at the grain boundary depends on the temperature and the magnitude of the space charge potential. Early considerations by Mc Lean [2.90] gave the following for the temperature dependence of the segregation,

$$\frac{C_b}{C} = \frac{\exp(-\Delta G_a/kT)}{1+C\exp(-\Delta G_a/kT)} \qquad (2.10)$$

where C_b is the solute concentration at the grain boundaries, C is the bulk concentration and ΔG_a is the Gibbs free energy of adsorption. Guo and Maier [2.53] proposed the following relation regarding the effect of the space charge potential on segregation

$$\frac{C_b(x)}{C} = \exp(\frac{-Ze\Delta\emptyset_i(x)}{kT}) \qquad (2.11)$$

where $C_b(x)$ is the solute concentration in the space charge zone, x is the distance from the GB core, Z is the valence of the solute and $\Delta\emptyset_i$ is the electrostatic potential at the GB.

Additional calculations of the degree of solute segregation to the grain boundary in ionic ceramics had been made by Yan et al. [2.87] and by Grönhagen and Argen [2.91].

2.3.5 Grain boundary conductivity measurement

The conductivity of oxide ceramics can be clarified into ionic, electronic and mix-conducting [2.86, 2.92-94]. An electronic component may result from the free electrons excited across the band gap or from impurity ionization [2.33]. The ionic component results from ion vacancy motion [2.95].

The electrical conductivity of ceramics has been measured employing the conventional 4-probe method (AC and DC) and impedance spectroscopy (IS) methods [2.51-53, 2.55, 2.56, 2.96-102]. Using the IS method, the conductivity of the GBs and of the grain interior can be determined by analyzing the impedance performances in the time and frequency domains [2.51]. The IS methods are however limited for low temperature measurements. At high temperature, the conductive behavior of the ceramics was more likely to be performed using conventional 4-point probe [2.51]; see Fig.2.12. Recently, Conrad and Wang [2.103] developed a voltage-drop model to calculate the GB and bulk conductivities. This model is based on the measured grain size and corresponding current flow and the applied voltage during sintering and annealing of ZrO_2 ceramics.

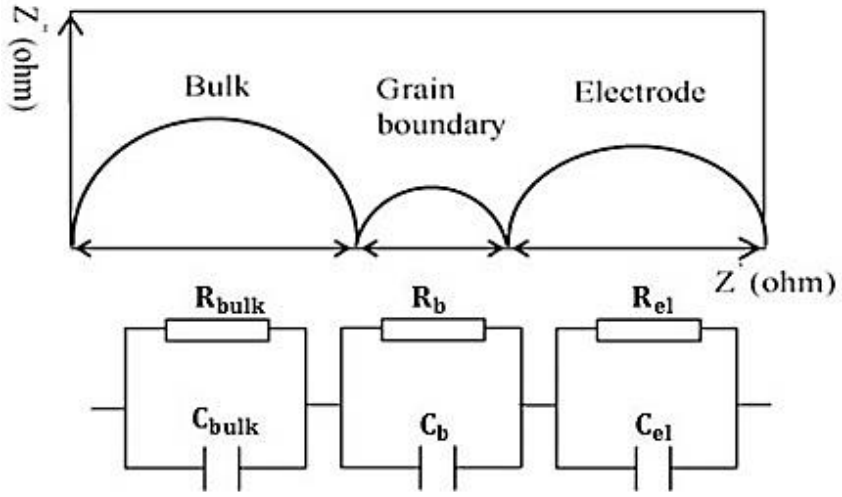

Fig.2.12 Schematic of a typical impedance spectroscopy plot for an ionic-conducting polycrystalline ceramic and the equivalent circuits.

The conductivity σ of ceramics is temperature dependent and in accord with the Nernst-Einstein equation,

$$\sigma = nq\mu = (A/T)\exp(\Delta H / kT) \qquad (2.12)$$

where n is the ion carrier concentration, q is the charge (in coulombs) and μ is the mobility of the charge carriers (in $cm^2s^{-1}V^{-1}$), kT has it's usual meaning and ΔH is the enthalpy pertaining to the charge carrier mobility.

The bulk ionic conductivity ($\sigma = \rho^{-1}$) of ceramics is considered to consist of the sum of the conductivity of the grain interior and that of the grain boundary. Expressed in terms of the resistivity one obtains

$$\rho = \rho_g + \rho_b = \rho_g + \rho_b^* \delta_b / d \qquad (2\text{-}13)$$

where ρ_g is resistivity corresponding to the grain interior, ρ_b is the contribution of the GB resistivity to the bulk, ρ_b^* is the specific GB reisistivity, δ_b is the GB width and d is the grain

size. The magnitude of the GB resistivity ρ_b^* ("specific GB resistivity") can be derived from ρ_b employing the so-called brick layer model [2.51, 2.57, 2.104-107], see Fig. 2.13.

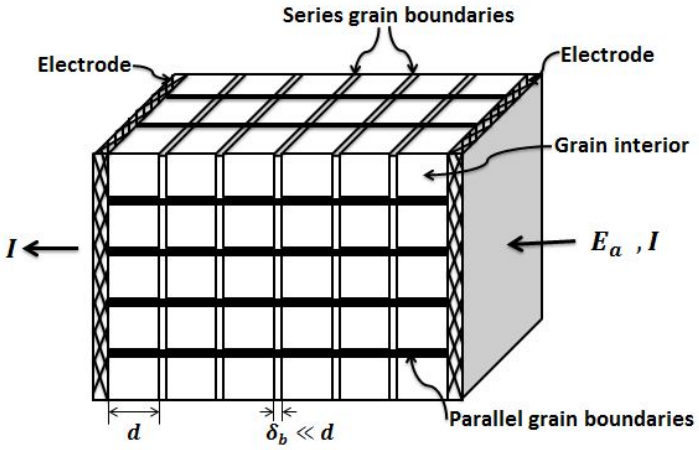

Fig. 2.13 Schematic of the brick layer model for calculating the GB conductivity.

Employing the brick layer model and assuming that the conductivity of the GBs both parallel and perpendicular to the applied electric field vector (as well as the grain interior) obey the Nernst-Einstein equation, N*ä*fe [2.57] developed the following equation for the temperature dependence of the bulk ionic conductivity,

$$\sigma T = \frac{(2\delta_b/d)A_b \exp(-\Delta H_b/kT) + A_g \exp(-\Delta H_g/kT)}{1 + (\delta_b/d)(A_g/A_b)\exp[(\Delta H_b - \Delta H_g)/kT]} \qquad (2.14)$$

where δ_b is the GB width including the core and space charge, d is the grain size, A_g and A_b are the respective grain interior and grain boundary pre-exponentials in the Arrhenius equation and ΔH_g and ΔH_b the respective activation enthalpies. For the case where $(\delta_b/d)(\sigma_g/\sigma_b) \ll 1$, Eq.2.14 gives the bulk resistivity at a constant temperature

$$\rho = \rho_g + (\rho_b \delta_b/d) \qquad (2.15)$$

i.e. the bulk resistivity increases with decrease in grain size. The form of Eq.2.13 has also been considered by other investigators [2.104-107]. Impedance spectroscopy measurements on Y-SZ in terms of Eq.2.13 [2.51, 2.52,2.108]. have reported $\rho_b/\rho_g \approx 10^1 - 10^3$(the ratio tending to increase with decrease in grain size), $\Delta H_b \approx 1.0{\sim}1.2\ eV$ and $\Delta H_g \approx 0.8{\sim}1.1\ eV$.

2.4 Effect of electric field on the processing and properties of ceramics

In the recent decade, many efforts had been devoted to utilizing an electric field (or current) in sintering [2.9, 2.10, 2.17-19, 2.109-111], isothermal annealing [2.112, 2.113] and plastic deformation [2.114, 2.115] of the ceramics. Compared to the conventional methods, in addition to achieve a higher density at shorter time, the products could be built a smaller grain size and in turn with better ductility when processed with electric field or current.

2.4.1 Effect of electric field on the sintering and isothermal annealing

Well-documented is that application of the electric field enhanced the sintering rate, sinter-ability and densification rate of the ceramics [2.17]. The enhanced sintering and densification rates were attributed to the observed finer grain size, which resulted from application of the field. Using 2.4 GHz microwave, Agrawal [2.9] reported that full density could be obtained in 3-8 mol. % YSZ at a temperature of 100 ^{o}C lower than the conventional procedure. A concurrent finer grain size was confirmed by Janney et al. [2.10]. Enhanced sintering and densification rates were also observed by Shen et al. [2.116] in alumina employing the “spark plasma sintering” (SPS) process. The Al2O3 was fully densified at 1150 ^{o}C (much lower than conventional) within much shorter time due to the enhanced GB diffusion and migration by the electric field which occurred along with the strong pulsed

current.

Extensive investigations of the effect of electric field on processing of ceramics has been conducted by Conrad and Co-workers [2.13-22] and by Raj and coworkers [2.117-120]. Di Yang and Conrad [2.17] reported that an enhancement of sintering rate and reduction of grain growth rate in 3Y-TZP were observed under the influence of a modest dc electric field. Using a 20 V/cm dc electric field at a constant heating rate, the densification rate of 3Y-TZP shifted to a significantly lower temperature regime. This was also observed in their subsequent work employing a relatively small dc field strength of 14 V/cm [2.18] or even smaller strength of 4 V/cm. A reduction in grain growth rate by a dc field was also confirmed by S. Ghosh [2.120]. Increased retardation of grain growth occurred with increase in field strength was up to 25 V/cm, but no further effect was observed when the field strength was further increased up to ~60 V/cm [2.19]. The enhancement of sintering rate and reduction of grain size were attributed to the reduction of GB energy due to the interaction of the applied electric field with the space charge. An even finer grain size was obtained employing AC electric field, compared to the same strength of dc field [2.121, 2.122]. A possible factor for the greater effect of 60 Hz AC field was attributed to the root mean square value in AC being root square 2 with that of dc field [2.8].

Besides the investigations reported by Conrad's group [2.13-22,2.121, 2.122] regarding the enhanced sintering rate and retarded grain growth which occurs employing a small or modest electric field, the phenomenon of rapid sintering ("flash sintering") in zirconia with application of a higher strength dc electric field has been reported by Raj et al.

[2.117, 2.123,124],. It was shown [2.117] that a fully dense YSZ product was achieved at 850 ^{o}C from an initial green density 0.5 in mere seconds with application of the high dc electric field strength of 120 V/cm. The sintering temperature could be further reduced to 750 ^{o}C as the field strength was increased up to 150 V/cm [2.124], see Fig. 2.14. The excited "flash sintering" with the application of high strength electric field was attributed to the localized Joule heating at the GB, which promoted GB diffusion, and retarded the grain growth by the field.

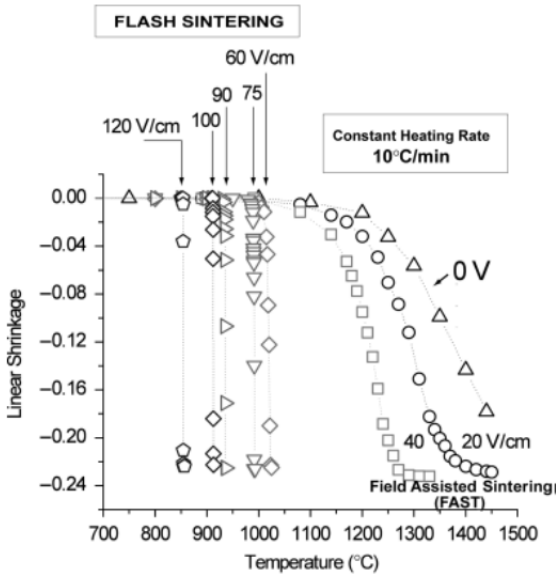

Fig.2.14 Effect of dc electrc field on linear shrinkage of 3 YSZ. From Ref. [2.117]

In addition to the studies cited above in which an electric field had a significant influence on the sintering behavior of the ceramics, the effect of electric field on annealing of ceramics was investigated by both Teong et al. [2.126] and Quach et al. [2.112]. Teong et al. reported that the GB mobility of bilayer alumina was significantly affected with the

application of 200 V/cm dc electric field. When annealed at 1600 ^{o}C for 2 hrs, the scale of the influence of the field was dependent on the field bias direction. Since the GBs of alumina have a positive charge potential [2.81], a positive bias had a stronger effect than a negative one. In the latter study, Quach et al. found that the grain growth was retarded in 8 mol.% YSZ under the SPS consolidation conditions. The grain size evolution showed a best-fit curve based on grain growth retardation in the temperature range from 1030 ^{o}C to 1180 ^{o}C.

Regarding the observations of the enhancement of sintering rate and densification rate, and the retardation of grain growth during sintering and annealing processes by employing an electric field or corresponding current, the explanations included the contributions of: (a)Joule heating [2.119], (b)electrostatic interaction with space charge [2.18,2.32],(c)the evolution of grain boundary characterizations [2.33, 2.127, 2.128].

2.4.2 Effect of electric field on superplastic deformation

Electric fields (simple two electrodes or current induced field) have been shown to reduce the time and temperature of sintering and retard the grain growth rate in the literature cited above. Mechanisms were inferred in terms of the influence of electric field on the grain boundary energetics and kinetics due to the electrostatic interaction between the fields and the GB character [2.129]. Furthermore, the application of electric field was proposed to accelerate the plastic deformation rate in ceramics [2.130-133] and in metals [2.134, 2.135]. The effect of electric field on superplastic deformation was attributed in different materials systems to many roles, including: (a) enhanced dislocation mobility[2.114, 2.115], (b) field

assisted dislocation generation [2.129], reduced rate-controlling activation energy [2.115] and (c) improved dislocation climb/cross-ship ability [2.135].

Since the charged dislocation in ceramics were pinned with charged point defects "cloud" to maintain neutrality [2.136], dislocation motion in the deformation of ceramics then requires unpinning the dislocation from the charge "cloud" interaction. Zuel et al. [2.137] reported that due to the electric field and charged dislocation interaction the velocity of edge dislocations in single crystal KCl increased significantly with the application of 13 kV/cm electric field at a given shear stress level. The observation of a reduction of the flow stress was presented by Conrad in single crystal [2.115]with dc internal electric field of the order of 10-100 kV/cm, and then confirmed by using a field strength of 1 kV/cm during compressing polycrystalline NaCl [2.138, 2.139]. Possible explanations for the reduced flow stress in ionic solids at elevated temperature were: (a) the dislocation mobility was enhanced by the field bias and (b) the rate-controlling activation energy was reduced with the application of electric field. Employing magnesia, alumina and YSZ, Conrad and coworkers [2.14, 2.15, 2.20, 2.22] further verified the significant influence of an electric field on plastic deformation, in that they found that the flow stress at high temperature was reduced even with a modest field strength, see Fig. 2.15. The contributions to the reduction in flow stress by the field were proposed to be: (a) Joule heating, (b) the reduced electrochemical potential due to field generated cation vacancy formation and (c) field-induced grain growth retardation.

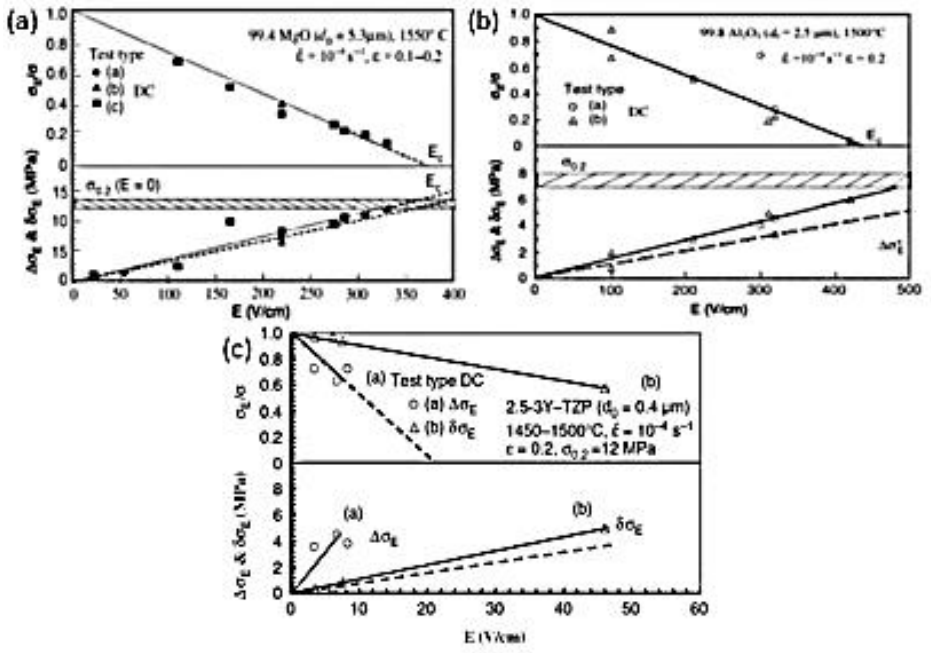

Fig.2.15 The effect of dc electric field strength, E, on the tensile flow stress: (a) MgO at 1550 ^{o}C (ε=0.1-0.2); (b) Al_2O_3 at 1500 ^{o}C (ε= 0.2) and (c) Y-TZP at 1450-1500 ^{o}C (ε=0.2). From Ref. [2.22].

2.5 References

[2.1] J. Caputo, C. C. Chao, Z. Huang, : ME: Introduction to Molecular Simulations, Final report, March 23, 2007.

[2.2] H. G. Scott, :J. Mater. Sci., 10(1975)1527-1535.

[2.3] H. P. Ding, A. V. Virkar, F. Liu, :Solid State Ionics, 215(2012)16-23.

[2.4] X. Guo, Z. Wang,:J. Euro. Ceram. Soc., 18(1998)237-240.

[2.5] Y. B. Khollam, A. S. Deshpande, A. J. Patil, H. S. Potdar, S. B. Deshpande, S. K. Date, : Mater. Chem. & Phys., 71(2001) 235-241.

[2.6] M. Biswas, P. K. Ojha, E. M. Jayasingh, C. D. Prasad,:Nanomater. Nanotechnol., 1(2011) 55-58.

[2.7]S.-J. L. Kang, Sintering: Densification, Grain Growth, and Microstructure. Elsevier Butterworth-Heinemann, Boston, p. 39-55(2005)

[2.8]R. H. R. Castro, Sintering: mechanisms of conventional nanodensification and field assisted processes, K. V. Benthem Eds., Springer, New York, p.14(2012).

[2.9]D. Agrawal,:Trans. Indian Ceram. Soc., 65[3] (2006)129-144.

[2.10]M. A. Janney, C. L. Calhoun, H. D. Kimrey, : J. Am. Ceram.Soc. 75[2](1992)341-346.

[2.11]Z. A. Munir, U. Anselmi-tamburini, M. Ohyanagi,: J. Mater. Sci., 41(2006) 763-777.

[2.12]J. R. Groza, A. Zavaliangos,:Adv. Mater. Sci., 5(2003)24-33.

[2.13]Di Yang, H. Conrad,: Scripta Mater., 36(1997)1431-1435.

[2.14]Di Yang, H. Conrad,: Scripta Mater., 38(1998)1443-1448.

[2.15]Di Yang, H. Conrad,: J. Mater. Sci., 43(2008)4475-4482.

[2.16]Hans Conrad, : in H. Wang Ed. Acta Mater., Gold Metal Symp., 2011, Thomas Telford Ltd., London, in print.

[2.17]Di Yang, R. Raj, H. Conrad,: J. Am. Ceram. Soc., 43 (2010)2935- 2937.

[2.18]Di Yang, H. Conrad,: Mater. Sci. Eng. A 528(2011)1221-1225.

[2.19]Hans Conrad, Di Yang,: Mater. Sci. Eng. A 528(2011)8523-8529.

[2.20]H. Conrad, Di Yang,: Acta Mater. 556(2007)789-6797.

[2.21]H. Conrad, Di Yang, P. Becher,: Mater. Sci. Eng. A 477(2008)358-365.

[2.22]H. Conrad, Di Yang, : Phil. Mag., 90(2010)1141-1157.

[2.23]J. E. Burke, : J. Am. Ceram. Soc., 40(1957)80-85.

[2.24]I.-W. Chen, X.-H. Wang, : Nature, 404(2000)168-171.

[2.25]M. N. Rahaman, Ceramic Processing and Sintering, 2nd Ed., Marcel Dekker Inc, New York (2003)pp.498.

[2.26]P. R. Rios,: Act Metall. Mater. 40(1992)2765-2768.

[2.27]W. D. Kingery, H. K. Bowen, D. R. Uhlmann, Introduction to Ceramics, Wiley, New York (1976).

[2.28]M. W. Barsoum, Fundamentals of Ceramics. The McGraw-Hill Companys, Inc., New York, (1997).

[2.29]M. Hillert,: Acta Metall.,13(1965)227-238.

[2.30]H. V. Atkinson, : Acta Metall. 36[3](1988)469-491.

[2.31]J. E. Burke, D. Turnbull, : Prog. Metal. Phys.,3(1952)220-292.

[2.32] H. Conrad,:Emerging Mater. Res., ICE 1(2012)11-16.

[2.33]J. Narayan,: Scripta Mater., 68(2013) 785-788.

[2.34]R. A. Vandermeer, :Acta Metall. 15(1967)447-458.

[2.35]M. F. Yan, R. Cannon, H. Bowen, :Ceramic Microstructures'76, R. M. Fulrath, J. A. Pask, eds., Westview Press, Bounlder, CO. (1977) pp.276-307.

[2.36]J. W. Cahn, : Acta Metall., 10(1962)789-798.

[2.37] K. L*ü*cke, H. P. St*ü*we, :Acta Metall., 19(1971)1087-1099.

[2.38]J. D. Powers, A. M. Glaeser, : Interface Science, 6(1998) 23-39.

[2.39]A. Michels, C. E. Krill, H. Ehrhardt, R. Birringer, D. T. Wu, : Acta Mater.,47[7](1999) 2143-2152.

[2.40]F. Liu, R. Kirchheim, : J. Crystal Growth, 264(2004)385-391.

[2.41]W. D. Kingery, : J. Am. Ceram. Soc., 57[2](1974)74-83.

[2.42]R. Kirchheim, : Acta Mater. 50(2002)413-419.

[2.43]J. P. Drolet, A. Galobois, :Metall. Trans., 2(1971)53-64.

[2.44]M. P. Harmer, R. J. Brook, :J. Mater. Sci. 15(1980)3017-3024.

[2.45]T. G. Langdon, : Acta. Metall. Mater., 42(1994)2437-2443.

[2.46]W. A. Rachinger,: J. Inst. Metals, 81(1952)33.

[2.47]F. Wakai, S. Sakaguchi, Y. Matsuno, : Adv. Ceram. Mater., 1(1986)259-263.

[2.48]J.- M. Manuel, D. – R. Arturo, B. – L. Alfonso, : J. Am. Ceram. Soc., 81(1998)2761-2776.

[2.49]S. Swaroop, M. Kilo, C. Argirusis, G. Borchardt, A. H. Chokshi, : Acta Mater. 53 (2005)4975-4985.

[2.50]M. C. Martin, M. L. Mecartney, : Solid State Ionics, 161(2003)67-79.

[2.51]S. Hui, J. Roller, S. Yick, X. Zhang, C. Decés-Petit, Y. Xie, R. Marc, D. Ghosh,: J. Power Sources, 172(2007)493-502.

[2.52]S. H. Chu, M. A. Seitz, : J. Solid State Chem., 23(1978)297-314.

[2.53]X. Guo, J. Maier, : J. Electrochem. Soc., 148 (2001)E121-E126.

[2.54]X. Guo, R. Waser, : Prog. In Mater. Sci., 51(2006)151-210.

[2.55]X. Guo, Z. Zhang, :Acta Mater., 51(2003)2539-2547.

[2.56]S. P. S. Badwal, F. T. Ciacchi, V. Zelizko: Ionics, 4(1998)25-32.

[2.57]H. Näfe, : Solid State Ionics, 13(1984)255-263.

[2.58] Y. Y. Lei, Y. S. Ito, N. D. Browning, : J. Am. Ceram. Soc., 85[9](2002)2359-2363.

[2.59]M. Aoki, Y.-M. Chiang, I. Kosacki, L. J. Lee, H. Tuller, Y. P. Liu,: J. Am. Ceram. Soc.,79[5](1996)1169-1180.

[2.60]G. S. A. M. Theunissen, A. J. A. Winnubst, A. J. Burggraaf, :J. Mater. Sci., 27(1992) 5057-5066.

[2.61]X. Guo, S. Mi, R. Waser, : Electrochem. and Solid-State Lett., 8(1) (2005) J1-J3.

[2.62]A. E. Hughes, B. A. Sexton, J. Mater. Sci. 24(1989):1057-1061.

[2.63]A. E. Hughes, S. P. S. Badwal, Solid State Ionic, 40/41(1990):312-315.

[2.64]S.P. S. Badwal, J. Drennan, Solid State Ionics, 40/41(1990):869-873.

[2.65]J. Tanaka, J. F. Baumard, P. Abelard: J .Am. Ceram. Soc., 70(1987)637-643.

[2.66]T. Masaki, : J. Am. Ceram. Soc., 69(1986)638-640.

[2.67]S. P. S. Badwal, S. Rajendran, : 70-71(1994)83-95.

[2.68]F. Wakai, T. Nagano, : J. Mater. Sci., 26(1991)241-247.

[2.69]T. Nagano, H. Kato, F. Wakai, : J. Mater. Sci., 27(1992) 3575-3580.

[2.70]S. Schlag, H.-F. Eicke, :Solid State Commun., 91(1994)883-887.

[2.71]S. Wada, T. Suzuki, T. Noma, : J. Mater. Res. 10(1995)306-311.

[2.72]J.-H. Choy, Y.-S. Han, S.-W. Song, : Mater. Lett. 19(1994)257-262.

[2.73] H. T. Martirena, J. C. Burfoot, :J. Phys. C: Solid State Phys., 7(1974)3182-3192.

[2.74] F. Micheron, G. Bismuth, : Appl. Phys. Lett., 79(1972) 79-81.

[2.75] S. P. S Bawal, F. T. Ciacchi, Ionics, 6(2000)1-21.

[2.76] S. Jiand, W. A. Schulze, V. R. W. Amarakoon, G. C. Stangle, : J. Mater. Res., 12 (1997) 2374-2380.

[2.77] X. J. Chen, K. A. Khor, S. H. Chan, L. G. Yu, : Mater. Sci. & Eng. A, 335(2002)246-252.

[2.78]J. Frenkel, Kinetic Theory of Liquids, Oxford University Press, New York, 1946 pp.36-48.

[2.79] J. D. Eshelby, E. Newey, P. Pyatt, A. Lidiard, :Philos. Mag., 3(1958)75-89.

[2.80] K. L. Kliewer, J. S. Koehler, : Phys. Rev., 140[4A] (1965) A1226-1240.

[2.81] W. D. Kingery,:J. Am. Ceram. Soc., 57(1)(1974)1-8.

[2.82] K. L. Kliewer, : Phys. Rev. 140(1965)A1241-1246.

[2.83]J.-H. Han, D.-Y. Kim, : J. Am. Ceram. Soc., 84(2001)539-550.

[2.84] S.-J. I. Kang, Sintering, Elsevier, New York (2005)pp.181-196.

[2.85] J. Maier, : Ber Bunsenges Phys Chem, 90(1986)26-33.

[2.86] R. Waser, R. Hagenbeck,: Acta Mater., 48(2000)797-825.

[2.87] M. F. Yan, R. M. Cannon, H. K. Bowen, : J. Appl. Phys. 54(1983)764-778.

[2.88] W. C. Johnson, :Metall. Trans A, 8A(1977) 1413-1422.

[2.89] S.- L. Hwang, I.-W. Chen, : J. Am. Ceram. Soc. 73(1990)3269-3277.

[2.90] D. Mc Lean, Grain Boundaries in Metals, Clarendon Press, Oxford (1957).

[2.91] K. Grönhagen, J. Ågren, : Acta Mater. 55(2007)955-960.

[2.92] M. Lrvy, J. Fouletier, M. Kleitz, J. Electrochem., 135(1988)1584-1589.

[2.93] R. I. Merino, V. M. Orera, Solid State Ionics 76(1995)97-102.

[2.94] V. M. Orera, R. I. Merino, Y. Chen, R. Cases, P. J. Alonso, Phys. Rev. B., 42 (1990)9782-9789.

[2.95] R. Ramamoorthy, D. Sundararaman, S. Ramasamy, Solid State Ionics, 123(1999)271-278.

[2.96] M. Weller, H. Schubert, : J. Am. Ceram. Soc., 22(1987) 573-577.

[2.97] S. P. S. Badwal, J. Drennan, : J. Mater. Sci., 22(1987) 3231-3239.

[2.98] S. P. S. Badwal, F. T. Ciacchi, M. V. Swain, V. Zelizko, : J. Am. Ceram. Soc., 73 (1990)2505-2507.

[2.100] T. Tsubakino, H. Ikeda, H. Maeda, B. Zang, : Am. Ceram. Soc. (1996)pp.213-224.

[2.101] A. Pimenov, J. Ullrich, P. Lunkenheimer, A. Loidl, C. H. Rüscher, :Solid State Ionics, 108(1998)111-118.

[2.102] T. Uchikoshi, Y. Sakka, K. Hiraga, : Jnl. Electroceram, 4:S1(1999)113-120.

[2.103] H. Conrad, J. Wang, Unpublished research, NCSU (2013).

[2.104] J. E. Baurle, : J. Phys. Chem. Solids 30(1969)2657-2670.

[2.105] D. Wang, A. Nowick, : J. Solid State Chem. 35(1980)325-333.

[2.106] R. Gerhardt, A. Nowick, : J.Am. Ceram. Soc. 69(1986)641-646.

[2.107] J .MacDonald, Impedance Spectroscopy: Emphasizing Materials and Systems, Wiley-Intersciences, New York (1987).

[2.108] M. C. Martin, M. L. Mecartney, : Solid State Ionics, 16(2003)67-79

[2.109] M. Tokita,: Mater. Sci. Forum, 308-311(1999)83-88.

[2.110] M. Omori, : Mater. Sci. & Eng. A 287(2000)183-188.

[2.111] Z. Shen, M. Johnsson, Z. Zhao, M. Nygren, : J. Am. Ceram. Soc.85(2002)1921-1927.

[2.1112] D. V. Quach, H. Avila-Paredes, S. Kim, M. Martin, Z. A. Munir, Acta Mater., 58 (15)(2010)5022-5030.

[2.1113] J. Wang, A. Du, Di Yang, R. Raj, H. Conrad, : J. Ceram., 2013, Article ID 370603.

[2.114] S. D. Antolovich, H. Conrad, : Mater. and Manufact. Pro., 19(2004) 587-610.

[2.115] H. Conrad, : Mater. Sci. and Eng. A, 287(2000) 276-287.

[2.116] Z. J. Shen, M. Johnsson, Z. Zhao, M. Nygren, J. Am. Ceram. Soc., 85[8](2002)1921-1927.

[2.117] S. Ghosh, A. H. Chokshi, P. Lee, R. Raj, : J. Am. Ceram. Soc. 92(2009)1856-1859.

[2.118] R. Raj, M. Cologna, J. S. C. Francis, J. Am. Ceram. Soc., 94(7)(2011)1941-1965.

[2.119] M. Cologna, B. Rashkova, R. Raj, J. Am. Ceram. Soc., 93(11)(2010)3556-3559.

[2.120] M. Cologna, R. Raj, J. Am. Ceram. Soc., 94(2)(2011)391-395.

[2.121] Di Yang, H. Conrad, Scripta Mater., 63(2010) 328-331.

[2.122] J. Obare, J. Wang, H. Conrad, Scripta Mater., 68(2013)111-113.

[2.123] J. S. C. Francis, M. Cologna, R. Raj, : J. Euro. Ceram. Soc., 32(12)(2012) 3129-3136.

[2.124] M. Cologna, A. L. G. Prette, R. Raj, J. Am. Ceram. Soc., 94(2) (2011)316-319.

[2.125] J. S. C. Francis, R. Raj, J. Am. Ceram. Soc., 95(1)(2012)138-146.

[2.126] J. W. Teong, J. H. Han, D. Y. Kim,: J. Am. Ceram. Soc., 83(4)(2000)915-918.

[2.127] J. Narayan,:MRS Commu. Cambridge Univ Press, 2013.

[2.128] J. Narayan,: Scripta Mater., 69(2)(2013)107-111.

[2.129] R. Raj, M. Cologna, J. S. C. Francis,: J. Am. Ceram. Soc., 94[7] (2011) 1941-1965.

[2.130] J. S. C. Francis, R. Raj,: J. Am. Ceram. Soc. 95[1](2012)138-146.

[2.131] Z. J. Shen, H. Peng, M. Nygren,: Adv. Mater.,15(2003)1006-1009.

[2.132] J. Campbell, Y. Fahmy, H. Conrad,: Metall. & Mater. Trans. A, 30A(1999)2817-2823.

[2.133] D. Yang, H. Conrad,: J. Mater. Sci., 43(2008)4475-4482.

[2.134] M. Q. Li, Y. L. Liu, S. C. Wu, X. W. Wu,: J. Mater. Proc. Tech., 40(1994)385-393.

[2.135] W. - D. Cao, X. - P. Lu, A. F. Sprecher, H. Conrad,: Mater. Sci. & Eng. A, 129 (1990) 157-166.

[2.136] T. Suzuki, M. Ueno, Y. Nishi, M. Fujimoto,: J. Am. Ceram. Soc., 84[1](2001)200-206.

[2.137] L. Zuev, V. Gromov, O. Alexankina, Sov. Phys. Crystallogr, 19(1975)553.

[2.138] Di Yang, H. Conrad, Mater. Sci. Eng. A 225(1997)173.

[2.139] Di Yang, H. Conrad, J. Am. Ceram. Soc. 80(1998)1389

CHAPTER THREE

3.0 EXPERIMENTAL PROCEDURE

3.1 Experimental Procedure

3.1.1 Starting material

The commercial 3 mol.% yttria-stabilized zirconia powders (3YB-TZ) with binder used in the present study was purchased from Tosoh Co, Japan. The grade, crystallite size and nominal chemical composition (wt. %) of the as-received powders are given in Table 3.1.The weight composition of the element Y_2O_3 in this powders is 5.15±0.20 wt.%; the specific surface area is 16±3 m^2/g. The green density and sintered density are 2.66 g/cm^3 and 6.05 g/cm^3, respectively.

Table 3.1 Grade, crystallite size d_0 and nominal chemical composition of the 3Y-TZP

Grade	d_0	Y_2O_3	Al_2O_3	SiO_2	Fe_2O_3	Na_2O	Lg. loss	ZrO_2	Binder
(TZ-3Y)	26nm	5.21	<0.005	0.005	<0.002	0.022	0.73	Reminder	Arcrylic

3.1.2 Specimen synthesis and processing

The powder compaction process is a versatile route for net-shaping specimens with a relatively complex geometry [3.1]. Before filling the powder into the die, the interior surface of the die (see Fig. 3.1) was lubricated by carefully smearing mold release wax (LECO Co.) on it and then heated so that the wax could spread over the entire surface. The purpose of the waxing was to ease the green specimen removal from the die after compaction. The as-received 3Y-TZP powders were filled into the stainless steel die with a dog-bone shaped cavity giving a specimen (see Fig. 3.2) with green density of 2.29 g/cm^3 and compacted with 98 MPa compressive force.

Following compaction the binder was removed by heating in air to 800 ^{o}C in 72 hr and holding at this temperature for 1 hr. The specimen was then furnace-cooled to room temperature and electrodes attached by tightly wrapping fine Pt wire (0.13 mm dia.) around each end of the gage section and in turn connected to the power supply (either Sorensen DCS 300-3.5 dc or 60 Hz ac (a vari ac transformer connected to the Laboratory power line). The specimen was then sintered at a constant heating rate(usually $\sim$ 10 ^{o}C/min to 1500 ^{o}C) without and with a constant applied voltage V ($\pm$0.1 V), giving an initial electric field E_0=V/l_0, l_0 being the distance between the Pt electrodes. Along with the voltage the specimen shrinkage Δl_s and the corresponding electric current I were measured throughout the sintering process. A schematic of the sintering apparatus and arrangements is shown in Fig.3.3. The magnitude of Δl_s (the degree of sintering) was measured to 0.01 mm by optically sighting by a low power telescope on the end of a Pt wire attached to the lower end of the specimen.

The isothermal annealing process was conducted at two selected temperatures, namely 1300 ^{o}C and 1400 ^{o}C. Following binder removal, the specimen was sintered without and with an initial dc electric field E_0 = 14 V/cm to 1300 ^{o}C or 1400 ^{o}C and then annealed at these respective temperatures for various times up to 24 hr, following which they were furnace cooled. The thermal history experienced by the specimens both without and with field is shown schematically in Fig.3.4. The linear shrinkage (which gave the relative density ρ_r and the corresponding increase in electric field E), the mean linear intercept grain size $\bar{d}$ (from SEM micrographs taken of mechanically-polished and thermal-etched(1 hr at 1200 ^{o}C) cross-sections and the electric current I were measured as a function of the annealing time.

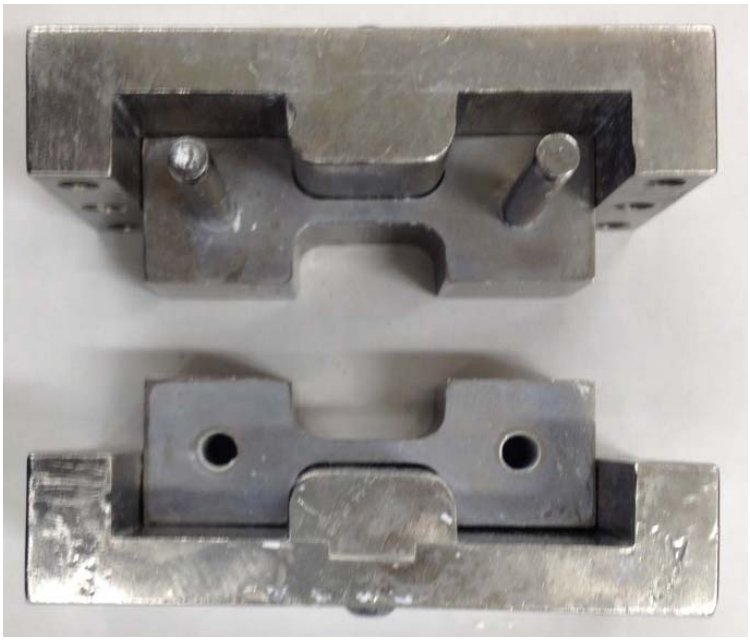

Fig. 3.1 Stainless steel fixture for compacting dog-bone shaped specimen.

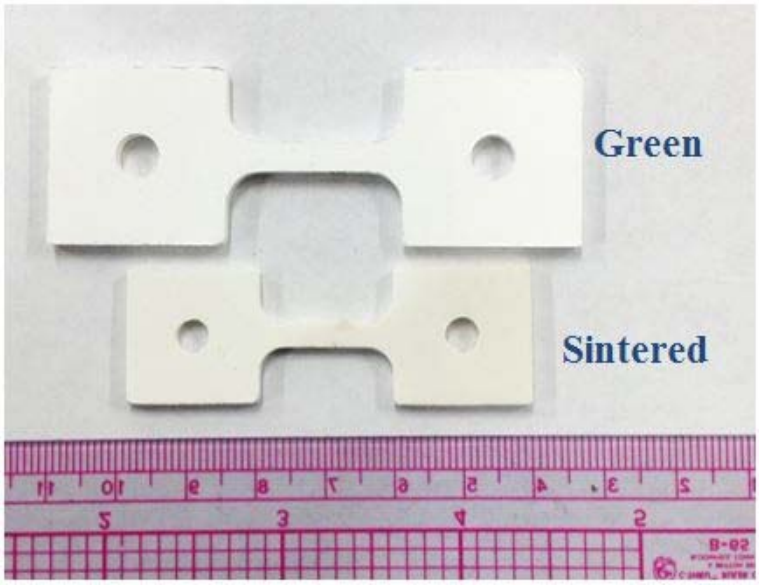

Fig. 3.2 Green and sintered specimens of 3Y-TZP.

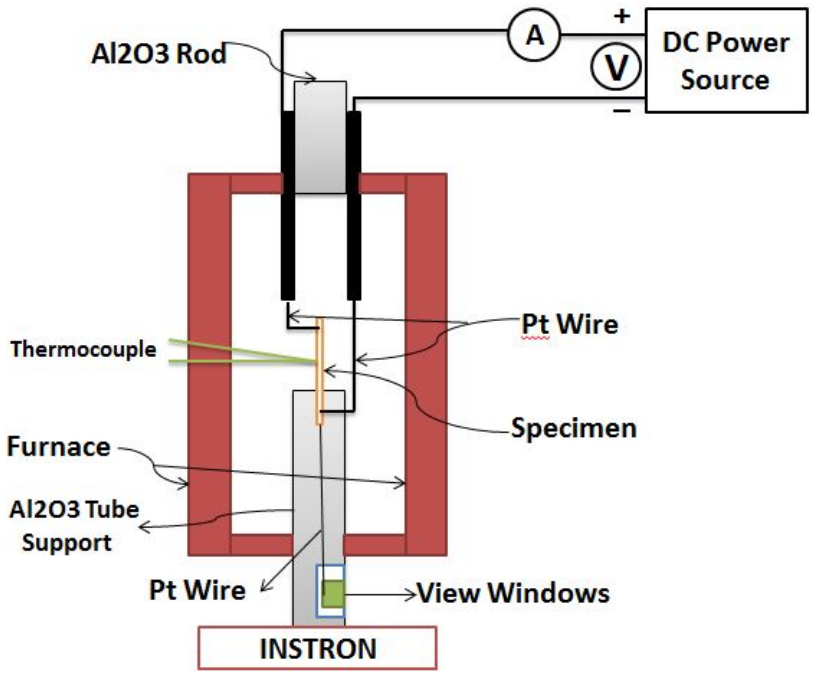

Fig.3.3 Schematic of sintering and annealing test arrangement.

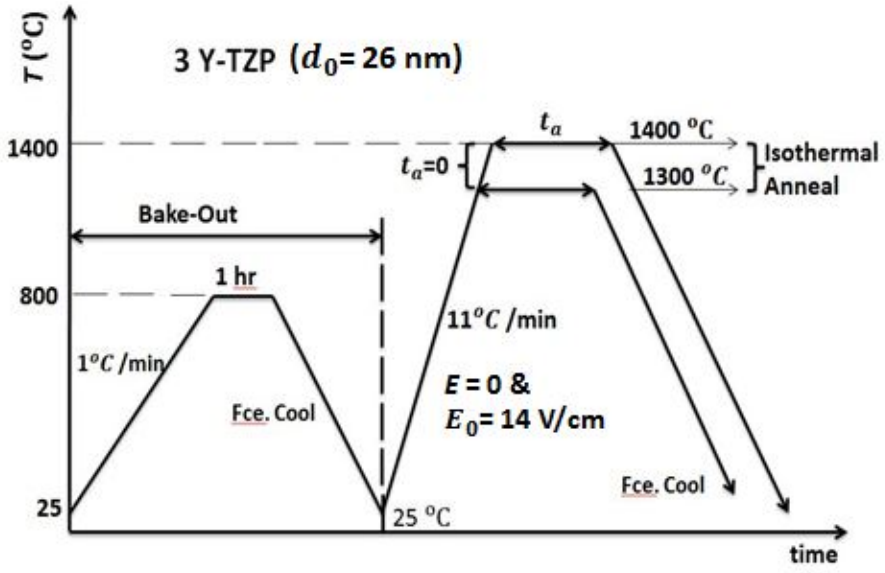

Fig.3.4 Schematic of the heating history experienced by the specimens subjected to the isothermal annealing tests.

3.2 Characterization

3.2.1 Density measurements and grain growth determination

The increase in the relative density ρ_r of the specimen during the sintering was determined employing the relation

$$\rho_r = \rho_0[(1+\epsilon_z)\rho_f]^{-1} \qquad (3.1)$$

where ρ_0=2.71 g/cm^3 is the green density following binder bake--out, $\epsilon_z = \Delta l_s / l_0$ is the negative longitudinal shrinkage strain and ρ_f=6.05 g/cm^3 is the final theoretical density of 3 Y-TZP. Both ρ_0 and ρ_f were checked by micrometer measurements and by the Archimedes method.

Since the sintering with field is performed at constant voltage and the specimen shrinks during sintering, the actual applied field E increases during sintering according to

$$E = E_0(1+\epsilon_z)^{-1} \qquad (3.2)$$

It is well-known that grain growth occurs during sintering of crystalline ceramics. The grain growth which occurred in the present sintering tests without and with electric field was both calculated and measured directly by scanning electron microscopy (SEM). The calculated values were obtained employing the general sintering equation[3.2]

$$\dot{\rho} = \frac{A}{T}\exp(\frac{-Q}{RT})\frac{f(\rho)}{d^n} \qquad (3.3)$$

where $\dot{\rho} = d\rho/dt$ is the densification rate, A a material constant, T the temperature, R the gas constant, Q an apparent activation energy of the governing diffusion process, f(ρ) is a function only of the existing density, d is the grain size and n is the grain size exponent, which is equal to 4 for grain boundary diffusion and 3 for lattice diffusion.

3.2.2 Microstructure characterization

Micrographs of the sintered and isothermally annealed grains of 3Y-TZP ceramics were determined by scanning electron microscopy (SEM) (Hitachi S-3200N). The thermally etched specimens were gold coated to prevent charging as the 3 Y-TZP is an insulator for electron microscopy determination. To check the validity of the calculated grain size values, they were also measured on SEM micrographs of both fractured and mechanically-polished and thermally-etched (1 hr at 1200 ^{o}C) surfaces of specimens sintered to specific relative densities between 0.5 and 1.0 (800 ^{o} to 1500 ^{o}C). The micrographs were taken at three locations along the specimen gage section: (a) ~5 mm below the upper (+) electrode, (b) midway between the two electrodes and (c) ~5 mm above the lower (−) electrode. On the order of 100 to 200 linear intercept counts were made on each SEM micrograph, giving a total of 300-600 counts for the reported mean linear intercept grain size $\bar{d}$ representing each test condition.

An exploratory study of the Joule heating which occurs during sintering with an electric field was made by inserting a fine Pt-PtRh thermocouple into a small hole (~ 1 mm dia × 0.5 mm deep) drilled at the center line of the gage section midway between the electrodes.

3.3 References

[3.1] N. A. Fleck, : J. Mech. Phys. Solids, 43(1995)1409-1431.

[3.2] J. Wang, R. Raj,: J. Am. Ceram. Soc., 73(1990)1172-1175.

[3.2] R. R. Bitti, P. E. N. Di, : Scripta Mater., 39(1998)335-340.

CHAPTER FOUR

4.0 EXPERIMENTAL RESULTS

4.1 Effect of a modest electric field on the sintering rate and related factors

4.1.1 Sintering rate

It was found that the application of a modest initial electric field E_0=1-50 V/cm (both dc and 60 Hz ac) during sintering increased the sintering rate. The degree of enhancement with the initial field strength E_0 is shown in Figs. 4.1 and 4.2. The corresponding increase in field strength E and current I with sintering temperature is given in Figs 4.3 and 4.4 for the dc and ac fields respectively.

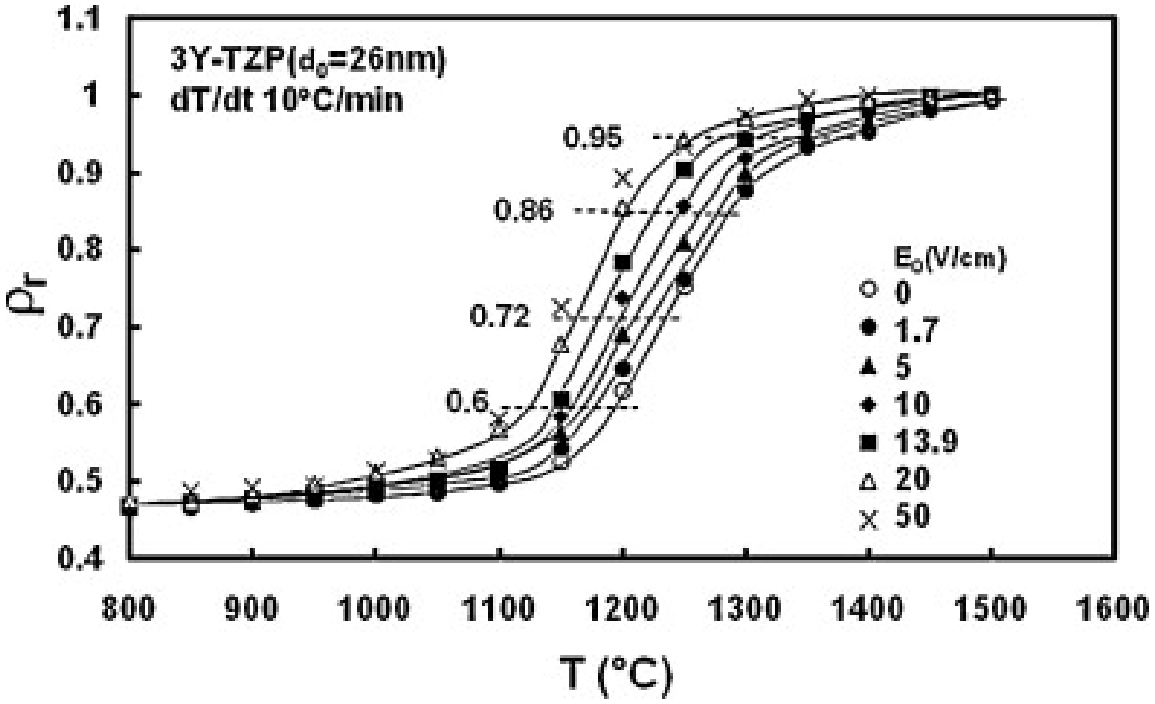

Fig.4.1 Relative density ρ_r vs sintering temperature as a function of the initial applied DC electric field strength E_0. The dashed lines indicate the relative densities where the effect of field strength on the sintering rate is considered. Adapted from Conrad, Di Yang [4.1].

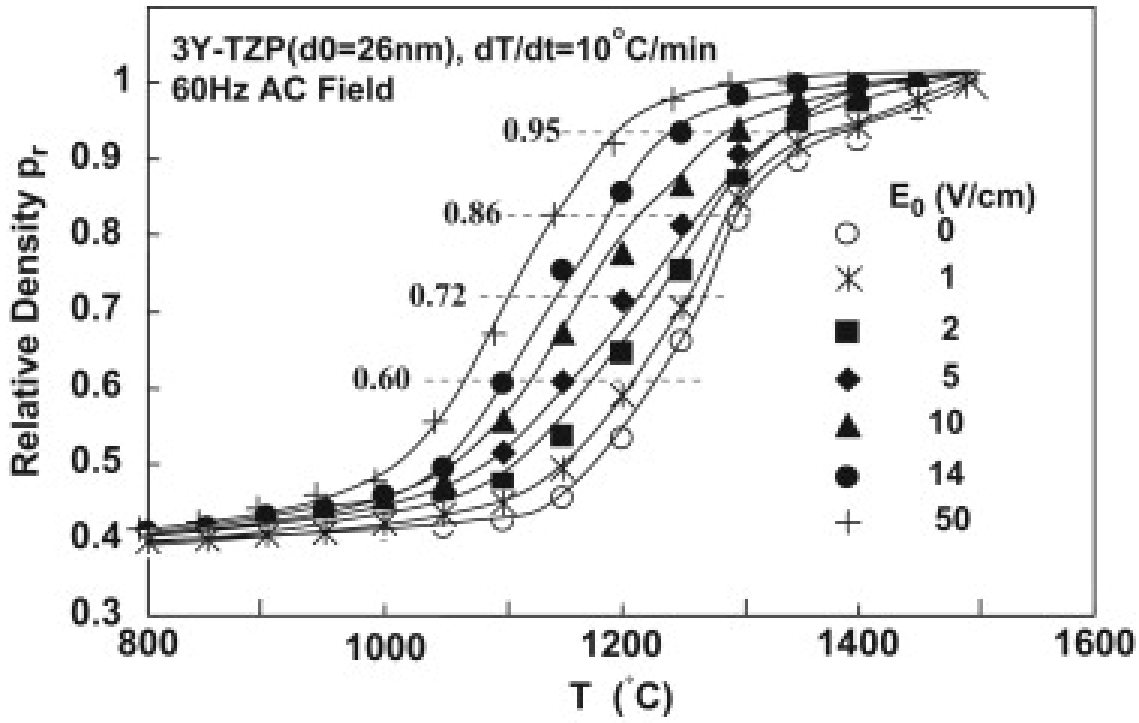

Fig.4.2 Relative density ρ_r vs sintering temperature as a function of the initial applied 60 Hz AC electric field strength E_0. The dashed lines indicate the relative densities where the effect of field strength on the sintering rate is considered. Adapted from Conrad, Di Yang [4.2].

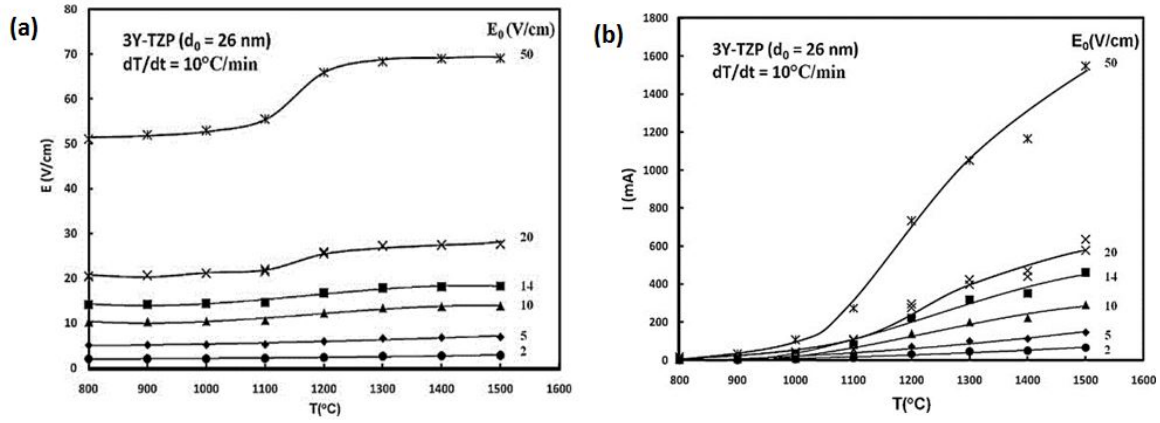

Fig. 4.3 (a) Increase in the applied dc field strength E with sintering temperature as a function of the initial field strength E_0 and (b) the corresponding electric currents I. Adapted from Conrad, Di Yang [4.1].

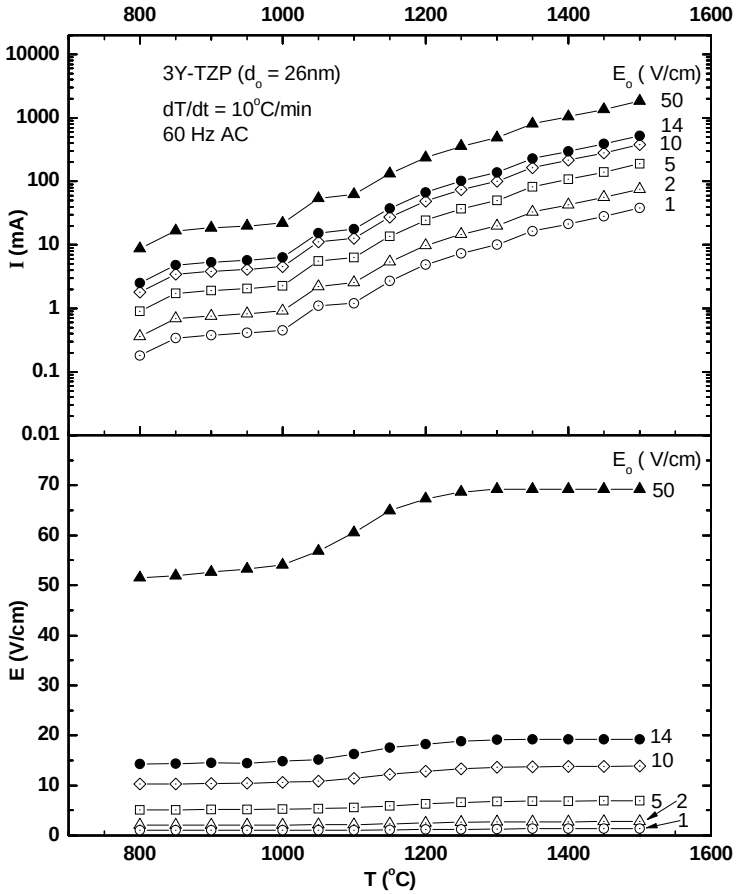

Fig.4.4 (a) Increase in the applied 60 Hz ac electric field strength E with sintering temperature as a function of the initial field strength E_0 and (b) the corresponding electric current I. Adapted from Conrad, Di Yang [4.2].

The dependence of the sintering rate (taken here as the temperature T_ρ to reach a specific relative density ρ_r) on the actual field strength E is shown in Fig. 4.5 for both the dc and the ac electric fields. To be noted is that for both field types T_{ρ_r} decreases (i.e., the sintering rate increases) with increase in field strength up to ~ 25 V/cm, but then remains relatively constant to ~60 V/cm. The ac field (rms) gives a greater effect than the dc field at all relative densities, the difference between the two however decreases with increase in ρ_r.

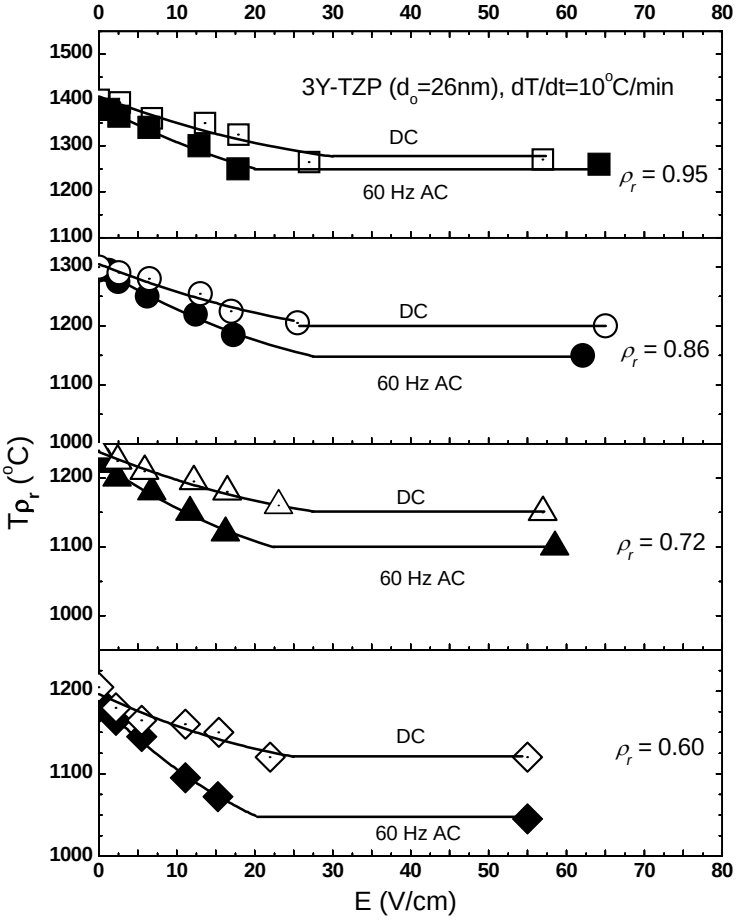

Fig.4.5 The temperature T_{ρ_r} at which the indicated relative density ρ_r was reached during sintering vs the actual dc and ac field strength. Adapted from Conrad, Di Yang [4.2].

4.1.2 Grain size

It is well-known that in general the grain size increases with the sintering temperature during sintering. The effect of an applied electric field on the grain size during sintering was calculated by taking the logarithm of Eq.3-3 and rearranging, which gives for a constant relative density and assuming that the field has essentially no effect on Q and n (which will be shown below to be the case):

$$nln\left(\frac{d}{d_E}\right) = \ln\left(\frac{\dot{\rho}_E}{\dot{\rho}}\right) + \ln\left(\frac{T_E}{T}\right) + \frac{Q}{R}(T_E^{-1} - T^{-1}) \qquad (4.1)$$

where the subscript E refers to the values with field and its absence without. The magnitudes of the grain size (GS) ratio d_E/d calculated during sintering with the *dc field* (Fig. 4.1) employing Eq. 4-1 (taking Q = 500 kJ/mole [4.3,4.4] and n=3 [4.3,4.5-4.7]) are presented in Fig.4.6. Included are the corresponding SEM measurements (see for example Fig. 4.7) to

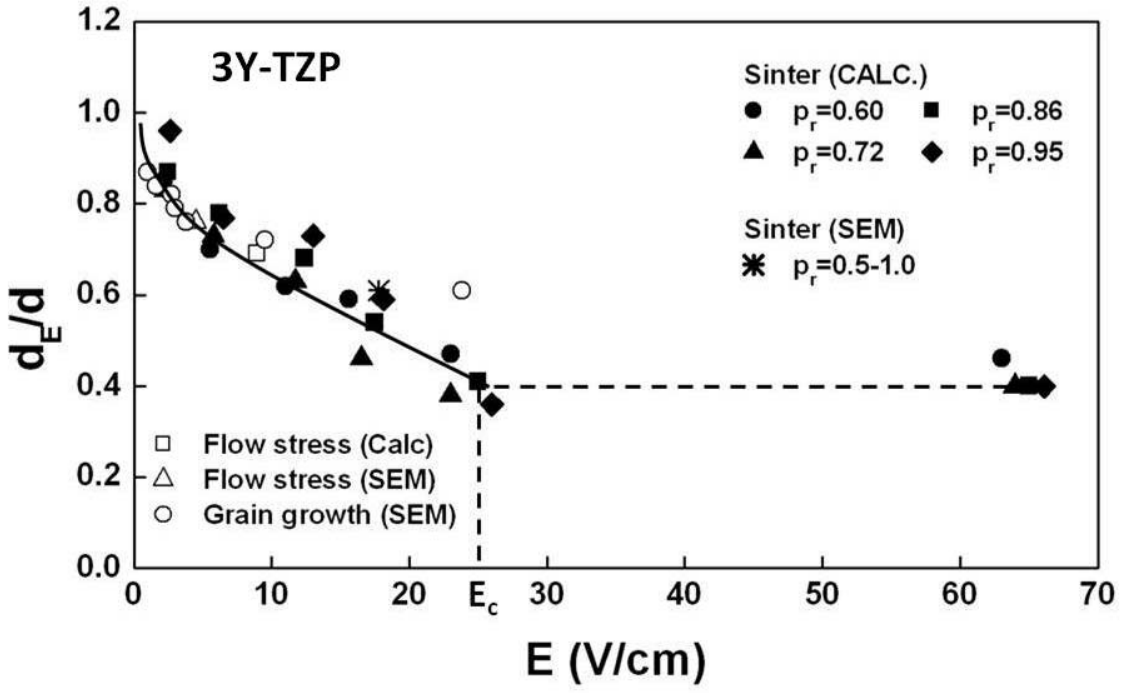

Fig.4.6 The calculated value of the grain size ratio d_E/d vs the dc electric field strength E as a function of the relative density ρ_r for sintering without and with a dc electric field. Included are corresponding SEM measurements and values from the literature on grain growth during plastic deformation [4.8] and during isothermal annealing [4.9]. Adapted from Conrad, Di Yang [4.1].

confirm the validity of the calculated values. Also included are *calculated* values from plastic deformation tests employing the relation in [4.8] and SEM values for the effect of a dc field

on the plastic deformation flow stress (see for example Fig. 4.8) and from SEM measurements in isothermal annealing tests [4.9].

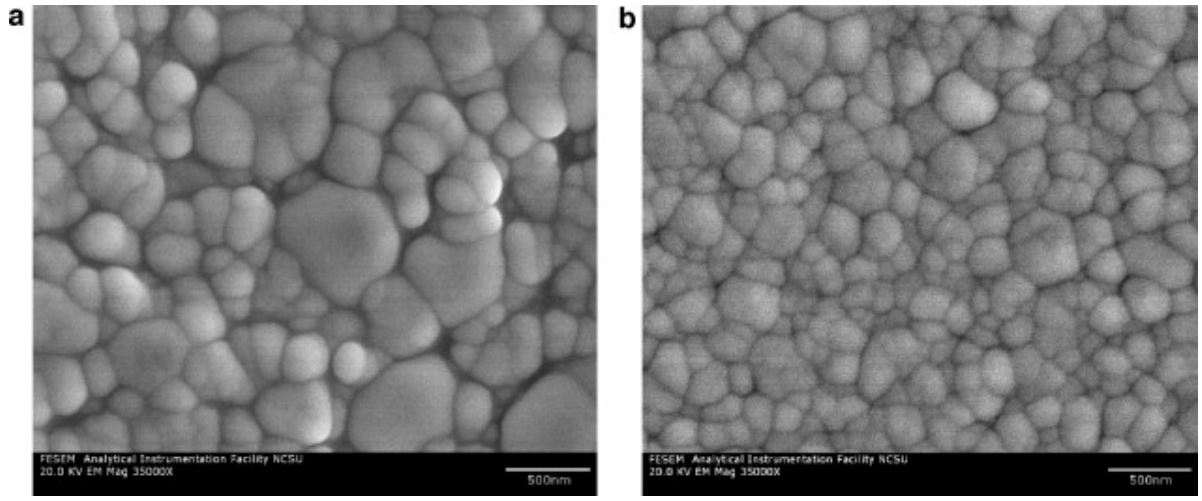

$\bar{d}$ = 350 nm $\bar{d}$ = 215 nm

Fig.4.7 SEM micrographs showing the retarding effect of a dc electric field on grain growth in fully-sintered (1500 ^{o}C) specimens: (a) E=0 and (b) E_0=14 V/cm dc. Adapted from Conrad, Di Yang [4.1].

To be noted regarding Figs. 4.6-4.8 are the following: (a) in all cases the application of a dc field retarded grain growth, i.e., the field decreased the grain size (GS) ratio d_E/d, (b) the degree of retardation increased with field strength E up to ~ 25 V/cm (designated E_c) and then remained essentially constant up to ~ 65 V/cm (the maximum applied field considered), (c) the degree of retardation by the field is essentially the same in the three processes, namely sintering, plastic deformation and isothermal annealing and (d) the calculated values of d_E/d for sintering and plastic deformation are in accord with those determined directly by SEM measurements.

Application of a 60 Hz ac field during sintering had a greater effect on retarding grain growth than an equivalent dc field; see Figs. 4.9 and 4.10. The form of the relationship

between d_E/d and E is however similar for the two field types, which suggest that the governing mechanism pertaining to retarding grain growth by the two field types is the same.

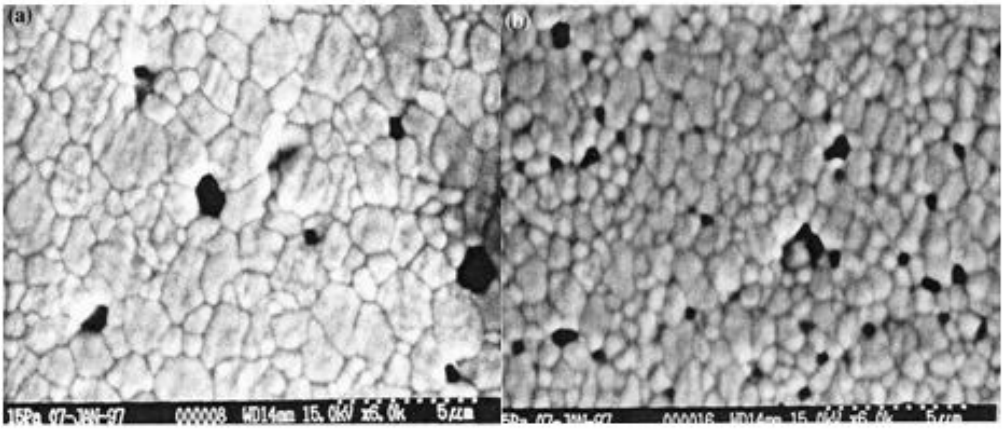

Fig. 4.8 SEM micrographs of specimens which had been fully sintered (1500 ^{o}C) without field and then plastically deformed (ϵ = 1.0) at 1500 ^{o}C: (a) E=0 and (b) E_0 = 14 V/cm. Adapted from Conrad [4.10].

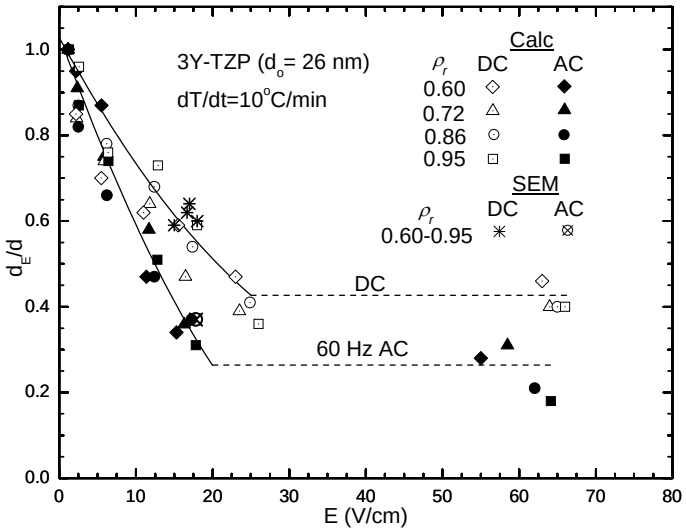

Fig. 4.9 The calculated value of the grain size ratio d_E/d vs the ac field strength E (rms) during sintering as a function of the relative density ρ_r.Included for comparison are the dc values in Fig.4.6. Also included are corresponding SEM measurements. Adapted from Conrad, Di Yang [4.2].

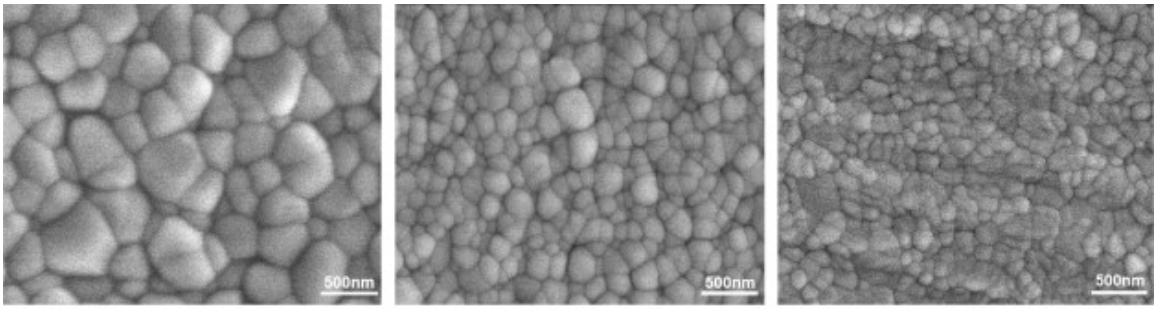

Fig. 4.10 SEM micrographs (polished and etched) showing the effect of a modest DC and AC electric field E= 19 V/cm on the grain size of fully-sintered ($\rho_r \approx 1.0$) specimens. Adapted from Di Yang, Conrad [4.11].

4.1.3 Grain Stereology

In the above it is found that the enhanced sintering rate which occurs with the application of an electric field results mainly from the retardation of grain growth by the field, either dc or ac. Of related interest is whether along with the retardation of grain growth there occurs any effect of the field on the stereology of the grains, i. e., on their 3-D form, shape isotropy or size distribution. Examples of the SEM microstructure and corresponding grain size distribution in specimens fully-sintered (1500 ^{o}C) without and with a field (dc and 60 Hz ac) are presented in Figs. 4.11-4.13, the stereology parameters pertaining to the grain size is shown in Table 4.1. Stereographic analysis [4.12.4.13] of these and other such micrographs gave the following: (a) the 3-D form of the grains is probably tetrakaidecahedral (Fig.4.11), (b) the grains are essentially isotropic in shape (Figs.4.11-4.13), (c) the grain size distribution is approximately log-normal(Figs. 4.11-4.13) and (d) the distribution is in accord with the Bitti-Di Nunzio model [4.14] (Figs. 4.14 and 4.15), which expresses the contribution of each grain of size d to the free energy of the system by the relation $\alpha\, \gamma_b^0$/d, where α is a

dimensionless geometric factor taking into account the grain shape and γ_b^0 the specific surface energy. In reaching thermoequilibrium their calculation give for the grain size distribution is given by the function

$$f(d) = A \exp[-(d_c/d + 2d/\bar{d} + d/d_m)] \qquad (4.2)$$

where A is a normalizing constant, d the size of a specific grain, $d_c \cong \bar{d}$ is the critical size corresponding to the mean energy of the distribution and d_m is the maximum size of the grains in the distribution. The grain size distribution results in Figs. 4.14 and 4.15 give that the field has little, if any, effect on the grain size distribution (GSD), but merely shifts the distribution to a smaller one that has the same mean grain size, but obtained without a field, e.g., increase in heating rate or decrease in temperature. The fit of the GSD with field to the Bitti-Di Nunzio model indicates that a major effect of the field on grain growth is through the factor $\alpha\ \gamma_b^0$/d.

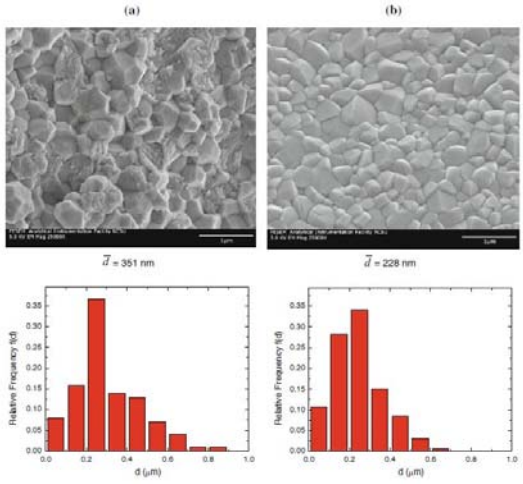

Fig. 4.11 SEM micrographs and the corresponding grain size distributions from fractured surfaces taken near the upper (+) location of fully sintered (1500 ^{o}C) specimens: (a) E=0 and (b) E_0=14 V/cm (DC). Adapted from Obare, Griffin, Conrad [4.12].

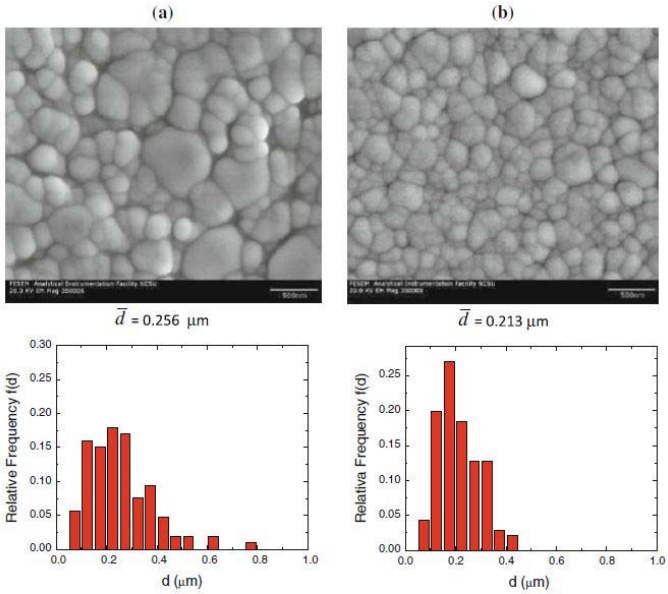

Fig.4. 12 SEM micrographs and the corresponding grain size distribution from mechanically polished and thermally etched (1 hr @ 1200 ^{o}C) surface taken near the lower (-) location of fully sintered (1500 ^{o}C) specimens: (a) E=0 and (b) E_0=14 V/cm (DC). Adapted from Obare, Griffin, Conrad [4.12].

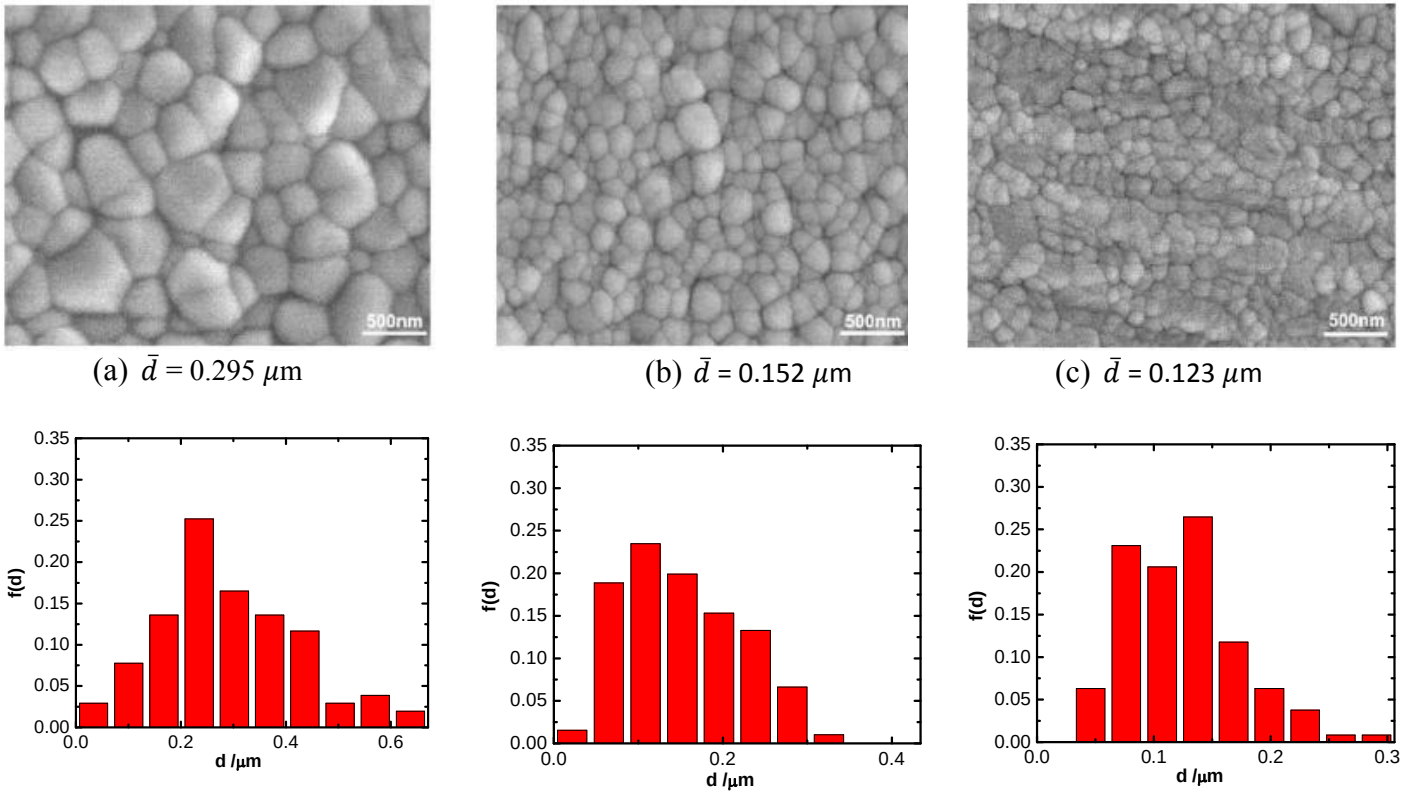

(a) $\bar{d}$ = 0.295 μm (b) $\bar{d}$ = 0.152 μm (c) $\bar{d}$ = 0.123 μm

Fig. 4.13 SEM micrographs and the corresponding grain size distribution and thermally etched (1hr @ 1200 ^{o}C) cross sections taken at the middle location of fully sintered (1500 ^{o}C) specimens: (a) E=0, (b) E_0=14 V/cm, DC and (c) E_0=14 V/cm, 60 Hz AC. Adapted from Obare, Wang and Conrad [4.13].

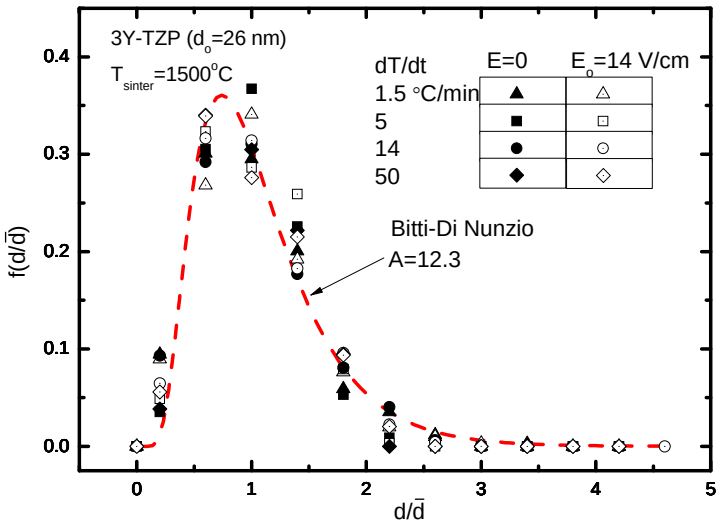

Fig.4.14 The normalized (with respect to the mean grain size) distribution curve from SEM micrographs of fractured surfaces from fully-sintered (1500 °C) specimens sintered at various heating rates without and with a dc electric field. Included is the curve predicted by the Bitti- Di Nunzio model. Adapted from Obare, Griffin, Conrad [4.12].

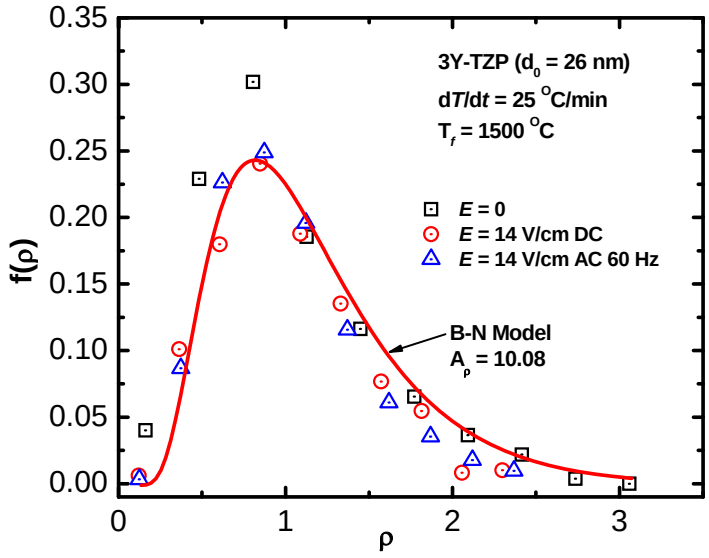

Fig.4.15 Fit of the grain size distributions in 3Y-TZP sintered without and with DC and AC fields to the Bitti-Di Nunzio grain coarsening model. Adapted from Obare, Wang, Conrad[4.13].

Table 4.1 Stereology parameters pertaining to the grain size in fully-sintered 3Y-TZP

E (V/cm)	Location[(a)]	N[(b)]	$(d/d_{max})^{(c)}$	$\bar{d}$ (nm)	d_{med} (nm)	$d_{med}/\bar{d}$	d_p (nm)	$d_p/\bar{d}$	d_{max} (nm)	$d_{max}/\bar{d}$	$f(d_p)$	R_A
0	U(+)	106	0.1	256	232	0.91	263	1.03	751	2.93	0.26	1.32
	M	104	0.1	295	275	0.93	235	0.80	671	2.27	0.25	0.96
	L(-)	66	0.1	402	363	0.90	344	0.86	984	2.45	0.23	1.25
	C	276	0.05/0.1	305	272	0.89	246/270	0.80/0.88	984	4.06	0.30/0.16	1.02
14 DC	U(+)	141	0.1	213	198	0.93	153	0.72	436	2.05	0.26	1.00
	M	197	0.1	152	140	0.92	109	0.72	434	2.86	0.23	1.05
	L(-)	158	0.1	186	175	0.94	161	0.87	461	2.48	0.28	1.06
	C	496	0.05/0.1	180	172	0.96	161/173	0.89/0.96	461	2.56	0.23/0.13	1.04
14 AC	U(+)	218	0.1	109	104	0.95	122	1.12	221	2.03	0.22	0.91
	M	239	0.1	123	120	0.98	138	1.12	306	2.49	0.26	0.95
	L(-)	167	0.1	176	169	0.96	149	0.85	331	1.88	0.22	0.90
	C	624	0.05/0.1	133	127	0.95	115/124	0.86/0.93	331	2.49	0.25/0.13	1.08

Notes: (a) U =upper, M=middle, L =lower, C = combined. (b) N = number of measurements, (c) d/d_{max} = classification size interval. (d) $R_A = \bar{d}_H/\bar{d}_L$ is a measure of the grain size shape anisotropy.

4.1.4 Grain growth kinetics

It was found in the above that the effect of the field on grain size ratio d_E/d was independent of the relative density ρ_r and in turn on the sintering temperature. Assuming that the rate-controlling mechanism obeys an Arrhenius-type equation of the form $d_E/d = Aexp(-Q/RT)$, the temperature independence of d_E/d indicates that the influence of the field on grain growth during sintering is mainly through its effect on the pre-exponential A rather than the activation energy Q. Support for this conclusion is provided by sintering tests with combined dc electric field and increasing heating rate, which show that the resulting GS ratio d_E/d is independent of the heating rate (Fig. 4.16). Additional support is provided by an analysis of the sintering curves without and with a dc electric field in terms of the Su, Johnson [4.16] "master sinter curve (MSC)" equation

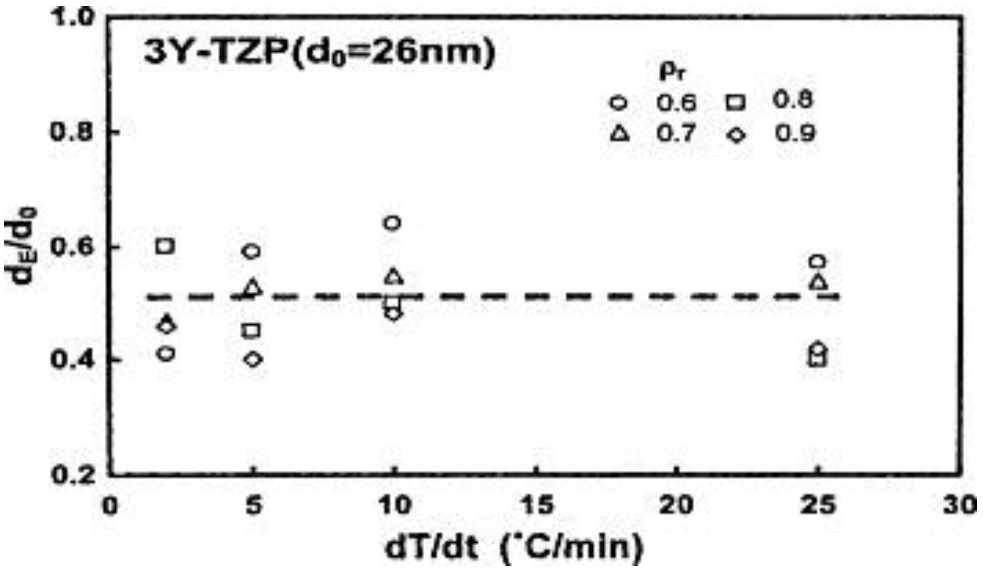

Fig.4.16 Ratio of the grain size with field to that without (d_E/d) vs the sintering heating rate in specimens sintered to various relative densities without and with a dc electric field E_0=14 V/cm. Adapted from Di Yang, Conrad [4.15].

$$\int_{\rho_0}^{\rho} \frac{[\bar{d}(\rho)]^n}{3\rho f(\rho)} = \int_0^t \frac{\gamma_s \Omega D_0}{kT} \exp\left(\frac{-Q}{kT}\right) dt \qquad (4.3)$$

where ρ is the density of the sintered compact, ρ_0 the green density, $\bar{d}$ the average grain size, n the grain size exponent, f(ρ) is only a function of ρ, γ_s is the surface energy, Ω the atomic volume, D_0 the governing diffusion coefficient pre-exponential, Q the apparent activation energy and t the sintering time. A best estimate of Q is obtained from the minimum value of a statistical analysis of the sintering curve based on the mean residual squares of errors (MRSE) of the data points with respect to fitted lines based on a range of selected Q values. The MRSE vs Q curves obtained in this manner for the sintering of 3Y-TZP with and without an electric field E_0=14 V/cm is presented in Fig. 4.17. To be noted is that the minimum values give Q = 500±5 kJ/mole for both sintering without field and with a field, i.e., the field

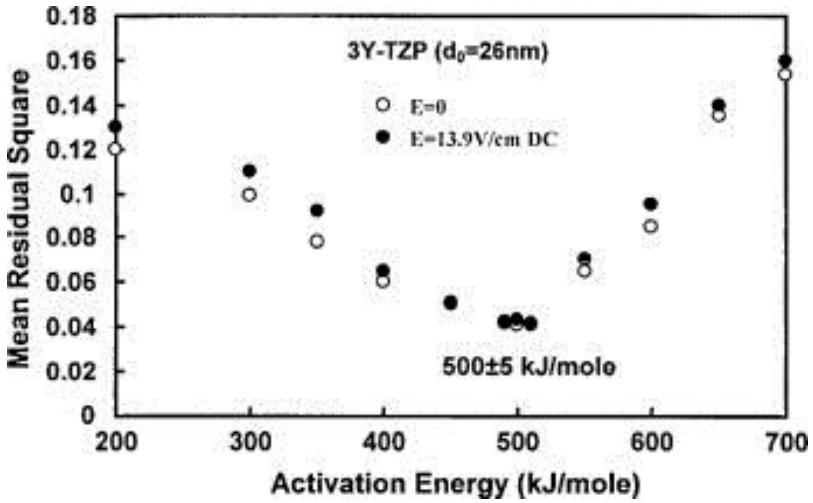

Fig.4.17 Mean residual squares errors (MRSE) based on the SU-Johnson master sintering curve euationvs selected values of the activation energy for the sintering of 3Y-TZP without and with a dc electric field E_0=14 V/cm. Adapt from Di Yang, Conrad [4.15].

has essentially no effect on Q. The present MSC value of 500 kJ/mole for conventional

sintering without field is in accord with that (485±12 kJ/mole) obtained by Mazaheri et al. [4.3] employing the MSC method. Furthermore, these authors further obtained Q=546±23 kJ/mole from their corresponding grain growth studies, which value compares favorably with that (580 kJ/mole) reported by Nich and Wadsworth [4.4] and that (516±24 kJ/mole) by Theunissen et al. [4.5]. Taking Q= 500 kJ/mole the good fit of our sintering curves for different heating rates to a single master sintering curve for E =0 and E_0 =14 V/cm is shown in Figs. 4.18 and 4.19. These agreements support the results in Fig. 4.17 which give that the field has only little, if any, effect on Q and therefore the retardation of grain growth by the field is mainly through a reduction in the pre-exponential A of the applicable Arrhenius equation.

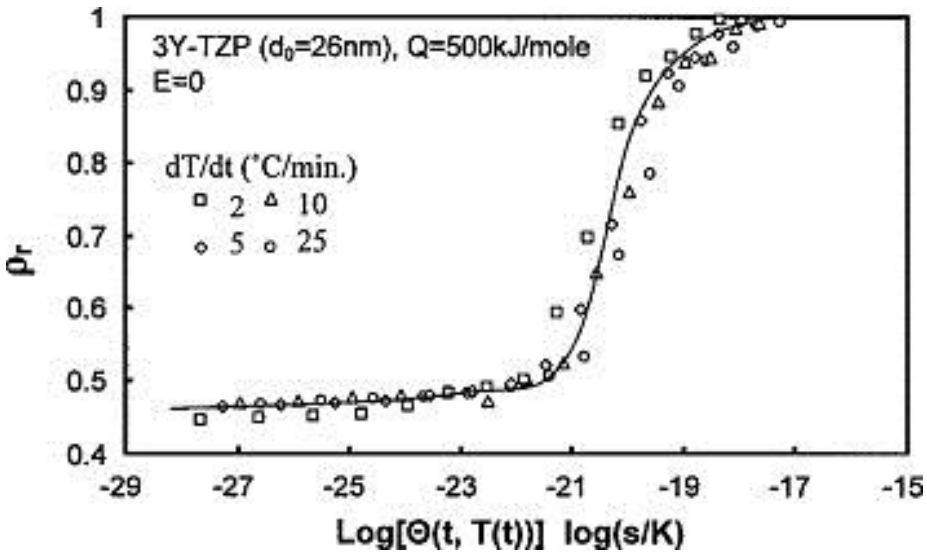

Fig.4.18 Relative density vs log $\theta = \int_0^t \frac{1}{T} \exp\left(\frac{-Q}{RT}\right) dt$ for the sintering tests without field and with various heating rates. Adapted from Di Yang, Conrad [4.15].

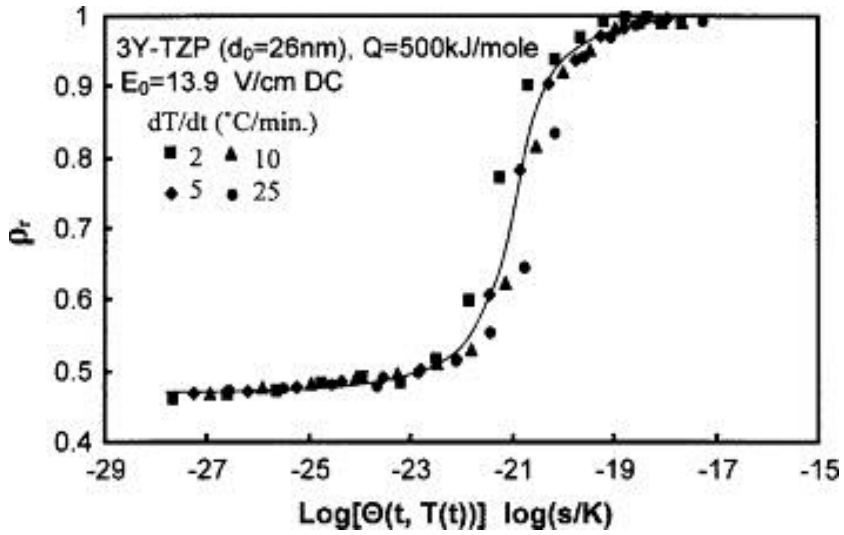

Fig.4.19 Relative density vs log $\theta = \int_0^t \frac{1}{T}\exp\left(\frac{-Q}{RT}\right) dt$ for the sintering tests with dc field E_0=14 V/cm and with various heating rates. Adapted from Di Yang, Conrad [4.15].

All of the above considerations thus lead to the conclusion that the major effect of an electric field on retarding grain growth in 3Y-TZP is through its effect on the pre-exponential of the governing Arrhenius-type equation rather than that on the activation energy Q.

4.1.5 Electric resistivity

It is well-known that polycrystalline yttria-stabilized zirconia has a relatively high ionic conductivity, which makes this material attractive for solid oxide fuel cells (SOFCs) and sensors [4.17,4.18]. The conductivity however decreases with decrease in grain size, which is attributed to the fact that the grain boundaries have a higher resistivity than the grain interior [4.17-19]. Information on the effect of grain size (whose growth during sintering is retarded by an electric field) on the bulk resistivity (ρ_Ω) of 3Y-TZP is thus desirable from both a technological and scientific viewpoint. To obtain ρ_Ω, it is recognized that the ionic conductivity (σ_Ω) of ceramics obeys Ohms law, which then gives for the bulk resistivity

$$\rho_\Omega = (\sigma_\Omega)^{-1} = E/j \qquad (4.4)$$

where E is the applied electric field and j=I/A is the current density, I being the ionic electric current, and A=$A_0[(1+\epsilon_z)^2\rho_r]^{-1}$ the effective specimen cross section area, with A_0 being that following binder burn-out.

Plots of ρ_Ω (=E/j) (based on the values of E and I in Figs. 4.3 and 4.4) vs the applied field E for dc and ac fields are given in Figs. 4.20 and 4.21, respectively. To be noted are the following: (a) the form of the curves is similar for the two fields types, i.e. ρ_Ω increases with E to ~ 20-25 V/cm and then becomes relatively independent of E with further increase to ~ 65-70 V/cm, i. e. the reciprocal of ρ_Ω(the conductivity $\sigma_\Omega = \rho_\Omega^{-1}$)vs field strength E has a form similar to that for the effect of E on grain size, see Fig.4.6.

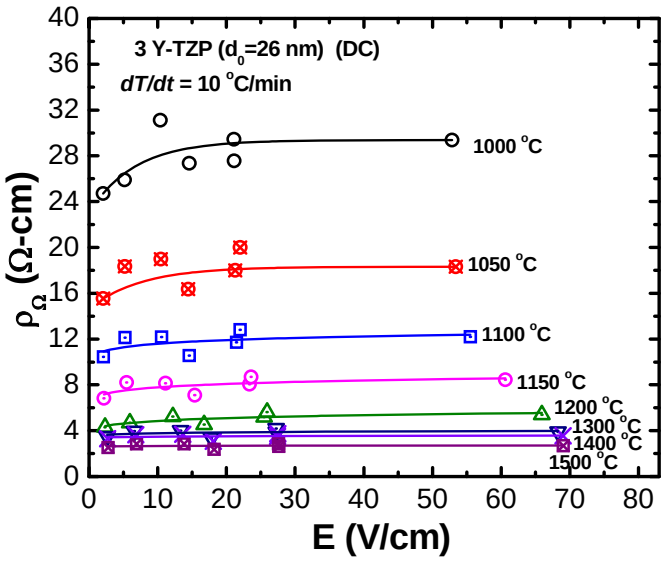

Fig.4.20 The bulk resistivity ρ_Ω(DC) vs the applied DC field strength E(DC) as a function of the attained sintering temperature.

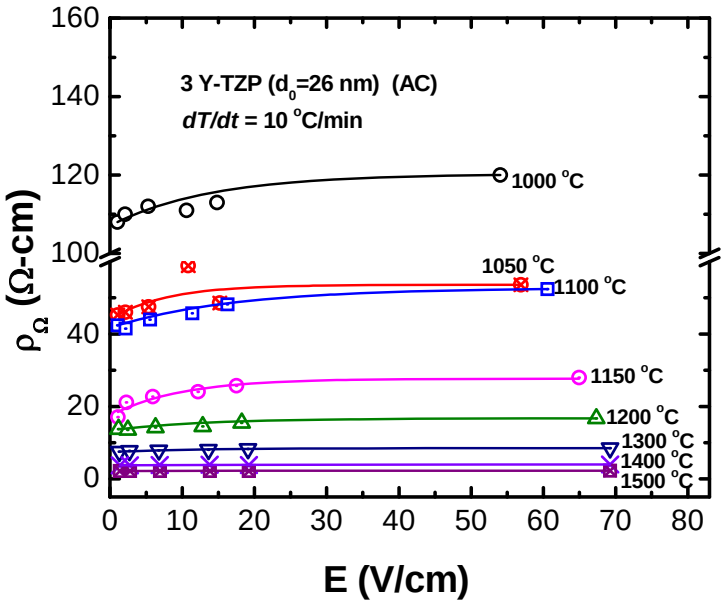

Fig.4.21 The bulk resistivity ρ_Ω(AC) vs the applied AC field strength E(rms) as a function of the attained sintering temperatures.

Comparing the bulk resistivity with ac field (ρ_Ω(AC)) in Fig. 4.21 with that for dc field (ρ_Ω(DC)) in Fig. 4.20, we find for a constant E that ρ_Ω(AC) > ρ_Ω(DC) at all, but the highest sintering temperatures. The variation in the ratio ρ_Ω(AC) / ρ_Ω(DC) with sintering temperature as a function of the field strength is shown in Fig.4.22. It is seen that the ratio is relatively independent of the applied field strength, but decreases from ~4 at 1000 ^{o}C to 0.8 at 1500 ^{o}C.

Plots of ρ_Ω vs the reciprocal of the mean grain size $\bar{d}$ (varied electric field employed) as a function of temperature were given in Figs. 4.23 and 4.24. To be noted is that the resistivity of both AC field and DC field is temperature dependent, and slightly electric field dependent, if any.

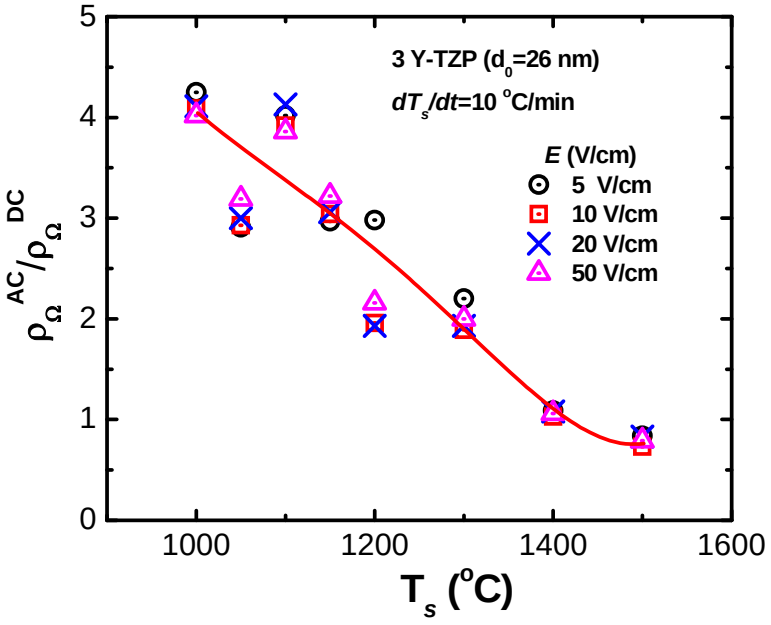

Fig.4.22 The ratio of the bulk resistivity during the sintering with AC field (ρ_Ω(AC)) to that with DC field (ρ_Ω(DC)) vs the attained sintering temperature T_s as a function of the applied initial field strength E_0.

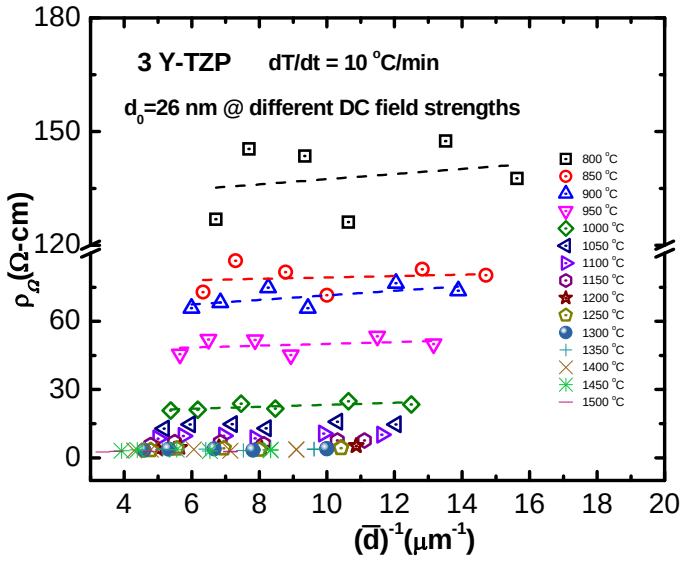

Fig. 4.23 The bulk resistivity ρ_Ω(DC) vs the reciprocal of grain size ($\bar{d}^{-1}$) as a function of the attained sintering temperatures.

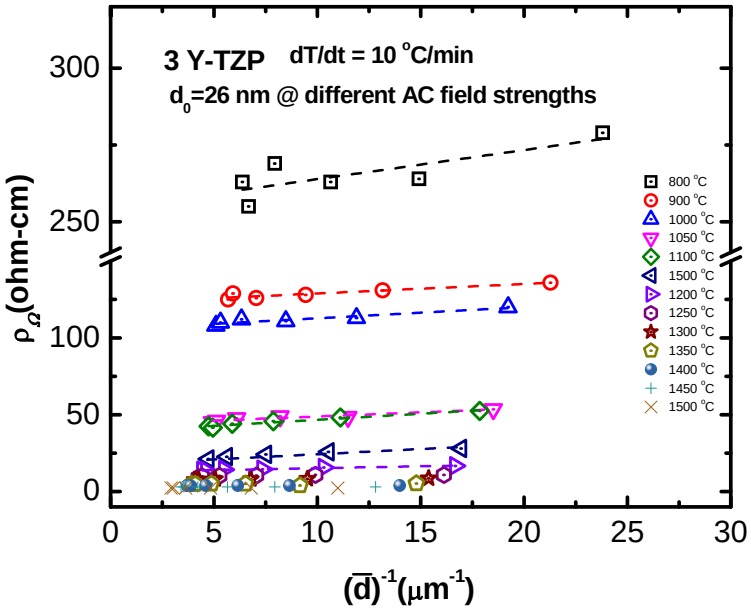

Fig. 4.24 The bulk resistivity ρ_Ω(AC) vs the reciprocal of grain size ($\bar{d}^{-1}$) as a function of the attained sintering temperatures.

4.1.6 Joule heating

The increase in temperature ΔT_J due to Joule heating measured by the embedded Pt-PtRh thermocouple which occurred during sintering with an applied initial electric field E_0 = 14 V/cm and heating rate of 10 °C/min is presented vs the electric power W=VI in Fig.4.25. The listed temperatures on the plot are the increasing sintering temperatures at which the Joule heating was measured. To be noted in Fig. 4.25 is that ΔT_J is proportional to W, i. e. $\Delta T_J \approx \alpha_J W$ with α_J= 1°C per watt.

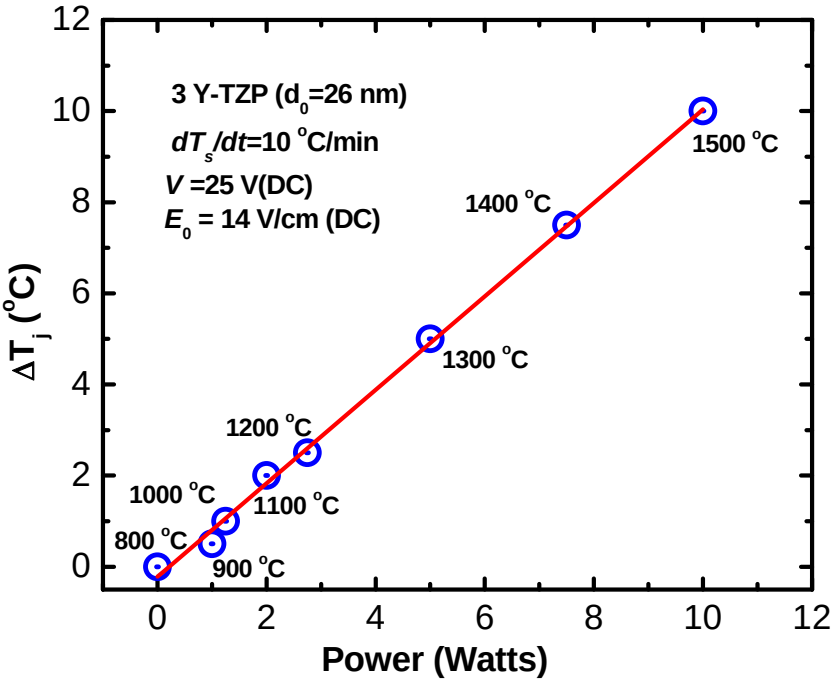

Fig.4.25 The increase in temperature ΔT_j due to Joule heating during sintering with a constant applied voltage of 25 V vs the corresponding electric powder W =IV, shown are the temperatures at which the current I was measured.

4.2 Effect of electric field on grain growth during isothermal annealing and related factors

4.2.1 Grain growth kinetics

Plots of ρ_r, $\bar{d}$ and electric current I without and with dc electric field E= 18 V/cm vs annealing time t_a at 1300 °C and 1400 °C are presented in Fig.4.26. To be noted are that: (a) ρ_r, $\bar{d}$ and I all increase with time at both temperatures, (b) the grain growth curves are parabolic in form and (c) the values of $\bar{d}$ with E are smaller than without.

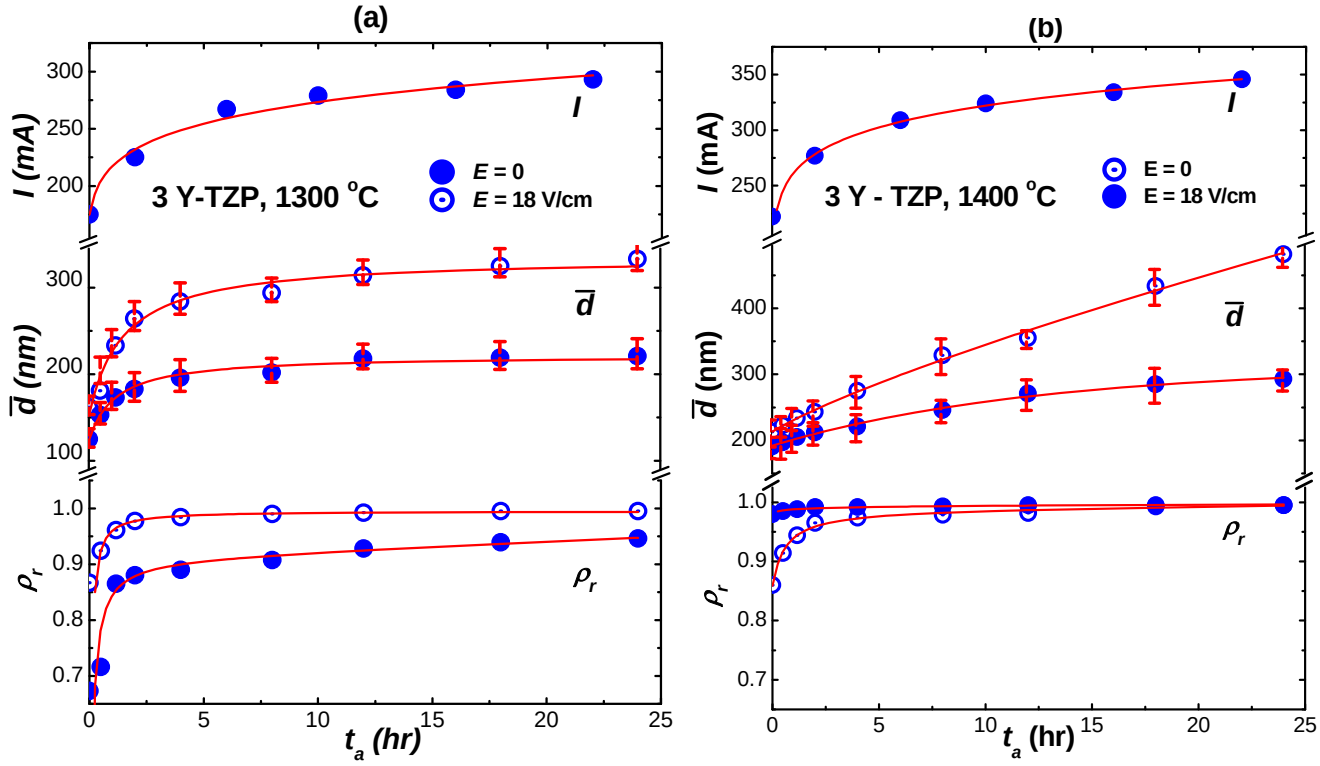

Fig.4.26 ρ_r, $\bar{d}$ and I vs annealing time for specimens annealed with E=0 and with E =18 V/cm at: (a) 1300 °C and (b) 1400 °C.

Since it is well-established that yttria segregates to the grain boundaries in 3Y-TZP [4.17-20], solute drag is the generally considered to be the governing grain growth rate mechanism[4.21]. Theoretical considerations give for this mechanism [4.22, 4.23]

$$\dot{d} = P^m M = \frac{AD}{kT}\left(\frac{\alpha\gamma_b}{d}\right)^m \qquad (4.5)$$

where $\dot{d}$ is the grain growth rate, $P = \alpha\gamma_b/d$ is the capillary driving force with $\alpha \approx 2$, $\gamma_b$the grain boundary energy and d the grain size. $M = AD/kT$ is the mobility with A a constant and D the diffusion coefficient of the rate controlling ion. m is the so-called driving force exponent, which has a value of one at both low and high values of $\dot{d}$ and appreciably larger values in between, i.e., in the so-called "transition regime" m with the values of 1-4 have been reported for grain growth in 3Y-TZP without an electric field[4.24].

In keeping Eq. 4-5 a plot of of $log\dot{\bar{d}}\ vs\ log\bar{d}$ of the isothermal grain growth curves in Fig.4.26 is presented in Fig. 4.27. The bar over d designates that the measured grain sizes are mean linear intercept values. To be noted in Fig.4.27 is that the slopes of the lines give m values ranging from 1 to 15. The value of 15 is much higher than the values (m=1-3) generally reported in the literature for 3 Y-TZP. Values larger than 1or 2 are typical of the "transition regime" in the solute drag theory [4.22, 4.23]. Also to be noted in Fig.4.27 is that at a constant $\dot{\bar{d}}$ the ratio of the grain size $\bar{d}_E$ with field to that without (d), *i.e.* $\bar{d}_E/\bar{d}$ ranges between 0.5 and 0.68. These values of d_E/d are in accord with the average for the effect of E_a(DC) on grain size during sintering and plastic deformation, namely $d_E/d \approx 0.60$ relatively independent of temperature [4.25]. Taking $\gamma_{b,E}/\gamma_b^0 = d_E/d = 0.60$ and that A and D are not significantly influenced by the field [4.25], the resulting plot of $\log\dot{\bar{d}}\ vs\ log\ P/\alpha$ is

shown in Fig.4.28, It is seen that the data points with the applied field now closely match those without.

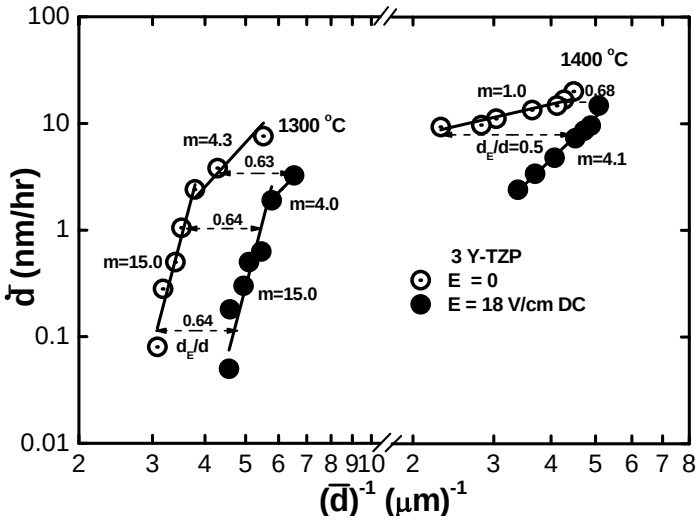

Fig. 4.27 Log grain growth rate $\dot{\bar{d}}$ vs log grain size $\bar{d}$ for annealing tests on 3Y-TZP at 1300 °C and 1400 °C without and with an applied DC electric field E=18 V/cm.

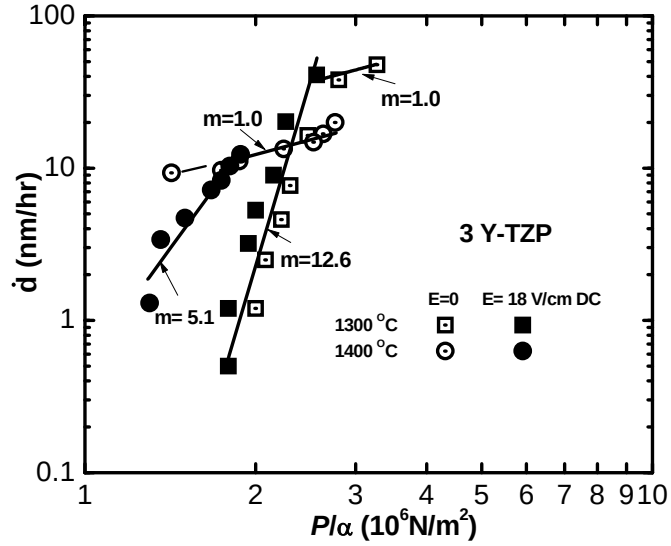

Fig.4.28 Log grain growth rate $\dot{\bar{d}}$ vs log driving force P/α for annealing 3 Y-TZP at 1300 °C and 1400 °C without (open symbols) and with (filled symbols) electric field E=18 V/cm. $P = \alpha\gamma_b/d$ and $\gamma_b^E = 0.6\gamma_b^0$; m=slope

4.2.2 Grain stereology

An example of the microstructure showing the reduction in grain size which occurred with the application of dc electric field during isothermal annealing is presented in Fig.4.29. The grains are relatively equiaxed both with and without field. SEM micrographs and corresponding grain size distributions (GSDs) during the isothermal annealing are shown in Fig. 4.30. They further indicate that the grain shape is isotropic and that the GSD is approximately log-normal. Fig.4.31 shows that the field had no significant effect on the GSD, which again is in accord with the Bitti-Di Nunzio model [4.14]. The stereology parameters pertaining to the grain size in isothermally annealed 3Y-TZP is shown in Table 4.2.

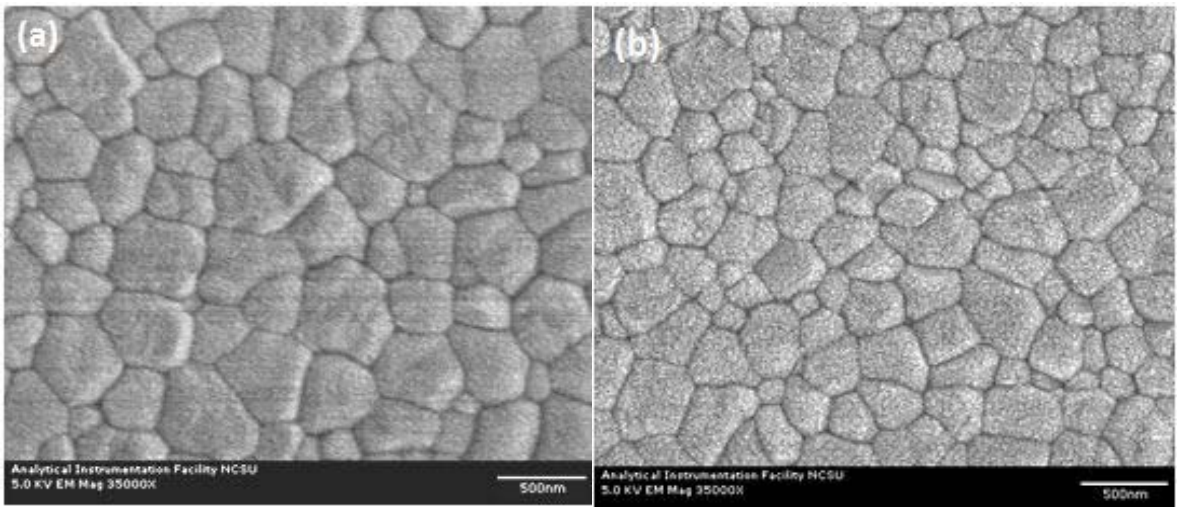

(a) $\bar{d}$ = 314 nm, (b) $\bar{d}_E$ = 218 nm

Fig.4.29 SEM micrographs of specimens annealed for 12 hr at 1300 ^{o}C: (a) E =0 and (b) E_0= 14 V/cm.

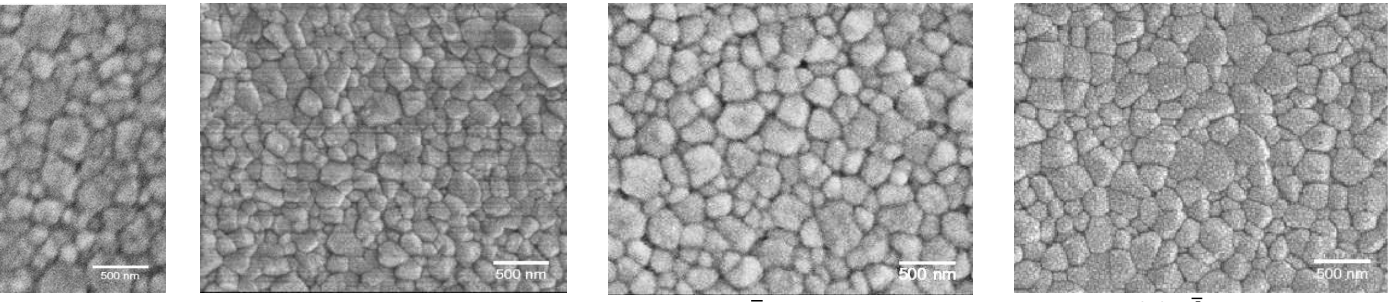

94 nm (b) $\bar{d}$= 152 nm (c) $\bar{d}$= 211 nm (a) $\bar{d}$= 190 nm

EM micrographs and the corresponding grain size distribution at the middle location in sintered specimens with: and (c) E =0 @, respectively; (b) and (d) E_0 =14 V/cm @ 1300 °C and 1400 °C, respectively.

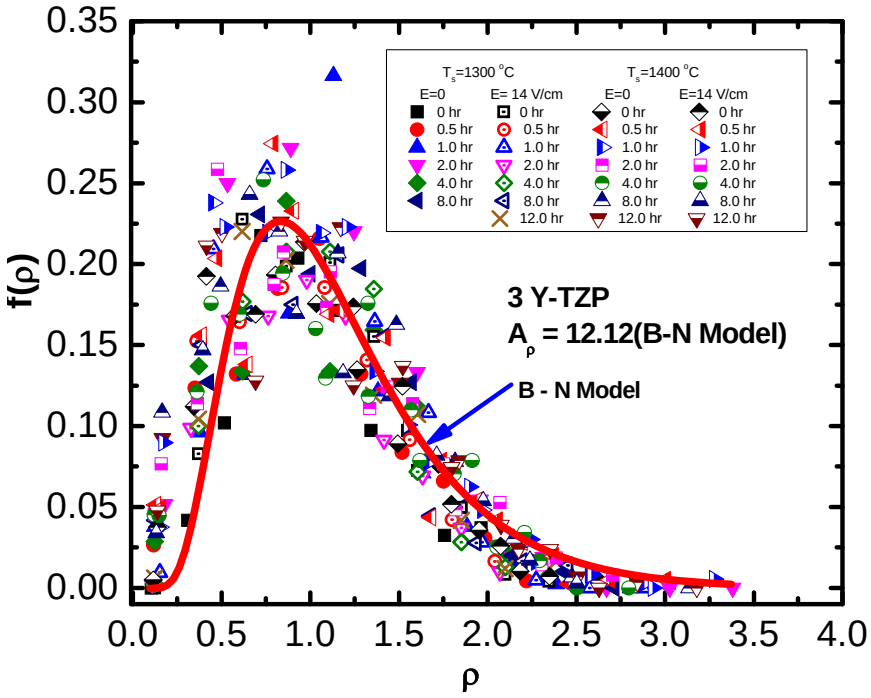

Fig. 4.31 Fit of the grain size distribution for isothermal annealing (1300 °C and 1400 °C with dc field and without) to the Bitti-Di Nunzio grain coarsening model.

Table 4.2 Stereology parameter pertaining to the grain size in isothermally annealed 3Y-TZP

T (^{o}C)	E (V/cm)	Location[(a)]	N[(b)]	$\bar{d}$ (nm)	d_{med} (nm)	$d_{med}/\bar{d}$	d_p (nm)	$d_p/\bar{d}$	d_{max} (nm)	$d_{max}/\bar{d}$	$f(d_p)$	R_A
1300	0	U(+)	134	192	189	0.98	185	0.96	411	2.14	0.20	1.04
		M	125	211	209	0.99	146	0.69	417	1.98	0.23	1.00
		L(-)	135	197	175	0.89	115	0.58	459	2.33	0.19	1.14
		C	394	200	192	0.96	161	0.81	459	2.30	0.19	1.05
	14DC	U(+)	145	177	164	0.93	176	0.99	504	2.85	0.25	1.06
		M	136	194	186	0.96	208	1.07	463	2.39	0.19	1.07
		L(-)	146	176	161	0.91	99	0.56	395	2.24	0.18	1.07
		C	427	182	168	0.92	176	0.97	504	2.77	0.21	1.00
1400	0	U(+)	72	201	200	1.00	154	0.77	400	1.99	0.24	1.00
		M	76	190	200	1.05	132	0.69	400	2.11	0.20	1.02
		L(-)	75	188	200	1.06	154	0.82	400	2.13	0.33	1.16
		C	223	193	200	1.04	147	0.76	400	2.07	0.26	1.05
	14 DC	U(+)	157	158	147	0.93	161	1.02	357	2.26	0.24	1.15
		M	169	152	146	0.96	111	0.73	317	2.09	0.25	1.04
		L(-)	148	171	167	0.98	99	0.58	396	2.32	0.20	1.01
		C	484	160	150	0.94	99	0.62	396	2.48	0.23	1.02

Notes: (a) U =upper, M=middle, L =lower, C = combined. (b) N = number of measurements.

4.2.3 Grain boundary resistivity: Brick layer model

Of both scientific and technological interest is grain boundary resistivity ρ_b^* and the governing mechanism. Impedance spectroscopy (IS) and the 4-probe method are commonly used for this purpose. Assuming that the grains are cubic in form ("brick layer model" [4.26]) IS measurements give for the bulk resistivity in YSZ

$$\rho_{bulk} = \rho_g + \rho_b^* \delta_b / d \qquad (4.6)$$

where ρ_g is the resistivity of the grain interior, ρ_b is the so-called " specific grain boundary resistivity, $\delta_b \cong 3 - 10$ nm is the GB width including the space charge zone and d is the grain size. IS measurements on YSZ give $\rho_b/\rho_g \cong 10^1 - 10^3$. An alternative method was used by us to determine the grain boundary resistivity ρ_b from the isothermal annealing data

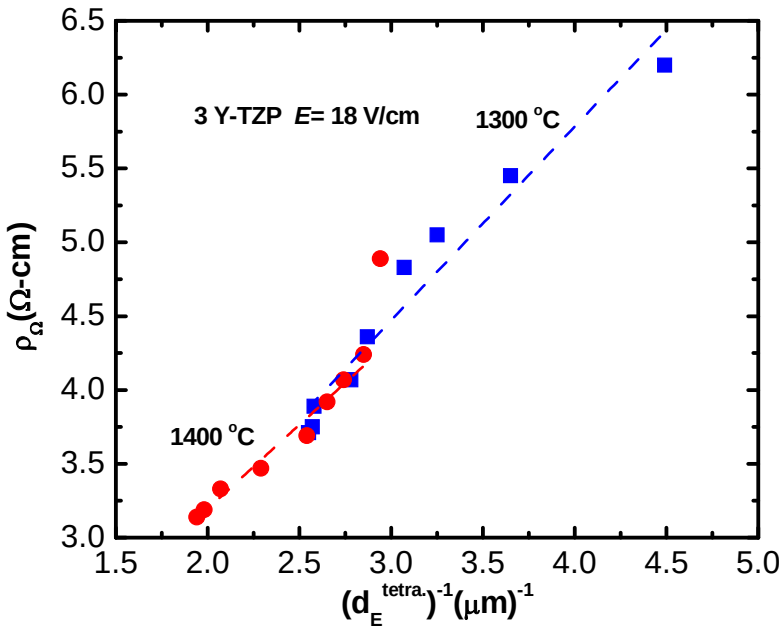

Fig. 4.32 Bulk resistivity ρ_Ω vs the reciprocal of the 3-D grain size $d_{tetra.} = 1.78\bar{d}$ in 3 Y-TZP during isothermal annealing.

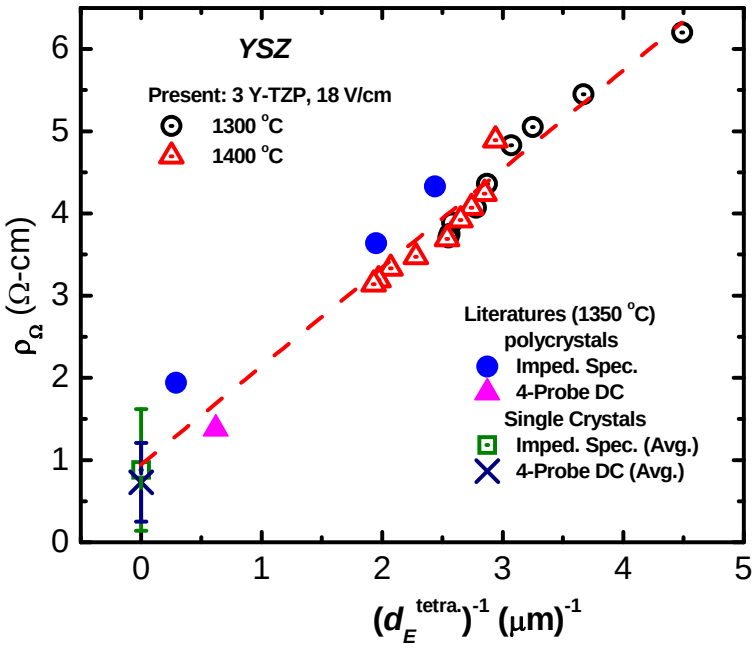

Fig. 4.33 Bulk resistivity ρ_{Ω} vs the reciprocal of the 3-D grain size $d^{tetra.} = 1.78\bar{d}$ in 3 Y-TZP during isothermal annealing. Also combined with the datas for single [4.33-38] and polycrtsals [4.29-32].

in Fig.4.26. For this we took the bulk resistivity $\rho_{bulk} = E/j$(where E is the applied field and j =I/A the current density) and $d^{tetra.} = 1.78\bar{d}$[4.27]. A plot of ρ_{bulk}vs $d_{tetra.}^{-1}$ is presented in Fig. 4.32. The least-squares values of the intercept and slope of the line for the measurements at 1300 ^{o}C is 0.54 ohm-cm and 1.31 (ohm-cm)μm respectively with a correlation coefficient(cc) of 0.98, and that at 1400 ^{o}C is 0.91 ohm-cm and 1.14 (ohm-cm)μm respectively with cc =0.99. Employing Eq.4.5 and taking δ_b=10 nm [4.28] the slope of the line gives ρ_b=131 and 114 ohm-cm at 1300 ^{o}C and 1400 ^{o}C, respectively. Further, taking the intercept to be ρ_g, one obtains ρ_b/ρ_g= 257 and 124, which is in reasonable accord with that reported for IS measurements. This is further shown in the plot of ρ_{bulk}vs $d_{tetra.}^{-1}$of values

from IS and 4-probe methods on polycrystals and single crystals of YSZ, see Fig.4.33, which gives the least-squares values of the intercept and slope of the line to be 0.98 ohm-cm and 1.20 (ohm-cm)μm with a correlation coefficient of 0.98. Employing Eq.4.6, this value of ρ_b= 120 ohm-cm by. To be noted is that the resistivity measurements from the isothermal annealing tests are in good accord with that of IS and 4-probe.

Knowing the magnitude of j and ρ_b, the electric field E_b across the grain boundary width can be calculated using the conventional ohmic equation

$$E_b = \rho_b \, \mathrm{j} \qquad (4.7)$$

Taking the values ρ_b=131 and 114 ohm-cm from the annealing tests at 1300 ^{o}C and 1400 ^{o}C and the values of j calculated from the measured values of the current I, the magnitude of E_b and the ratio E_b/E_a as a function of grain size are presented in Figs. 4.34. The magnitude of E_b at 1300 ^{o}C increase from 382 V/cm to 639 V/cm and in turn the ratio E_b/E_a from 21.25 to 35.52, respectivelywith increase in grain size from ~0.2 to ~ 0.5 μm, using the corresponding values of the electric current. In the meanwhile, The magnitude of E_b and in turn the ratio E_b/E_a at 1400 ^{o}C increase from 452 V/cm to 657 V/cm and from 23.43 to 36.48, respectively.

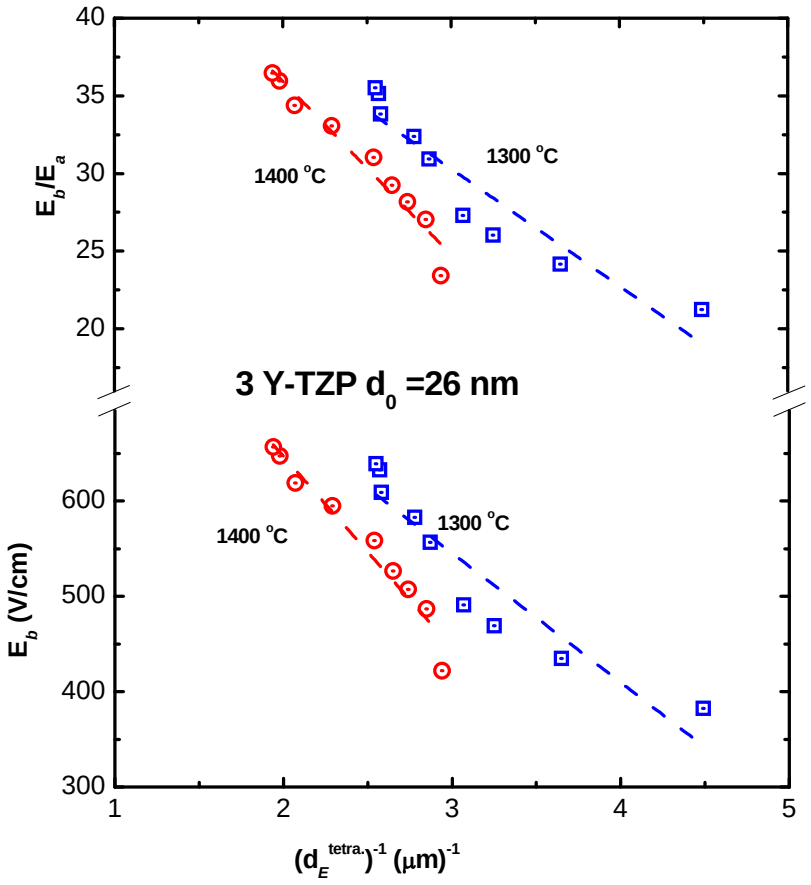

Fig.4.34 Magnitudes of E_b and the ratio E_b/E_a vs $d_{tetra.}{}^{-1}$ at 1300 °C and 1400 °C with dc electric field of 18 V/cm.

4.3 References

[4.1] H. Conrad, Di Yang, : Mater. Sci. Engr., A528(2011)8523-8529.

[4.2] H. Conrad, Di Yang, : Mater. Sci. Eng. A 559(2012)591-594.

[4.3] M. Mazaheri, A. Simihi, M. Dourandish, F. Golestanin-Fard, :Ceram. Int., 35 (2009) 547-554.

[4.4] T. G. Nieh, J. Wadsworth, : J. Am. Ceram. Soc., 72(1989)1469-1472.

[4.5] G. S. A. M. Theumissen, A. J. A. Winnubst, A. J. Burggrat, : J. Eur. Ceram. Soc, 9(1992)251-263.

[4.6] T. Stoto, M. Nauer, C. Carry, : J. Am. Ceram. Soc., 74(1991)2615-2621.

[4.7] T. Sakuma, Y. Yoshizawa, : Mater. Sci. Forum,94-96(1992)865-870.

[4.8]H. Conrad, Di Yang, : Phil. Mag., 90(2010)1141-1157.

[4.9] S. Ghosh, A. H. Chokshi, P. Lee, R. Raj, : J. Am. Ceram. Soc., 92(2009)1856-1859.

[4.10] H. Conrad, : Emerging Mater. Res., ICE, 1(2012)11-15

[4.11] Di Yang, H. Conrad,: Scripta Mater., 43(2010)328-331.

[4.12] J. Obare, W. D. Griffin, H. Conrad, : J. Mater. Sci., 47(2012) 5141-5147.

[4.13] J. Obare, J. Wang, H. Conrad, : Scripta Mater., 68(2013)111-113.

[4.14]R. Ricci Bitti, P. E. Di Nunzio, : Scripta Mater., 39(1998)335-340.

[4.15] Di Yang, H. Conrad, : Mater. Sci. Eng. A528 (2011) 1221-1225.

[4.16] H. Su, D. L. Johnson,: J. Am. Ceram. Soc., 79(1996)3211-3217.

[4.17] J. Wang, H. Conrad, in “Grain oundary resistivity in yttria-stabilized zirconia”, Processing and Properties of Advanced Ceramics and Composites V: Ceramic Trans. Vol

240, eds. N. P. ansal, J. P. Singh, S. Ko, R. Castro, G. Pickrell, N. J. Manjooran, M. Nair, G. Singh, Wiley, New York (June 2013)pp.175-188.

[4.18] M. C. Martin, M. I. Mecartney,: Solid State Ionics, 161(2003)67-79.

[4.19] S. Hui, J. Roller, S. Yick, X. Zhang, C. Decès-Petit, Y. S. Xie, R. Maric, D. Ghosh, : J. Power Sources, 172(2007) 493-502.

[4.20]S. H. Chu, M. A. Seitz, :J. Sol. State Chem., 23(1978)297-314.

[4.21] R. Chaim, Mater. Sci. Eng. A 486(2008)439-446.

[4.22] J .W. Cahn, : Acta Metall., 10(1962)789-798.

[4.23] R. A. Vandermer,: Acta Metall., 15(1967)447-458.

[4.24] J. Zhao, Y. Ikuhara, T. Sakuma, J. Am. Ceram. Soc., 81(1998)2087-2092.

[4.25] H. Conrad, Di Yang, : Mater. Sci. Eng. A, 528(2011)8523-8529.

[4.26] J. Fleig, J. Maier,: J. Euro. Ceram. Soc., 19(1999)693-696.

[4.27] M. I. Mendelson, : J. Am. Ceram. Soc., 52(1969)443-446.

[4.28] K. Matsui, H. Yoshida, Y. Ikuhara, : Acta Mater., 56 (2008)1315-1325.

[4.29] X. Guo, J. Maier, :J. Electrochem. Soc., 148E(2001)121-126.

[4.30] S. P. S. Badwal, J. Drennan, : J. Mater. Sci., 22(1987)3231-3239.

[4.31] T. Uchikoshi, Y. Sakka, K. Hiraga, :Jnl. Electroceram, 4:S1(1999)113-120.

[4.32] Y. Shiratori, F. Tietz, H. Penkalle, J. He, D. Stöver, : J. Power Sources 14(2005)832-842.

[4.33] J. D. Solier, I. Cachadiña, A. Dominguez-Rodriguez, :Phys. Rev. B 48(1993-II)3704-3712.

[4.34] S. Ikeda, O. Sakurai, K. Uematsu, N. Mizutani, M. Kata, :J. Mater. Sci. 206 (1985)

4593-4600.

[4.35] A. L. Dragoo, C. K. Chiang, A. D. Franklin, J. Bethin, A grain boundary in yttria-stabilized zirconia, in Science and Technology of ZrO_2 (1993) pp.184-195.

[4.36] X. Guo, E. Vasco, S. Mi, K. Szot, E. Wachman, R. Waser, : Acta Mater. 53(2005) 5161-5166.

[4.37] A. Pimenov, J. Ullrich, P. Lukenheimer, A. Loidl, C. R*ü*scher, : Solid State Ionics 109(1998)111-117.

[4.38] I. Kosacki, C. Rouleau, P. Becher, J. Bentley, D. Lowndes, : Solid State Ionics, 176 (2005)1319-1326.

CHAPTER FIVE

5.0 DISCUSSION

5.1 Model and physical mechanisms: Grain growth retardation by an applied electric field

It is well-known that grain size is an important microstructure parameter in the processing and properties of ceramics [5.1]. It was discovered by Yang and Conrad [5.2] and subsequently confirmed by Ghosh et al. [5.3] that a modest applied dc electric field retards grain growth in 3 mol% yttria-stabilized zirconia (3YSZ). Subsequent work by Conrad and coworkers [5.4, 5.5] established that the retarding effect increased with field strength up to ~ 26 V/cm and then retained essentially constant to ~ 60 V/cm, the effect being similar in the processing methods of sintering, annealing and plastic deformation; see example of Fig.4.6. Furthermore, the retarding effect by the field was found to be relatively independent of temperature and porosity. Stereology studies gave that the field had no detectable influence on the grain shape nor on the grain size distribution [5.6,5.7]. Based on these characteristics it was proposed [5.4,5.5] that the retardation of grain growth in 3YSZ by an electric field results from a reduction in the capillary driving force (namely, the grain boundary energy) by the interaction of the field with the space charge at the grain boundaries.

A schematic of the energetics pertaining to the proposed mechanism is presented in Fig.5.1. To be noted is that the effect of the field is to give a decrease in ΔG_d, which corresponds to the driving force for grain growth, i.e., the GB energy (capillary energy). The evaluation of grain growth rate experimental data in terms of Eq. 4.5 generally only considers the forward ionic diffusion jumps, which give an increase in the grain size. The more rigorous thermodynamic absolute reaction rate theory considers the reverse jumps as well as

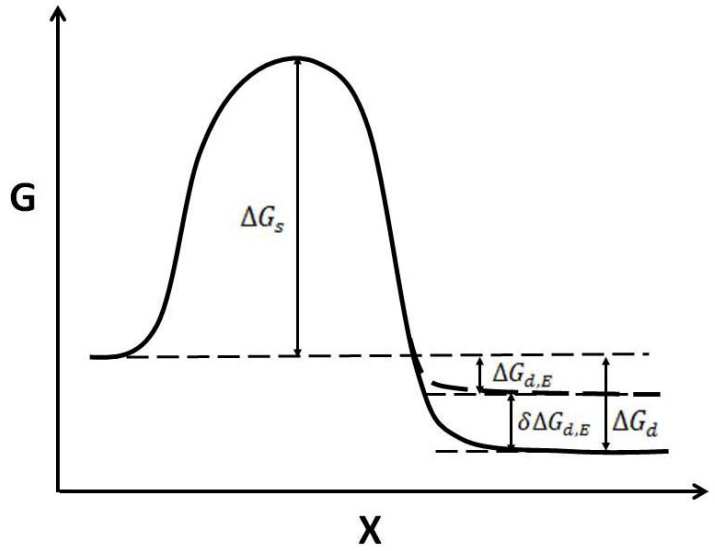

Fig. 5.1 Schematic of the absolute reaction rate theory applied to the effect of an electric field on grain growth in 3 Y-TZP. Adapted from Conrad [5.11].

the forward jumps [5.8, 5.9]. This gives for the grain growth rate

$$\dot{d} = \frac{A'_g}{kTd^m}\exp\left(-\frac{\Delta G_s}{kT}\right)\left[1-\exp\left(-\frac{\Delta G_d}{kT}\right)\right] \qquad (5.1)$$

Integration of Eq. 5.1 gives

$$d^n - d_0^n = \frac{A't}{kT}\exp(-\frac{\Delta G_s}{kT})[1-\exp\left(-\frac{\Delta G_d}{kT}\right)] \qquad (5.2)$$

where n=m+1 and d_0 is the grain size at t=0. Taking $\Delta G_s \neq$f(E) and $d^n \gg d_0^n$ one obtains for the effect of E on d

$$(\frac{d_E}{d})^n = [\frac{1-\exp(-\Delta G_{d,E}/kT)}{1-\exp(-\Delta G_d/kT)}] \qquad (5.3)$$

where $\Delta G_{d,E} = \Delta G_d - \delta\Delta G_{d,E}$ with $\Delta G_{d,E}$ being the decrease in ΔG_d by the field. Taking the experimental values d_E/d =0.4 for E = E_c (26 V/cm and $\Delta G_{d,E}$=0.064 ΔG_d[5.10]. Solution of Eq. 5.3 gives ΔG_d=0.36-0.54 eV for n=2 and 3 respectively. Taking the reasonable value

$$\gamma_b^0 = \Delta G_d/\Omega^{2/3} \qquad (5.4)$$

gives γ_b^0 =0.54-0.81 J/m^2 at 1250 ^{o}C, which is in reasonable accord with 0.67 J/m^2 reported by Tsoga and Nikolopoulus [5.11]. Further, assuming that γ_b^0 is mainly due to the space charge potential energy $e\emptyset_i$ one obtains

$$e\emptyset_i = \Delta G_d/Z \qquad (5.5)$$

where Z =3 is the valence of the yttrium ion. Inserting ΔG_d=0.36-0.54 eV into Eq. 5.5 gives $e\emptyset_i$=0.12-0.18 eV, which is within the range reported in the literature (0.1-1.0 eV).

In the rest of this chapter section, we develop a new electrostatic model for this mechanism and employ the annealing tests on 3 mol% yttria-stabilized zirconia polycrystals (3Y-TZP) at 1300 ^{o}C and 1400 ^{o}C to ascertain its validity.

New Electrostatic Model: Fig.5.1 presents the factors involved in our model. It was now well-established that yttria segregates to the grain boundary in polycrystalline yttria-stabilized zirconia (YSZ) [5.12-19]. A major factor proposed to be responsible for the segregation is the grain boundary space charge. In view of the segregation, it is generally considered that the mechanism governing grain growth rate in YSZ is "solute drag" [5.20]. Theoretical considerations give for this mechanism [5.21, 5.22] was presented as Eq.4.5. Employing this equation and assuming that a major effect of an applied electric field E on $\dot{d}$ is through a reduction in γ_b^0, and dividing the grain growth rate with an applied field $\dot{d}_E$ by that without ($\dot{d}$), one obtains

$$\frac{\dot{d}_E=\frac{A_E D_E}{k_B T}[\frac{(\gamma_b^0-\Delta\gamma_b^E)}{d_E}]^{m_E}}{\dot{d}=\frac{AD}{k_B T}[\frac{\gamma_b^0}{d}]^m} \qquad (5.6)$$

where $\Delta\gamma_b^E$ is the reduction in γ_b^0 by the applied field E. The subscript E in Eq.5.6 refers to the parameter with applied field and its absence without field. In prior work [5.4,5.5,5.23] it was found that the parameters A, D and m are relatively independent of E. Rearranging Eq.5.6 then gives for a constant temperature

$$\Delta\gamma_b^E \cong [1 - (\dot{d}_E/\dot{d})^{1/m}\,(d_E/d)]\gamma_b^0 \qquad (5.7)$$

The magnitude of $\Delta\gamma_b^E$ as a function of E at a constant T can thus be obtained experimentally from a knowledge of the values of γ_b^0 and the effect of E on the grain size ratio(d_E/d), i.e., the results in Fig.4.6. In our model we will take that γ_b^0 in YSZ consists of the sum of three major components (see Fig.5.2), namely

$$\gamma_b^0 = \gamma_b^\Sigma + \gamma_b^s + \gamma_b^e \qquad (5.8)$$

where γ_b^Σ results from the crystallographic misorientation between contacting grains, γ_b^s the

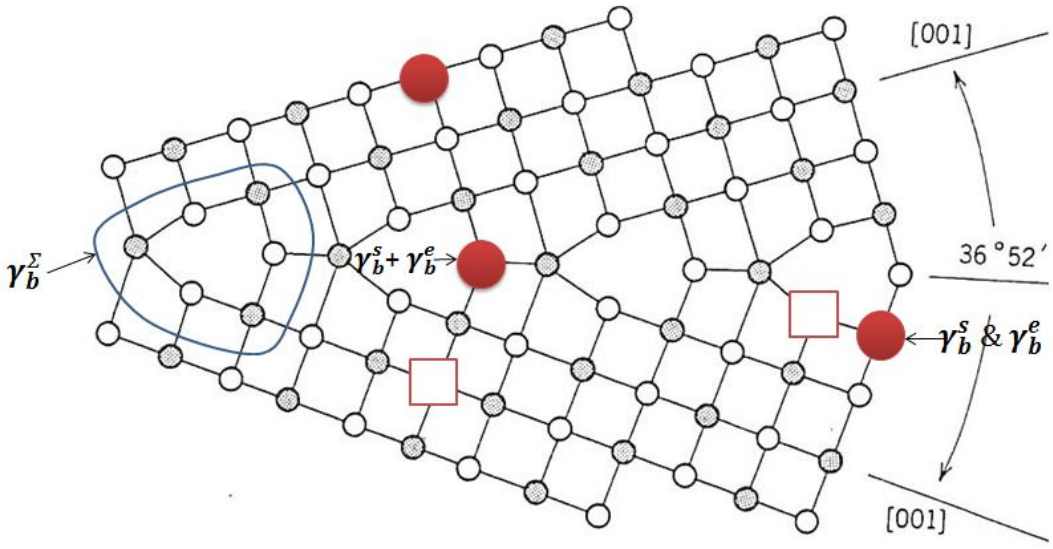

Fig. 5.2 Schematic of a large angle grain boundary in an ionic ceramic illustrating the three major contributions to the grain boundary energy.

ionic size misfit between the solute (yttrium) and solvent (zirconium) ions and γ_b^e the electrostatic (space charge) which results from the segregated, aliovalent yttrium ions at the GB.

A rough theoretical estimate of γ_b^Σ is [5. 24]

$$\gamma_b^\Sigma = \lambda_b^c \, k_B T/\Omega \qquad (5.9)$$

where λ_b^c is the width of the GB *core*, Ω the atomic volume of the host lattice and k_B Boltzmann's constant. Regarding the solute ion size misfit, estimates of the elastic strain energy U based on considerations by Eshelby [5.26, 5.27] are given in Table 5.1; included are the calculated magnitudes of U. Further, taking into account the number of solute ions in the total grain boundary width δ_b(core plus the dual Debye space charge zones) one obtains for the size misfit energy per unit GB area

$$\gamma_b^s \approx U\delta_b \, \bar{C}_b/\Omega \qquad (\text{J/m}^2) \qquad (5.10)$$

where $\bar{C}_b$ is the integrated average solute ion concentration within the total GB width δ_b.

Table 5.1 Estimates of the ionic size misfit energy U in yttria-stabilized zirconia.

Authors	Equation	Ref.	U (10^{-21}N-m)
Yan et al [5.25]	$U = \frac{6\pi {r_1}^3 (\frac{r_2 - r_1}{r_1})^2 B}{(1 + 3B/4\mu)}$	Eshelby [5.26]	5.7
Hwang, Chen [5.12]	$U = \frac{2}{9}\mu\Omega[\frac{(1+\nu}{(1-\nu)}]\Gamma^2$	Eshelby [5.27]	6.9
		Avg.	6.3

Notes:
μ =shear modulus (80 GPa); B= bulk modulus (174 GPa); γ=Poissons ratio (0.3).
r_1=ionic radius of the host (0.084 nm); r_2= ionic radius of the solute (0.102 nm); Γ= Vegards slope for volume misfit (0.077);
Ω= molecular volume ($3.5\times 10^{-29} m^3$).

Regarding the electrostatic component of the GB energy γ_b^e, the number of *excess* segregated aliovalent solute ions per unit GB area is

$$N_b^S = \delta_b \overline{\Delta C}_b / \Omega \qquad (m)^{-2} \qquad (5.11)$$

where $\overline{\Delta C}_b$ is the integrated average *excess* segregated solute concentration. The corresponding electrostatic energy per unit GB area is then

$$\gamma_b^e = N_b^S Ze\emptyset = \delta_b \overline{\Delta C}_b \, Ze\emptyset/\Omega \qquad (eV/m^2) \qquad (5.12)$$

Assuming that $\Delta\gamma_b^E$ (in Eq.5.2) results from the reduction in γ_b^e by the applied field bias and taking β as the average orientation between the applied electric field vector and the pertinent GB curvature, Eq.5.12 gives for the applied electric field $E = E_c$

$$\Delta\gamma_b^E = \beta\gamma_b^e = \beta\delta_b \overline{\Delta C}_b Ze\,\emptyset/\Omega \qquad (eV/m^2) \qquad (5.13)$$

where β can have a value of the order of ~ 0.5 to unity. Taking $E = E_c$ and rearranging Eq.5.13 gives for the space charge potential energy due to the segregated aliovalent ions

$$Ze\emptyset = \Delta\gamma_b^{E_c}\Omega/\beta\delta_b\overline{\Delta C}_b \qquad (5.14)$$

where E_c is the critical field shown in Fig.4.6.

The pertinent plots of ρ_r and $\bar{d}$ vs annealing time t_a without and with applied electric field (E= 18 V/cm) at 1300 ^{o}C and 1400 ^{o}C are presented in Fig.4.26. To avoid the value of the driving force parameter *m* in the solution of Eq.5.7 one needs to know the magnitude of the GS ratio $\bar{d}_E/\bar{d}$ at a constant grain growth rate ratio $\dot{\bar{d}}/\dot{d}$. For this, values of $\dot{\bar{d}}_E/\dot{\bar{d}}$ were determined by taking the slopes of the $\bar{d}$ vs t_a curves in Fig.4.26. The slopes (derived manually) are plotted vs the reciprocal of the grain size $(\bar{d})^{-1}$ in Fig.5.3. The hatched region defines where the magnitude of $\bar{d}_E/\bar{d}$ can be obtained at a constant $\dot{\bar{d}}_E/\dot{\bar{d}}$, and in turn the

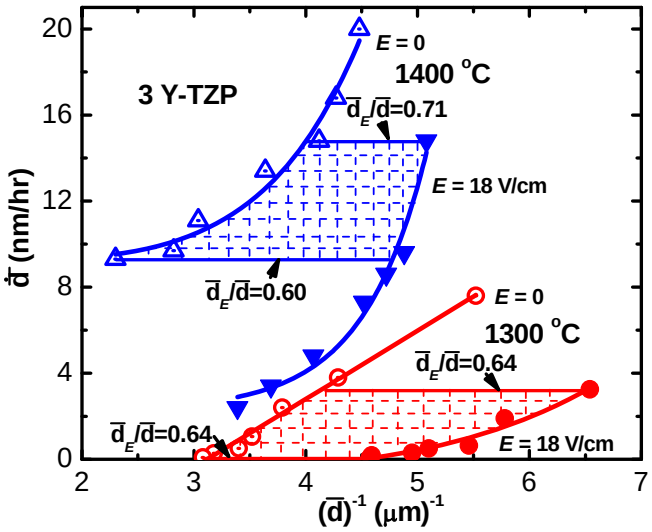

Fig. 5.3 Grain growth rate ($\dot{\bar{d}}$) vs the reciprocal of the grain size $(\bar{d})^{-1}$ for the present annealing tests without and with applied dc electric field $E = 18$ V/cm at 1300 °C and 1400 °C.

corresponding constant driving force for grain growth. Also shown in Fig.5.3 are the values of $\bar{d}_E/\bar{d}$ at constant $\dot{\bar{d}}$, which values range from 0.60 to 0.71 with an average of 0.65. Of significance is that these values of d_E/d (E=18 V/cm) are in accord with those in Fig.4.6 obtained at this field strength for other processing conditions and by other means.

The GB energy components γ_b^{Σ} and γ_b^{s} represent atomic displacements, which are essentially independent of the applied electric field E. The effect of E on grain growth is therefore taken to be entirely through its influence on the electrostatic component γ_b^{e} as a result of the action of the field bias on the space charge potential $\emptyset$. The form of the $\bar{d}_E/\bar{d}$ vs E curve in Fig.4.6 thus gives that the regime $E \leq E_c$ corresponds to γ_b^{e} and that for $E > E_c$ corresponds to $(\gamma_b^{\Sigma} - \gamma_b^{s})$. γ_b^{s} is subtracted from γ_b^{Σ} because the ionic radius of Y^{3+} is larger than that of Zr [5.13]. Now, since d_E/d =0.4 at $E = E_c$, Eq.5.2 gives $\gamma_b^{e} = 0.6\gamma_b^{0}$ and

in turn $(\gamma_b^{\Sigma} - \gamma_b^{s}) = 0.4\gamma_b^0$. Based on these values we will compare the experimentally-derived GB energy components with predictions.

Regarding γ_b^{Σ}, employing Eq.5.9 and taking the reasonable value $\lambda_b^c = 2\Omega^{1/3}$($\Omega$=35×10^{-30}m^3) one obtains γ_b^{Σ}=0.42 J/m^{2}for the average test temperature T_{avg} = 1350 ^{o}C. Regarding γ_b^{s}, employing Eq.5.5 and taking U =6.3×10^{-21}N-m (Table 5.1), δ_b= 8 nm [5.19], $\bar{C}_b$=0.092 (core plus Debye zone [5.19]) and Ω=35×10^{-30}m^3 gives γ_b^{s}=0.13 J/m^2. The difference $(\gamma_b^{\Sigma} - \gamma_b^{s})$is 0.29 J/m^2, is thus in reasonable accord with that predicted for $E > E_c$ (Fig.4.6), namely that $(\gamma_b^{\Sigma} - \gamma_b^{s}) = 0.4\gamma_b^0$=0.24 J/m^2 at 1350 ^{o}C [5.11]. Regarding γ_b^{e}, according to Eq.5.13 $\Delta\gamma_b^{e}$ is proportional to $\Delta\gamma_b^{E}$, the latter being given by Eq.5.7. Employing Eq.5.8 and taking γ_b^0=0.61 J/m^2 [5.11] the effect of E on $\Delta\gamma_b^{E}$ at 1350 ^{o}C determined from the results in Figs. 4.6 and 5.3 is shown in Fig.5.4. To be noted is that in keeping with Fig.4.6 an approximately linear reduction in the GB energy by the applied field occurs up to the critical field E_c ≅26 V/cm, with no further effect at higher fields to 65 V/cm. The rate of reduction in γ_b^0 by the field $d\gamma_b^{E}/dE$ is 1.42×10^{-2} (J/m^2)(V/cm)$^{-1}$, and the total reduction at E=26 V/cm is ~0.37 J/m^2.

Of further interest, regarding the electrostatic grain boundary energy component γ_b^{e} is a comparison of the magnitude of the space charge potential obtained from the present isothermal annealing tests with that determined by impedance spectroscopy measurements and by atomic simulations. Taking for the parameters in Eqs.5.14 and 5.15, $\Delta\gamma_b^{Ec} = 0.60\,\gamma_b^0$ (Eq.5.8), γ_b^0=0.61 J/m^2(T_{avg} =1350 ^{o}C) [5.11], Ω=35×10^{-30}m^3, δ_b= 8 nm [5.19], $\overline{\Delta C}_b$=0.032 [5.19] and β =0.5, one obtains $Ze\emptyset$ = 0.66 eV. Taking Z =3 for the Y ions gives $e\emptyset$ =

Table 5.2 Comparison of the space charge potential $\emptyset_i$ obtained in the present isothermal grain growth tests with those by the absolute reaction rate (ARR) theory, by impedance spectroscopy (IS) and by atomic simulation (AS).

Authors	Material	Method	$d^{(1)}(\mu\text{m})$	T(^{o}C)	$\emptyset_i(V)$	$\delta_b^{(2)}$(nm)
Present	3 YSZ	Grain growth:$\dot{d}$=const.	0.1-0.5	800-1500	0.22	8.0
Conrad[5.5]	3 YSZ	Grain growth: ARR	0.1-0.5	800-1500	0.12-0.18	—
Verkerk et al [5.25]	8 YSZ	IS	0.28	600-1000	0.20-0.23	9.0
Guo, Maier [5.26]	8 YSZ	IS	16	200-800	0.25	~5.0
Guo [5.27]	8 YSZ	IS	1.4	400	0.26	3.5
Guo et al [5.28]	8 YSZ	IS	16	250-500	0.20-0.27	~4.0
Guo, Zhang [5.29]	3 YSZ	IS	0.12-1.3	250-600	0.18-0.24	5.6
Guo, Zhang [5.29]	8 YSZ	IS	0.25-13.5	450	0.21-0.27	4.8
Bingham et al[5.30]	6 YSZ	AS	<0.5	1700	0.15-0.22	1.7

Notes: (1) d= grain size; (2) δ_b= total grain boundary width.

$0.22\ eV$, which is in accord with the values obtained by impedance spectroscopy measurements [5.28-32] and atomic simulation [5.33]; see Table 5.2. Moreover, it is within

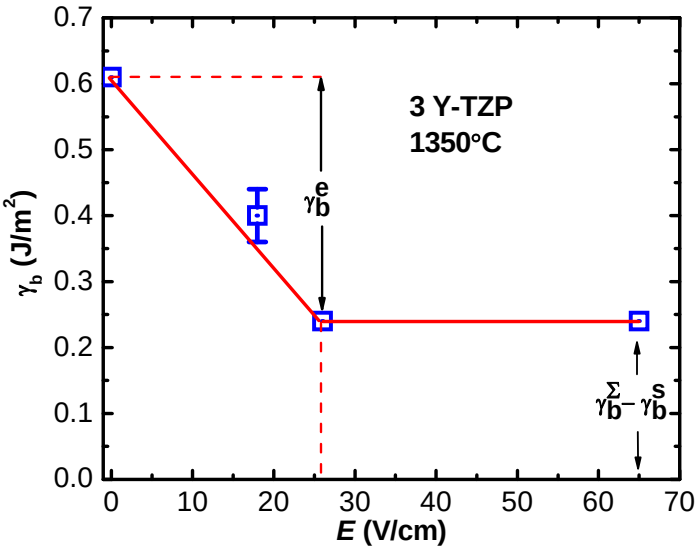

Fig. 5.4 Effect of the applied dc field on the grain boundary energy in 3 Y-TZP at T_{avg}=1350 ^{o}C.

the range reported for crystalline oxides in general [5.34-38]. This agreement provides support for the model proposed here for γ_b^e(Eqs. 5.8 and 5.9) whereby the applied electric field exerts a bias on the space charge potential which results from the segregation of Y^{+3} ions to the GBs; see Fig.5.5. It should also be mentioned that atomic simulation calculations [5.33, 5.39] gives that both yttrium ions and oxygen vacancies segregate to the GBs in ZrO_2 giving Y'_{Zr}- oxygen vacancy complexes. One such complex is $[Y'_{Zr} - V_o^{\cdot\cdot}]^{\cdot}$ $(e\emptyset \cong 0.4\ eV)$ which could be a factor of the magnitude of γ_b^e.

The contribution of the space charge $\emptyset_i$ to each of the components of γ_b^0 is obtained from cross plots of the results in Figs 5.4 and 5.5. The results are shown in Fig.5.6. This

figure shows the variation of γ_b with $\emptyset_i$ and therefore any physical property which is a function of γ_b (e.g. grain growth rate) will depend on the valence of the solute as well as its size misfit, which was found to be so for YSZ by Hwang and Chen [5.13]. Thus, the properties relating to γ_b can be varied by the addition of selected solutes and the application of an electric field.

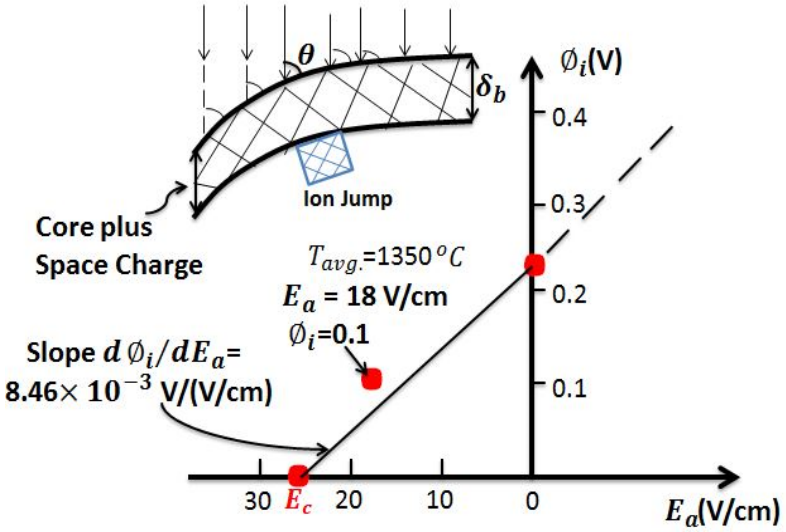

Fig. 5.5 The bias exerted at 1350 °C by the applied dc electric field E on the space charge potential $\emptyset_i$ in 3YSZ due to the segregation of yttrium ions at the grain boundary.

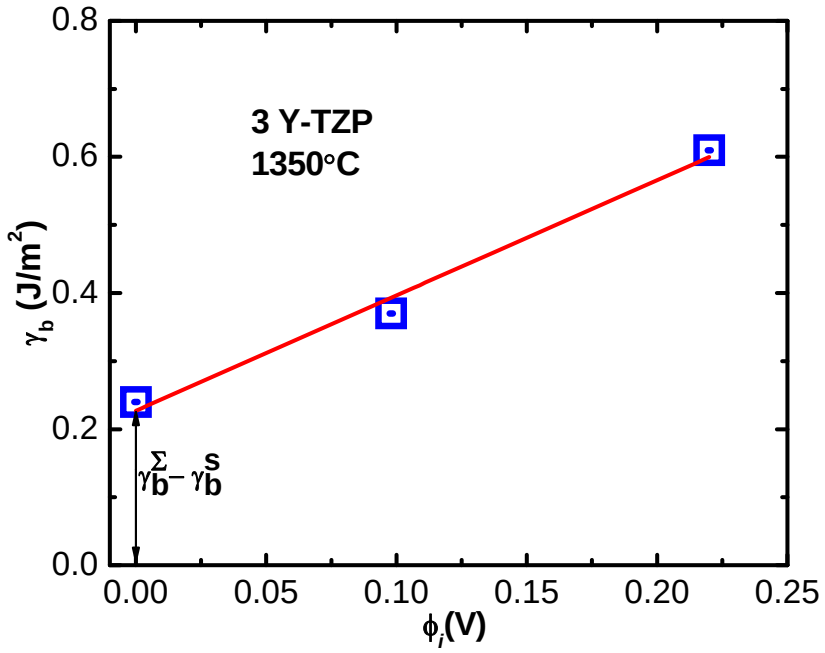

Fig. 5.6 Grain boundary energy γ_b vs the magnitudes of the space charge potential $\emptyset_i$ in 3YSZ at 1350 ^{o}C.

5.2 Equivalence of AC and DC electric field on grain growth retardation

It is now well-established that a modest applied dc electric field retards grain growth in yttria-stabilized zirconia (YSZ) [5.2-6, 5.23, 5.40]. It is proposed that the retardation results from a reduction in the driving force for grain growth (namely, the grain boundary (GB) energy) by the interaction of the applied field bias with the space charge potential Ø at the GB [5.4,5.5,5.38]. It was further found that a 60 Hz ac electric field (rms) had a greater retarding effect on grain growth in 3YSZ than a dc field [5.41,5.42]; see Fig.5.7. The ratio d_E/d is the grain size with field to that without for otherwise the same conditions. The present section examines the reason for the greater effect of the rms ac field compared to dc in Fig.5.7. It is shown that the full-cycle mean (average) value of the ac field strength gives agreement with the dc field.

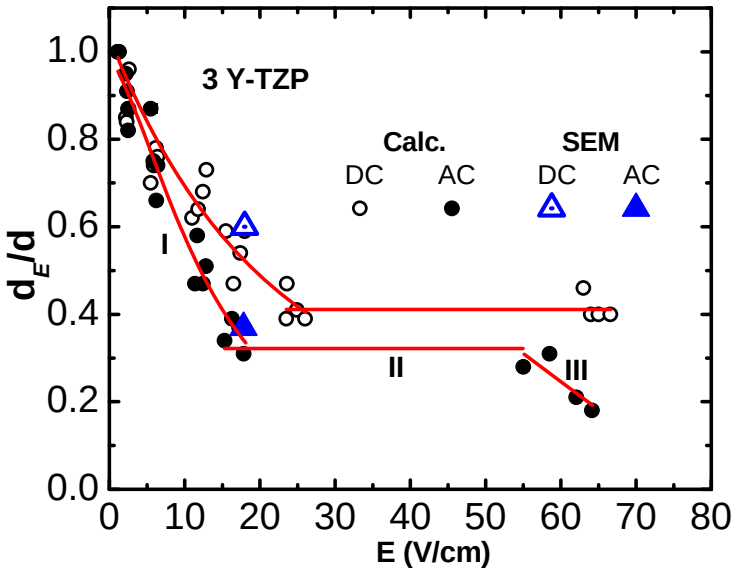

Fig. 5.7 Ratio of the grain size with field (d_E) to that without (d) vs electric field strength E (DC and rms AC). Data from ref. [4.2].

The 60 Hz ac field employed in Fig.5.7 was sinusoidal in form given by

$$E = E_{max}\sin 2\pi ft = E_{max}\sin\theta \qquad (5.15)$$

where E_{max} is the maximum value, f the frequency, t the time and θ the angular velocity. The effective value of an ac field can be defined by either its root mean square (rms) value or by its mean (average) value. For a sinusoidal wave, $E_{rms} = E_{max}/\sqrt{2}$ and E_{mean}(half-cycle) $=2\,E_{max}/\pi = 2\sqrt{2}\,E_{rms}/\pi$. The voltage and corresponding ac field strength reported in Fig.5.7 is the rms value measured by a commercial meter. It is well-known that the rms value of an ac field is equivalent to a dc field regarding Joule heating.

Upon reviewing the results for Regime I in Fig.5.7 ($E \leq 26$ V/cm) it was found that the ratio of the ac rms field to the dc field (E_{rms}/E_{dc}) was essentially constant (0.51 ± 0.5) for the entire range in grain size ratios d_E/d = 0.9 to 0.4; see Fig.5.8. Also, the effect of the field on d_E/d was essentially independent of temperature over the range of 800 ^{o}C to 1500 ^{o}C[5.4] thereby negating *bulk* Joule heating as a significant factor. Further, a linear bias effect of the field on ∅ is in better accord with theory than a root mean square bias [5.38]. Moreover, the squared nature of the rms field eliminates any directional effect of the field. Therefore, it is proposed that the rms value is not the appropriate "effective" field in grain growth, but rather the mean value $E_{mean} = 2\sqrt{2}\,E_{rms}/\pi$ for each half-cycle. Since both positive and negative radii of GB curvature will normally exist in a bulk specimen, the total, full-cycle effective mean ac value $E_{mean}^{total} = 4\sqrt{2}\,E_{rms}/\pi$; see Fig.5.9. Shown here as an example is a cubic grain whose opposite boundaries exhibit positive and negative radii of curvature regarding a possible reduction in GB energy by ionic diffusion. The applied

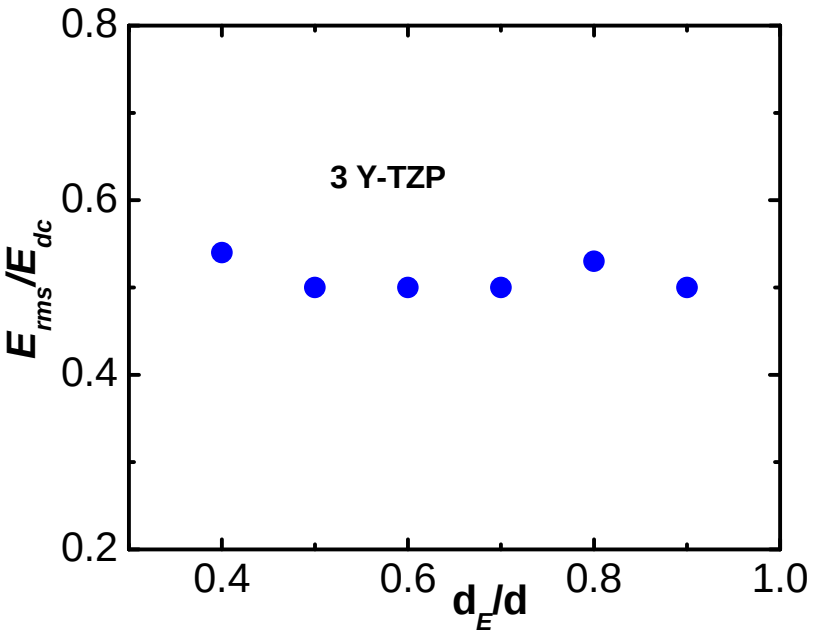

Fig. 5.8 Ratio of the rms ac electric field strength E_{rms} to the dc strength E_{dc} for each grain size ratio d_E/d in Regime I of Fig.5.7.

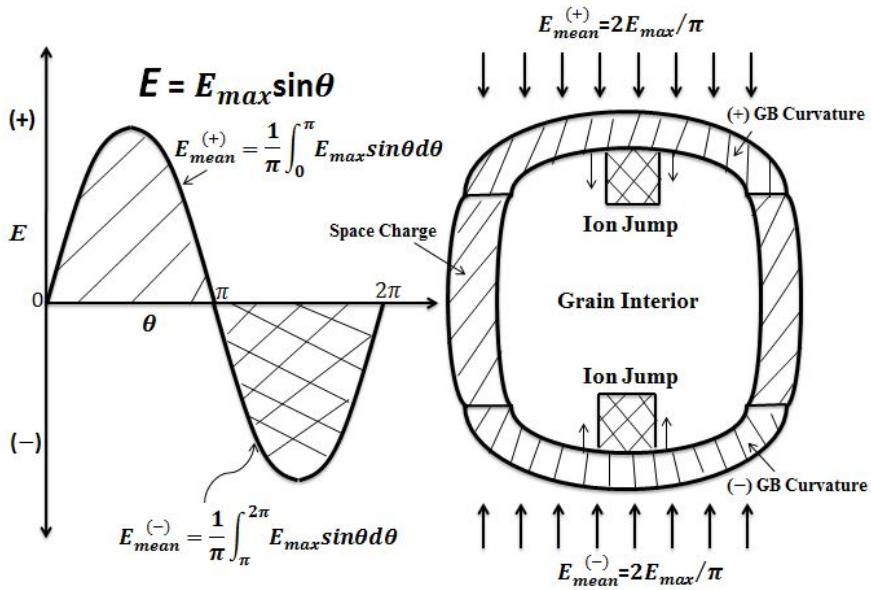

Fig. 5.9 Schematic employing a cubic grain geometry of the dual effect of a sinusoidal ac electric field on grain growth by the effective positive and negative mean fields acting on grain boundary segments having a positive or negative curvature.

sinusoidal ac field consists of positive and negative half-cycles with mean electric field values $E_{mean}^{(+)}=\frac{1}{\pi}\int_0^{\pi} E_{max} sin\theta\, d\theta$ and $E_{mean}^{(-)}=\frac{1}{\pi}\int_{\pi}^{2\pi} sin\theta\, d\theta$ which act respectively on the grain boundaries of the same sign radius of curvature. Since on the average equal numbers of GBs with positive and negative radii of curvature are expected to exist in the bulk specimen, the total effective mean ac field is $E_{mean}^{total} = 4\sqrt{2}\, E_{rms}/\pi$. Using $E_{mean}^{total} = 4\sqrt{2}\, E_{rms}/\pi$ for the total effective ac field strength the plots of d_E/d vs E for both ac and dc now overlap; see Fig.5.10.The overlap not only provides support for the use of E_{mean}^{total} but is in accord with the proposed physical mechanism for the retardation of grain growth by an electric field in 3YSZ, namely reduction in the GB energy through the bias interaction of the field with the space charge potential [5.4,5.5,5.38].

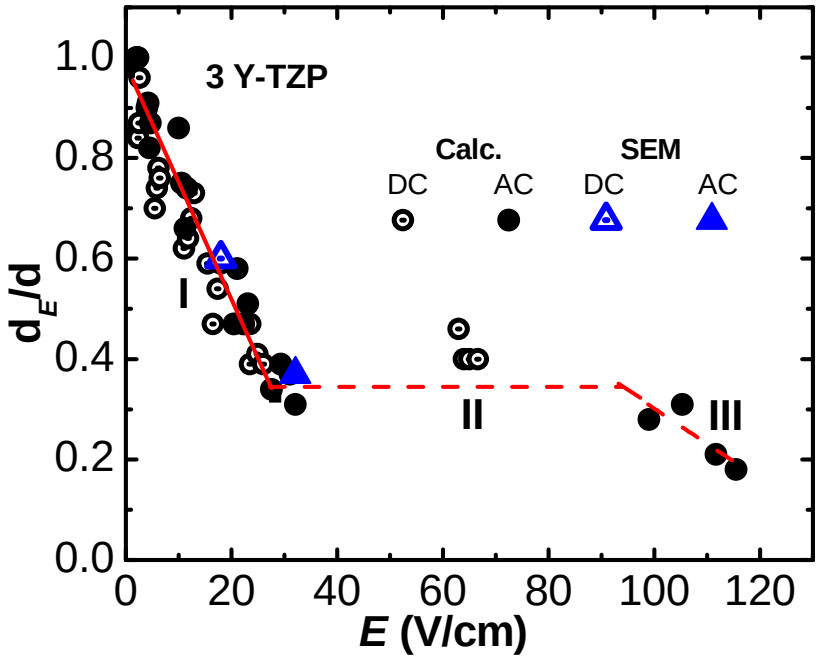

Fig. 5.10 Grain size ratio d_E/d vs dc and the total mean ac electric field strength.

Ghosh et al. [5.3] proposed an alternate explanation for the retarding effect of an applied electric field on grain growth in 3YSZ, namely that the high GB resistivity leads to excessive *local* Joule heating and to an increase in the GB entropy, which in turn gives a reduction in driving force for grain growth. It is however not clear why an equivalent rms ac field should have a greater effect than a dc field.

The overlap of the data for ac and dc fields in Fig.5.10 gives three regimes for the variation of d_E/d with applied field E: (a) Regime I for $E < E_c^I$(~26 V/cm), where d_E/d initially decreases with E, (b) Regime II for $E = E_c^I$ to E_c^{II} (~100 V/cm), where d_E/d is relatively independent of E and (c) Regime III for $E > E_c^{II}$, where d_E/d decreases again with field strength. Wang and Conrad [5.43] attribute Regime I to a reduction in the driving force (GB energy) for grain growth by the interaction of the field with the electrostatic space charge potential; Regime II is attributed to the combined crystallographic and ionic size mismatches at the GB core. Regime III could then result from a reduction in the GB core energy. A possible mechanism for this is the concept proposed by Narayan [5.44], where at sufficiently high field strength an excessive number of crystal defects can result at the GB core leading to a reduction in the *core* energy. Frenkel defects could provide this possibility. The critical field E_c^{III}(=~100 V/cm) may well be the precursor to "flash" sintering [5.45].

5.3 Grain boundary resistivity

5.3.1 Annealing tests

For comparison with the values reported in the literature, the brick-layer model (Eq.4.6) was first employed to determine the specific GB resistivity ρ_b^* from the present

isothermal annealing test results, i.e., from the slope of a plot of the bulk resistivity $\rho_{bulk}(= E/j)$ vs the reciprocal of the grain size. We assume that the grains approximate a tetrakaidecahedral shape and therefore that the effective grain size $d_E^{tetra.} = 1.78\bar{d}_E$. Plots of $\rho_\Omega$vs$(d_E^{tetra})^{-1}$ determined from our annealing tests at 1300 ^{o}C and 1400 ^{o}C are presented in Figs. 4.32 and 4.33. Included in Figs.4.33 for comparison are extrapolations of reported data obtained by impedance spectroscopy (lower temperatures) and 4-probe (similar temperatures) measurements on single and polycrystalline specimens. To be noted is that the resistivity behavior determined from the annealing tests is in reasonable accord with that by the more conventional measurements by impedance spectroscopy and 4-probe method.

A least-squares fit of the annealing test results for each temperature in Fig. 4.32 give for the intercept $\rho_g = 0.54$ Ω-cm, the slope $\rho_b^*\delta_g$=1.31 (Ω-cm)μm and Pearson's fit equal 0.98 at 1300 ^{o}C, and ρ_g=0.91 (Ω-cm), $\rho_b^*\delta_b$= 1.14 (Ω-cm)μm and 0.99, respectively at 1400 ^{o}C. Taking δ_b= 10 nm for 3 Y-TZP gave ρ_b^*=131 Ω-cm at 1300 ^{o}C and 114(Ω-cm) at 1400 ^{o}C, and in turn the ratio ρ_b^*/ρ_g=257 and 124 respectively. These values are all within the ranges of those reported in the literature for YSZ. Of special significance is that the calculated intercepts for the annealing tests are in accord with conventional measurements of the resistivity of single crystals.

5.3.2 Sintering tests

Of primary interest is an explanation for the increase in the bulk resistivity ρ_Ω with electric field strength shown in Figs. 4.20 and 4.21. Since the grain size decrease with increase in E and since the grain boundary resistivity ρ_b^* is orders of magnitude larger than

that for the grain interior it is expected that the bulk resistivity ρ_{Ω} will increase with increase in field strength E. According to the brick layer model the increase should vary with reciprocal of the grain size, which is found to be the case; see Figs. 4.23 and 4.24.

5.4 References

[5.1] W. D. Kingery, H. K. Bowen, D. R. Uhlmann, Introduction to Ceramics, 2nd Edition, John Wiley & Sons, New York (1996).

[5.2] Di Yang, H. Conrad, : Scripta Mater., 36(1997) 1431-1435.

[5.3] S. Ghosh, A. H. Chokshi, P. Lee, R. Raj, : J. Am. Ceram. Soc. 92 (2009) 1856-1859.

[5.4] H. Conrad, Di Yang, : Mater. Sci. Eng. A 528(2011)8523-8529.

[5.5] H. Conrad, : Emerging Mater. Res., Inst. Civil Engrs. 1 (2012)11-16.

[5.6] S. Starnes, H. Conrad, : Scripta Mater. 59(2008)1115-1118.

[5.7] J. Obare, W. D. Griffin, H. Conrad, : J. Mater. Sci. 47 (2012) 5141-5147.

[5.8] J. E. Burke, D. Turnbull,: Prog. Metal. Phys. 3(1952)220-292.

[5.9] W. D. Kingery, H. K. Bowen, D. R. Uhlmann, :Introduction to Ceramics, Wiley, New York(1976) 448-515.

[5.10] H. Conrad,:Emerging Mater. Res., ICE 1(2012)11-16.

[5.11] A. Tsoga, P. Nikolopoulos, : J. Mater. Sci. 31(1996)5409-5413.

[5.12] A. A. Winnubst, P. J. M .Kroot, A. J. Burggraaf, :J. Phys. Chem. Solids, 44(1983)955-960.

[5.13] S.-L. Hwang, I.-W. Chen, : J. Am. Ceram. Soc. 73(1990)3269-3277.

[5.14] G.S.A.M. Theunissen, A.J.A. Winnubst, A.J. Burggraaf, :J. Mater. Sci. 27(1992)5057-5066.

[5.15] S. Stemmer, J. Vdeugels, O. Vand der Beist, : J. Eur. Ceram. Soc., 18 (1998)1565-1570.

[5.16] J.A. Hines, Y. Ikuhara, A.H. Chokshi, T. Sakuma, : Acta Mater. 46(1998)5557-5568.

[5.17] E.C. Dickey, Z. Fan, S.J. Pennyeook, :J. Am. Ceram. Soc., 84 (2001)1361-1368.

[5.18] P.E.J. Flewitt, R.K. Wild, Grain Boundaries: Their Microstructure and Chemistry, John Wiley & Sons, Beffins Lane, Chichester, UK (2001).

[5.19] K. Matsui, H. Yashida, Y. Ikuhara, : Acta Mater. 56(2008)1315-1325.

[5.20] R. Chaim, : Mater. Sci. Eng. A 486(2008)439-446.

[5.21] J. W. Cahn, :Acta Metall., 10(1962)789-798.

[5.22] M. F. Yan, R. Cannon, H. Bowen, Ceramic Microstructures, R. M. Fulrath, J. A. Pask, eds. Westview Press, Boulder, CO(1977)pp.276-307.

[5.23] J. Wang, Di Yang, H. Conrad, : Scripta Mater. 69(2013) 351-353.

[5.24] G. Gottstein, L. S. Shvindlerman, Grain Boundary Migration in Metals, CRC Press, New York (1999) pp.112.

[5.25] M. F. Yan, R. M. Cannon, H. K. Bowen, :J. Apl. Phys. 54(1983)764-776.

[5.26] J. D. Eshelby, “The continuum theory of lattice defects” in Solid State Physics, F. Seitz, D. Turnbull, eds. (1956).

[5.27] J. D. Eshelby, : Proc. Roy. Soc. London A, 241 (1957) 376-396.

[5.28] M. J. Verkerk, B. J. Middelhuis, A. J. Burgraff, : Solid State Ionics, 6(1982)159-170.

[5.29] X. Guo, J. Maier, :J. Electrochem. Soc. 148(2001)E121-E126.

[5.30] X. Guo, : Phys. Status Sol. (a)183(2001)261-271.

[5.31] X. Guo, W. Sigle, J. Fleig, J. Maier, :Solid State Ionics, 154-155(2002) 555-561.

[5.32] X. Guo, Z. Zhang, :Acta Mater. 51(2003)2539-2547.

[5.33] D. Bingham, P. W. Tasker, A. N. Cormack, : Phil. Mag. A 60(1989)1-14.

[5.34] W. D. Kingery, : J .Am. Ceram. Soc. 57(1974)1-8.

[5.35] J. A. Ikeda, Y.-M. Chiang, : J. Am. Ceram. Soc., 76(1993)2437-2446.

[5.36] B. D. Huey, D. Lisjak, D. A. Bonnell, : J. Am. Ceram. Soc., 82(1999)1941-1944.

[5.37] J.-H. Han, D.-Y. Kim, : J. Am. Ceram. Soc., 84(2001)539-550.

[5.38] X. Guo, R. Waser, : Progress in Mater. Sci. 51(2006)151-210.

[5.39] W. C. Mackrodt, P. M. Woodrow, : J. Am. Ceram. 69(1986)277-280.

[5.40] Di Yang, R. Raj, H. Conrad, J. Am. Ceram. Soc. 93(2010)2935-2937.

[5.41] Di Yang, H. Conrad, Scripta Mater. 61(2010)328-331.

[5.42] H. Conrad, Di Yang, Mater. Sci. Eng. A 559(2013)591-594.

[5.43] J. Wang, H. Conrad,:J. Mater. Sci., accepted.

[5.44] J. Narayan, Scripta Mater. 68(2013)785-788.

[5.45] M. Cologna, B. Rashkova, R. Raj, J. Am. Ceram. Soc., 93(2010)3556-3559.

CHAPTER SIX

6.0 CONCLUSIONS

1. The grain growth rate of 3 Y-TZP is retarded with application of a modest electric filed during sintering, isothermal annealing and plastic deformation, which leads to an enhancement of these processing rates. The effect of an applied dc electric field E up to 60 V/cm on grain growth shows two regimes: (a) $E \leq E_c (\leq 26\, V/cm)$ where the grain size ratio d_E/d with field compared to without decreases with E and (b) $E > E_c$ where d_E/d is relatively independent of E, the transition occurring at E = 26 V/cm and the corresponding grain size ratio of $d_E/d \approx 0.4$. A 60 Hz AC(rms) field has a greater retardation of grain growth compared to DC field. This is attributed to the fact that the field vector with AC has both positive and negative components thereby interacting with grain boundaries of both positive and negative curvature.

2. Grain stereology studies suggest that for both tests with and without field the 3-D form of the grain is approximately tetrakaidecahedral and that he grains are relatively equiaxed, i.e., the grain shape is essentially isotropic. The grain size distribution of fully-sintered and isothermally annealed 3 Y-TZP is approximately log-normal and in accord with the Bitti-Di Nunzio model. The field has no effect on the stereological features but only shifts the size distribution to a smaller grain size.

3. Based on the classical solute drag mechanism, the present results in terms of grain growth rate in 3Y-TZP annealed at 1300 ^{o} and 1400 ^{o}C with and without an applied electric

field E = 18 V/cm gave that the grain growth rate exhibited $\dot{d}\ vs\ P$ behavior in the so-called transition regime with values of grain size exponent m in the range of 1-15.

4. The grain growth results also suggest that the retarding effect of an electric field on grain growth in 3Y-TZP is mainly due to the reduction of the grain boundary energy by the field, which results from the interaction of the field with the GB space charge.

5. A physical model is developed from the effect of E on the grain growth rate for the magnitudes of the GB energy components: γ_b^{Σ}(crystallographic mismatch), γ_b^{s}(solute ion size misfit) and γ_b^{e}(electrostatic), which provide the driving force for grain growth. It is proposed that the region with E ≤26 V/cm (the grain size ratio of $d_E/d > 0.4$)corresponds to the electrostatic (space charge) component γ_b^{e} of the grain boundary(GB) energy with E = 26 V/cm and that $d_E/d = 0.4$ corresponds to the difference between the crystallographic (γ_b^{Σ}) and the size misfit (γ_b^{s}) components. The former accounts for 60 % of the total GB energy and the latter for the remaining 40 %.

6. The proposed model gives reasonable agreement between the experimentally–derived values of the GB energy components and predictions. Further, the model gives the magnitude of the space charge potential energy $e\emptyset_i = 0.22\ eV$, which is in agreement with reported values employing impedance spectroscopy and atomic simulations.The agreement of the calculated values of $e\emptyset_i$ with reported values supports the model proposed here for γ_b^{e},

whereby the applied electric field provides a bias to the space charge which results from the segregation of the Y^{+3} ions to the GBs. The reduction in γ_b^e by the applied field is considered to be the major factor responsible for the retardation of grain growth in 3YSZ by an electric field.

7. Bulk resistivity ρ_Ω during sintering increases with E to ~ 25 V/cm and then becomes relatively independent of E with further increase to ~ 65-70 V/cm. The increase in ρ_Ω with E was attributed to the corresponding decrease in grain size with E. The resistivity ρ_Ω with both AC field and DC field for sintering is strongly temperature dependent.

8. The grain interior resistivity ρ_g and the grain boundary resistivity ρ_b^* were determined employing brick layer model from isothermal annealing test results. The values of ρ_b^* obtained employing the brick layer model are 131 Ω-cm and 114 Ω-cm at 1300 ^oC and 1400 ^oC, which gives that the ratio ρ_b/ρ_g equals 257 and 124 respectively. These results are in good accord with the reports by IS and 4-probe in the single crystal and polycrystals of YSZ.

CHAPTER SEVEN

7.0 FUTURE WORK

Future works: According to the results obtained to-date, the following aspects are rescommended for further research in this area:

1. Since a small or modest electric field has been found to improve the sintering rate and in turn retard the grain growth in YSZ, then it would promise that dense products can be obtained with application of a higher electric field targeting further lowering the sintering temperature, which would save the energy and reduce the contamination.

2. Further work needs to be conducted by processing the YSZ with application of AC field, i.e., determine the effect of the frequency and wave-form (i. e. sinusoidal, triangular and rectangular etc.) of an AC field.

3. Further grain boundary structure investigation is suggested. Experimental work or modeling regarding the effect of electric field on the structure of grain boundary would provide important information for further understanding mechanism(s) of the effect of electric field on grain growth.

4. Employed host materials and solute additions which give a variation in the valence difference between host and solute.

5. Study the effect of field bias on grain growth in laminar composites consisting of large grains on one side and smaller grains on the other.

6. Determine the ratio of space charge size to the grain size in the nanometer grain size range.

7. Employ impedance spectroscopy to measure the grain and grain boundary conductivity.

8. Measure the electric potential in the space charge at the grain boundaries directly using a scanning probe.

9. Study the mobility of a single grain boundary.

10. Measure the Joule heating by advanced techniques, e.g. infrared radiation technique.

APPENDIX

APPENDIX A: The brick layer model for grain boundary resistivity

Assume that the microstructure consists of cubic grains with edge length d separated by grain boundaries of width δ_b and that the electric current I due to the applied field E_a flows perpendicular to the grain boundary shown in Fig. A-1. Further assume that the resistivity of the grain boundaries ρ_b is considerably greater than that of the grain ρ_g so that essentially no electric current flows along the boundaries parallel to E_a. This gives for the total resistance due to the grain plus the boundary.

$$R_\Omega = R_g + R_b \qquad \text{(A-1)}$$

where R_g is that due to the grain interior and R_b that due to the boundary. Taking $R = \rho l/A$ for each of the two components in Eq. A-1, where l is the respective height and A = d^2 the cross section area, one obtains for $l_g = d$ and $l_b = \delta_b$

$$\rho_\Omega = \rho_g + \rho_b = \rho_g + \rho_b^* \delta_b d^{-1} \qquad \text{(A-2)}$$

where ρ_Ω is the total (bulk) resistivity, ρ_g that of the grain interior, $\rho_b = \rho_b^* \delta_b d^{-1}$ the contribution of the grain boundary resistivity to the total resistivity and ρ_b^* that of the "specific grain boundary resistivity".

A schematic of Eq.A-2 is shown in Fig.A-2. To be noted is that the contribution of the grain boundary resistivity to the total resistivity may be larger or smaller than the magnitude of the grain resistivity depending on grain size.

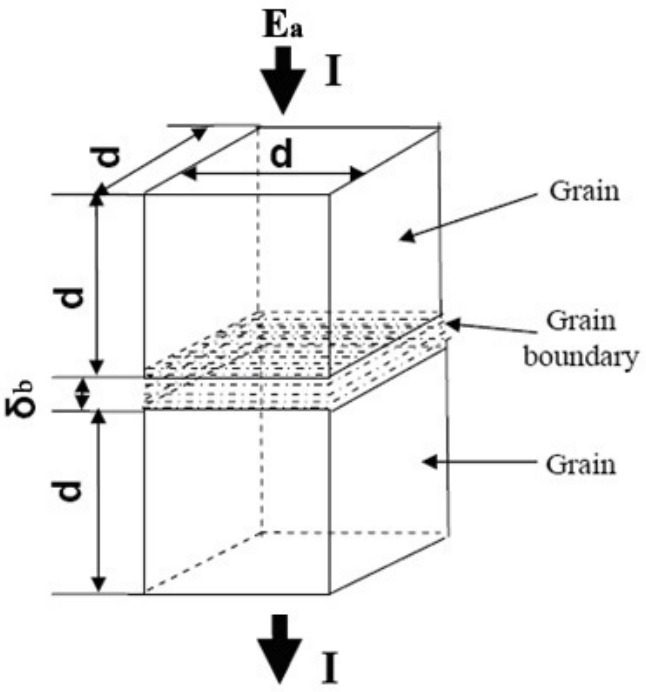

Fig.A-1. Schematic showing cubic grains with edge length d separated by a grain boundary of width δ_b subjected to an applied electric field E_a giving the electric current I.

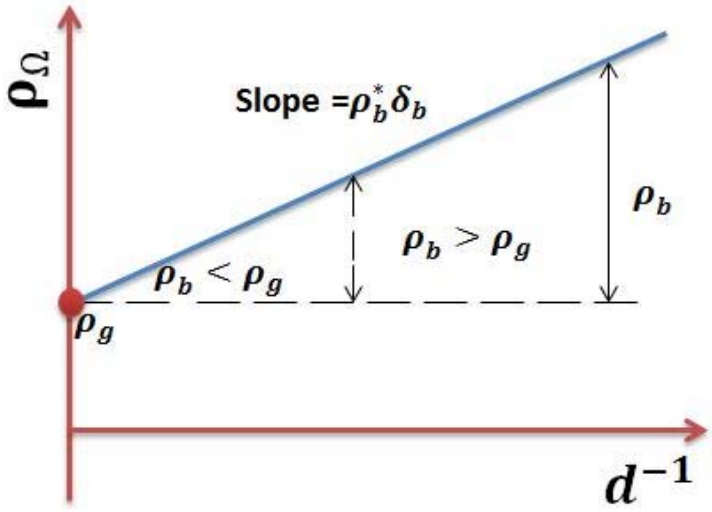

Fig.A-2. Schematic of the variation of the total resistivity ρ_Ω with the reciprocal of the grain size d^{-1} according to the brick layer model.